ELECTROSPINNING OF BIOCOMPATIBLE AND BIODEGRADABLE POLYMERS AND THEIR APPLICATION IN SCAFFOLD TISSUE ENGINEERING

A THESIS SUBMITTED TO THE

SAVITRIBAI PHULE PUNE UNIVERSITY

FOR THE DEGREE OF

DOCTOR OF PHILOSOPHY (Ph.D.)

IN

CHEMICAL ENGINEERING

BY

M. DHANALAKSHMI

DR. ASHISH LELE

(RESEARCH GUIDE)

DR. JYOTI JOG

(RESEARCH CO-GUIDE)

POLYMER SCIENCE AND ENGINEERING DIVISION
NATIONAL CHEMICAL LABORATORY
PUNE - 411008 (INDIA)

FEBRUARY 2015

CERTIFICATE

This is to certify that the work presented in the thesis entitled "**Electrospinning of biocompatible and biodegradable polymers and their application in scaffold tissue engineering**" by **M.Dhanalakshmi**, submitted for the degree **Doctor of Philosophy** in **Chemical Engineering** was carried out under our supervision at the Polymer Science and Engineering Division, National Chemical Laboratory, Pune, 411008, India. Such material as has been obtained from other sources has been duly acknowledged in the thesis.

Dr. Ashish Lele **Dr. Jyoti P. Jog**

(Research Guide) **(Research Co-Guide)**

Date:

Place: NCL, Pune

DECLARATION

I hereby declare that the work presented in the thesis entitled "**Electrospinning of biocompatible and biodegradable polymers and their application in scaffold tissue engineering",** submitted for Ph. D. Degree in **Chemical Engineering** to the Savitribai Phule Pune University, has been carried out under the supervision of **Dr. Ashish Lele and Dr. Jyoti P. Jog** at the Polymer Science and Engineering Division, National Chemical Laboratory, Pune. The work is original and has not been submitted in part or in full by me for any degree or diploma to this or any other University.

M.Dhanalakshmi

(**Research Student)**

Date:

Place: NCL, Pune

Dedicated to my beloved parents

Acknowledgements

First of all I would like to express my sincere gratitude to Dr. Ashish Lele for his invaluable guidance and support throughout this work. He has trained me and helped me develop my technical and writing skills. He is an excellent teacher and always gave me freedom to work in areas of my interest. I will always be grateful to him for giving me this opportunity to work with him.

I would like to express my sincere gratitude to Dr. Jyoti Jog for her valuable guidance. I have always been a great admirer of her sincerity and dedication to work. More than a Ph.D guide, she always cared about me. I sincerely thank Dr. Jog for all her well wishes, help and guidance.

I would like express my gratitude to Dr. Mugdha Gadgil to her valuable guidance in the cell culture studies. I would also like to thank Mrs. Ketaki for helping in the cell culture experiments. I would like to thank Dr. B.L.V. Prasad and Dr. Mansi for helping me in the gold nanoparticle synthesis and in fruitful scientific discussions. I would also thank Dr. C. Ramesh for his support.

I would like to thank Dr. M. G. Kulkarni, former Head, PSE Division. I would also like to thank the technical and non-technical staff of the Polymer Science and Engineering Division for their help. I would like to acknowledge CSIR, India for awarding me the Senior Research Fellowship.

I would like to thank Mr. Vivek Borkar for helping to setup the electrospinning equipment. I would also thank Mr. A. B. Gaikwad, Mr. Gholap, Pandi, Dr. Naren, Anuj and Ketan for their help in the Electron Microscopy studies.

I will take this opportunity to thank Mrs. Anuya Nisal for her continuous support. I would like to acknowledge her for the valuable suggestions given to me during the thesis writing. I would like to thank Sameer Huprikar for his encouragement and support.

It is my pleasure to thank pretty ladies Neelima mam, Sangeeta mam, Marathe mam, Poorvi mam, Amruta, Kalyani and Samruddhi for making my stay at NCL memorable. I would also thank all the CFPE group members.

I would like to thank my lab friends Amol Ridhore, Chetan Chenmal, Dr. Santosh Wanjale and Sunita Thombre for their moral support.

I would like thank to my friends, Kala, Raji, Anusha, Muruga Priya, Viswanath, Cynthia, Rathi priya, Sridhar Krishna, Palani, Silambarasi and Lenin for their moral support.

I would like to specially thank Mr. Prashant Patil for his help and encouragement throughout my Ph.D, His support during the initial stages for invaluable.

Finally, I would like to express deep gratitude to my brothers M. Velanprabu and M. Sathishkumar for their continuous support during this long journey. I would also thank my sister in law V. Dhanalakshmi.

M. Dhanalakshmi

Table of contents

LIST OF FIGURES

LIST OF TABLES

List of Abbreviations

N11	Nylon11
PHB	Polyhydroxybutyrate
ES	Electrospinning
UV-vis	Ultraviolet visible spectroscopy
SEM	Scanning electron microscope
TEM	Transmission electron microscope
XRD	X-ray diffraction
DSC	Differential scanning calorimetry
DMTA	Dynamic mechanical analysis
DRS	Dielectric relaxation spectroscopy
FTIR	Fourier transform infrared spectroscopy
ATR	Attenuated total internal reflection
TGA	Thermo gravimetric analysis
XPS	X-ray photoelectron spectroscopy
CA	Water contact angle measurement
3-D	Three dimensional
GNPs	Gold nanoparticles
ZnO	Zinc Oxide
HAP	Hydroxyapatite

List of symbols

□	Viscosity
σ	Conductivity
Tg	Glass transition temperature
Tm	Melting point
ΔH_f	Heat of fusion
T_c	Crystallization temperature
RF	Radio frequency
tan δ	Damping factor
tan δ	Dielectric loss tangent
α, γ	Shape parameters describing the symmetric and asymmetric broadening of relaxation, respectively.
E_a	Activation energy
T	Temperature
R	Gas constant
V	Voltage

ABSTRACT

This thesis is concerned with electrospinning of biocompatible polymers, studies on microstructure of the electrospun mats and viability of the mats for cell culture application. Electrospinning process offers a simple and scalable approach for fabrication of non-woven mats comprising fibers of diameters ranging from nanometer to micrometer. A wide variety of polymers ceramics and metal oxides can be electrospun. We have used Nylon11 for electrospinning nonwoven mats in this work. We had varied the Nylon11 electrospinning processing parameters such as concentration, viscosity and conductivity of the solution, applied voltage, flow rate and distance between the two electrodes to study their effects on fiber diameter and morphology. The physical properties of electrospun mats were measured and compared with the properties of melt pressed films and solvent cast films. The rapid evaporation of solvent and stretching of fibers during electrospinning gives rise to measurable differences in the properties of electrospun fibers. The Nylon11 melt pressed film and electrospun mats were used as scaffolds for growing cells.

Nylon11 electrospun mat exhibits hydrophobic nature with the water contact angle values of 135^{o}. To use the mats in cell culture studies, we need to make them hydrophilic and suitable for growing cells. We have used two surface modification techniques to convert hydrophobic Nylon11 electrospun mats to hydrophilic mat and facilitate the cell growth. The first surface modification was plasma treatment. Plasma treatment is a process by which we can incorporate desired functional groups on the surfaces. Followed by the plasma treatment, gold nanoparticles were attached to the electrospun mat. Contact angle measurements were performed to compare the longevity of the surface modification by plasma treatment and plasma treatment followed with attachment of gold nanoparticles.

One of the methods to increase the biocompatibility of polymer is to blend with biocompatible or biodegradable polymers and or by using biocompatible fillers. Nylon11/PHB biocompatible blends were prepared using different processing techniques such as melt blending, solution blending and electrospinning process. The effects of the processing conditions on the structure and morphology of the blends were studied. Finally, the electrospun mats of Nylon11, PHB and Nylon11/PHB (50:50) electrospun blends were tested in preliminary cell culture studies for their use

as scaffolding matrices in tissue engineering application. Nylon11/ZnO nanocomposites were prepared using electrospinning process. Nylon11/ZnO electrospun mats show better piezoelectric response when compared to the Nylon11 electrospun mats.

This thesis is organized into six chapters.

Chapter 1 provides introduction to of tissue engineering and scaffold fabrication methods. The basic concept of electrospinning process is described in detail. Different morphologies of electrospun fibers are also presented. Finally, the properties of Nylon11 and previous literature on electrospinning of Nylon11 and Nylon11 blends are given.

Chapter 2 presents the objectives of the thesis.

Chapter 3 describes electrospinning of Nylon11 by varying processing parameters such as concentration, applied voltage and distance between the electrodes. Structural analysis of the Nylon11 electrospun mats is compared with Nylon11 melt and solution cast films. Nylon11 melt pressed film and electrospun mats were used as scaffolds for cell culture applications.

Chapter 4 presents surface modification of Nylon11 electrospun mat, by virtue of which the hydrophobic Nylon11 electrospun mats are converted to hydrophilic mats that can support cells to grow.

Chapter 5 discusses Nylon11/PHB biocompatible blends prepared from melt, solution and electrospinning processes. The effects of the processing conditions on the structure and morphology of the blends were studied. The piezoelectric response of the Nylon11 electrospun mats was compared with that of Nylon11/ZnO biocompatible electrospun mats.

Chapter 6 gives specific recommendations for future work.

Chapter 1

Introduction

This chapter gives a brief introduction to electrospinning and tissue engineering. The electrospinning process is described in detail. The processing parameters of electrospinning and the different morphologies of electrospun fibers and mats are described. Next, a brief description of tissue engineering and different scaffold fabrication methods are provided with particular emphasis on the application of electrospun mats for tissue engineering. Finally, this chapter provides information about Nylon11, which has been used extensively in this work.

1.1 Introduction to Tissue Engineering

Scaffold based tissue engineering is an interesting and emerging field. The main role of a scaffold in tissue engineering is to provide support for cells to adhere and grow[1]. Ideally as cells start growing, the scaffold should degrade gradually and should not inhibit cell growth. The scaffold should have appropriate physical, chemical and mechanical properties to promote cell adhesion and tissue formation[2].

Polymers have been widely used as biomaterials for the fabrication of scaffolds. Biocompatible and biodegradable natural polymers such as silk, polyhydroxybutyrate, chitosan, gelatin and collagen has been successfully used to make scaffolds for tissue engineering applications[3–5]. A few synthetic polymers have also been utilized for fabricating scaffolds such as polyethylene oxide and polyvinyl alcohol[6].

The main requirements of a scaffold material are that it should be biocompatible and biodegradable.

The other basic requirements of a scaffold are that it should have

- Three dimensional structure.
- High surface area.
- High porosity and interconnected pores to allow cell migration and transfer of nutrition and metabolic waste.
- Adequate mechanical strength.
- Non-toxicity to the cells.
- Appropriate degradation rate to match the rate of new tissue formation.
- Positive interaction with cells to promote enhanced cell adhesion, growth, migration and differentiation.

1.2 Scaffolds Fabrication Methods

Many fabrication methods are available to make polymer scaffolds. The fabrication process should produce a scaffold with 3-D architecture because cells and tissue are organized into three-dimensional architecture. The choice of manufacturing method can influence different characteristics of the scaffolds such as structural architecture, porosity and mechanical properties. Figure 1.1 shows different fabrication methods of scaffold namely, solvent casting, particulate – leaching, drawing, template synthesis, phase separation, self-assembly, freeze drying and electrostatic spinning (electrospinning).

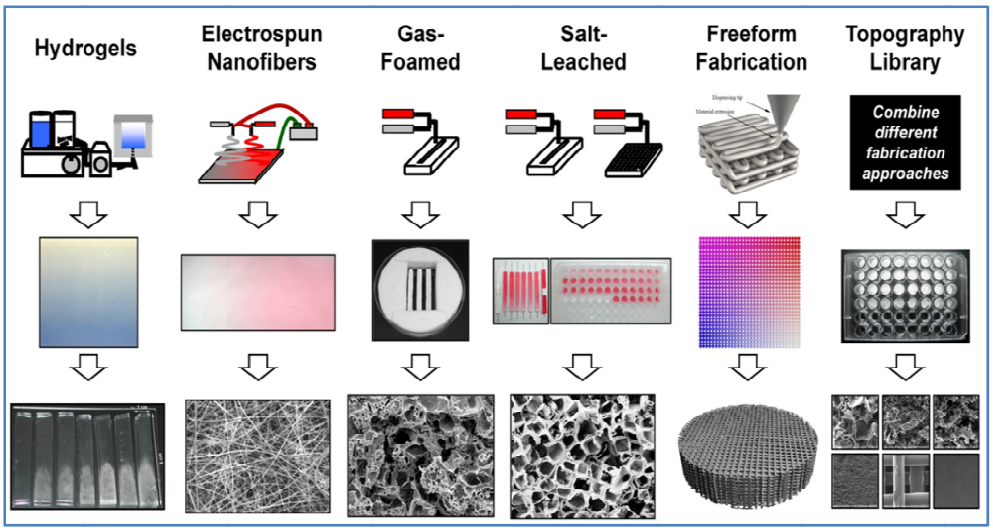

Figure 1.1 Different scaffold fabrication methods (http://www.nist.gov/mml/bbd/biomaterials/3dtissuescaffolds.cfm).

Solvent casting is a simple process and does not require large equipments. In this process, a mold is dipped into the polymer solution and allowed sufficient time to evaporate the solvent[7]. The main drawback of this process is that it is time consuming and involves potentially toxic solvents. Also, scaffolds of only simple architecture such as films or fibres can be made by this process.

Particulate leaching is one of the most popular technique for preparing scaffolds for tissue engineering applications. Porogens (such as salt, sugar and wax) are used to create pores or channels. In this process, a polymer solution is cast into a salt filled mold. Alternatively, the porogens can be mixed with the polymer solution[8]. After solvent evaporation, the salt crystals are leached away to produce pores. The pore size can be controlled by the amount and size of the porogens. The advantage of this process is that it is easy to implement. The drawback of this process is that there is little control on inter-connected porosity.

Microfibrous scaffolds can be made by drawing. Drawing is a process that can be used to produce very long fibers[9]. The disadvantage of this technique is that it is only suitable for viscoelastic materials. The material must be cohesive enough to support the stresses that develop during pulling.

Nanowires and nanorods can be fabricated using template synthesis method[10]. The most commonly used templates are aluminum oxide and polycarbonate membrane.

Phase inversion is also a popular technique to prepare scaffolds. The phase separation mechanism depends on the physical incompatibility of the constituents of the mixture. When a homogenous polymer solution undergoes a decrease in temperature at least two phases form, the first phase is a polymer rich phase and the second one is a polymer lean-phase. By extracting the solvent from the polymer rich phase, gelation occurs and results in formation of a network structure with the polymer lean phase occupying the pores[11]. Various porous structures can be achieved by this method by varying the thermodynamic and kinetic parameters. The disadvantage of this technique is that it is difficult to control the morphology of the scaffold.

Self-assembly process for making scaffolds involves the use of smaller molecules as basic building blocks[12]. The main mechanism for self-assembly is the intermolecular forces that organize the smaller units together and determine the shape of the macromolecular nanostructures such as nanofibers. The advantage of this process is that there is good control on the pore size and fiber diameter. The disadvantage is that it is a complicated process and expensive.

In the last two decades, freeze-drying method has been widely investigated for the fabrication of three-dimensional porous scaffolds for tissue engineering[13]. In freeze-drying, the solution is frozen at a low temperature (−70°C to −80°C). The solvent is removed by lyophilization under vacuum to produce interconnected porous structure. The pore size can be controlled by the freezing rate and pH of the solution. The advantage of this technique is that high temperatures are not required. The drawback is that the processing time is large.

Electrospinning process provides a simple route to fabricate non-woven fibrous scaffolds containing fibres of diameters ranging from nanometers to micrometers. It is a straight forward, inexpensive and scalable process that produces continuous nanofibers. Electrospun nonwoven mats have advantages such as high surface area, porosity and 3-D environment that allows cells to adhere and grow. Disadvantages of electrospinning process are that the mats have limited mechanical properties and the pore size is typically submicron.

Electrospinning is increasingly gaining popularity as the process of choice to fabricate biocompatible and biodegradable polymeric scaffolds. A wide variety of polymers, ceramics and metal oxides can be electrospun[14,15]. The usage of electrospun nanofibrous scaffolds for biomedical applications has attracted a great deal of

attention over the past ten years[16–20]. The bar chart in Figure 1.2 shows publications in the area of electrospinning from 1998 to 2012. It is clear that the interest in electrospinning and its applications is growing in recent years.

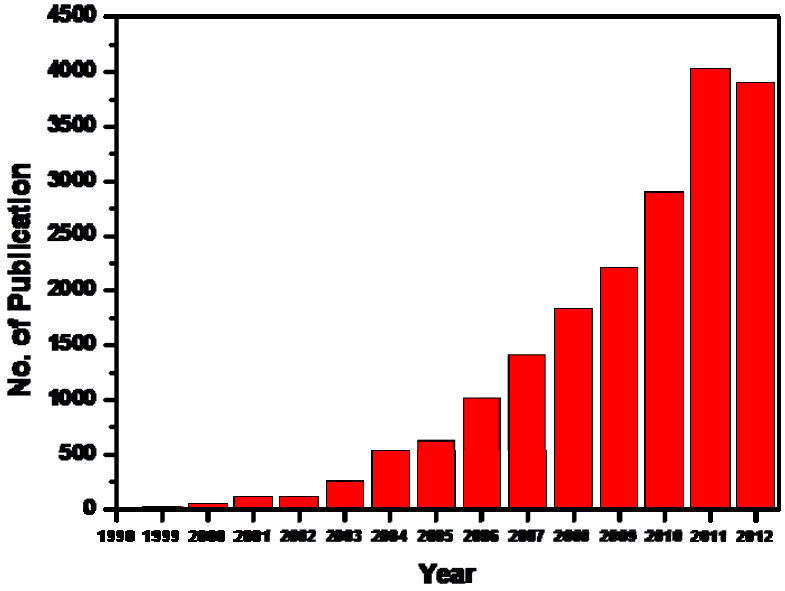

Figure 1.2 Year wise publications in the field of electrospinning (http://www.nafigate.com/en/section/portal/app/theme/detail/30-a-dramatic-rise-of-interest-in-nanofibers).

In the present work we have used the electrospinning process extensively to make non-woven fibrous mats from polymers, polymer blends and polymer nanocomposites. In the following section, we describe the electrospinning process in more detail.

1.3 History of Electrospinning Process

The origin of electrospinning can be traced back to 1600. William Gilbert, discovered that a spherical drop of water on a dry surface was drawn up in a conical shape when a piece of rubbed amber was brought within its proximity. Such shape deformation of liquid bodies in an external electrostatic field governs the modern electrospinning technology. In 1749 Jean-Antoine Nollet demonstrated that a water jet disintegrated when it was charged[21].

Nearly 250 years later in 1902 the fundamental idea of the term “electrostatic spinning or electrospinning” was patented by J.F Cooley and by W.J. Morton[22,23]. Cooley proposed four types of indirectly charged spinning heads, which includes

conventional head, coaxial heads, air assisted model and a spinneret featuring rotating distributor. He also proposed the recovery of a solvent and the use of dielectric liquid instead of a gas as a medium. In his work, Morton employed suitable sources of high tension of static electricity, such as a Holtz' static machine, induction coils of large size, or Tesla and Thomson machines to create fibrous masses by electrospinning .

In 1914 John Zeleny, published work on the behavior of fluid droplets at the end of metal capillaries. His effort began the attempt to mathematically model the behaviour of fluids under electrostatic forces. The principle of modern needle electrospinning originated through Zeleny's work, who designed a needle/capillary apparatus for studying electrical discharges from liquid points. His apparatus is, with some changes, employed by most research workers to date. The first U.S patent in electrospinning was granted to Anton Formhals in 1934 for a process that produced fine fibers from a cellulose acetate solution. Formhals had 22 patents on electrospinning process.

In 1969, Taylor published his work on the shape of the polymer droplet produced at the tip of the needle when an electric field was applied[24]. Taylor found that the pendant droplet developed into a cone when the surface tension was balanced by electrostatic force and that jets were ejected from the vertices of the cone with diameters significantly smaller than the diameter of the needle when the electrostatic force exceeded its surface tension. In a detailed report, Taylor determined that an angle of 49.3 ° is required to balance the surface tension of the polymer with the electrostatic forces. This conical shape of the jet was later referred as the "Taylor Cone" in subsequent works.

A large number of innovations in electrospinning happened around the year 2000, which includes oriented fibers, multilayer electrospinning, mixed electrospinning, fabrication of mats of dual porosity and fabrication of core shell nanofibers. More recently, researchers have focused attention on the modification and functionalization of electrospun fibers for specific applications. The usage of electrospun nanofibrous scaffolds for biomedical applications has attracted a great deal of attention over the past ten years.

1.4 Electrospinning Process

Electrospinning is a process by which sub-micron polymer fibers are produced using an electro statically driven jet of polymer solution or polymer melt[25]. Figure 1.3

shows a schematic representation of the electrospinning process. A metering pump is used to control the flow of polymer solution through a syringe. One electrode is connected to the needle and another electrode is connected to the collector plate. The collector is grounded. When no voltage is applied between the electrodes, the polymer solution through the needle falls down in hemispherical drops due to surface tension. As the intensity of electric field is increased, the hemispherical surface of the fluid starts to elongate to form a conical shape known as the Taylor cone. When a threshold value of electrostatic force is reached, it overcomes the surface tension of the polymer solution and a charged jet is ejected from the apex of the cone[26]. The charged jet travels linearly only for a short distance and then undergoes bending instability resulting in formation of looping trajectory of the jet. The charged jet elongates, the solvent dries out and fibres are finally deposited on the collector plate. The collected fibers are in the range of few nanometers to few microns depending on the processing conditions.

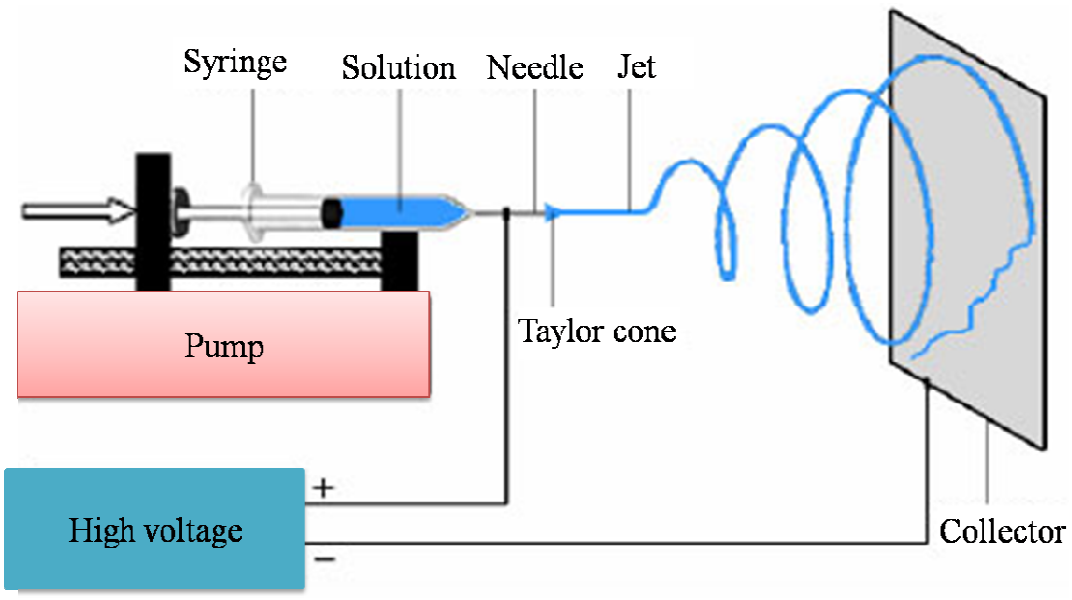

Figure 1.3 Schematic representation of electrospinning process (M. Ziabari et al[27]; Reproduced with permission from Brazilian Journal of Chemical Engineering).

Processing conditions play a major role in the electrospinning process. The entire process is governed by the external electric field produced by the applied voltage and the induced electric field caused by the free and induced charges on the jet surface. Hence, the electric field gradient and also other external parameters have a significant effect on the fiber diameter and morphology of the nanofibers. Many

researchers have studied the effect of proceeding variables on fiber diameter[28,29]. The electrospinning processing variables are listed in the Table 1.1.

Table 1.1 Electrospinning processing parameters.

Solution properties	Processing parameters	Ambient properties
Viscosity Surface tension Conductivity Dielectric constant Solvent volatility	Applied voltage Distance Flow rate Needle diameter	Temperature Humidity Pressure

In the following paragraphs we summarize the effects of the various parameters listed in Table 1.1 on the morphology of electrospun mats.

1.4.1 Viscosity

The viscosity of the solution is directly affected by the concentration of polymer present. Higher polymer concentration results in increased inter- polymer interactions which ultimately raise the solution viscosity. In the electrospinning process, for fiber to be formed a minimum viscosity is required. It is generally observed that increasing the viscosity of the solution increases the fiber diameter[30]. On the other hand, if the viscosity is too high, pumping the solution through the syringe pump will be difficult or the solution may dry on the tip of the needle before the electrospinning is initiated.

1.4.2 Conductivity

When the electrical conductivity of the solution is increased, a significant reduction in the fiber diameter occurs because the jet carries more charges. The repulsion of the charges at the surface of the electrospinning jet causes the solution to stretch and form the nanofibers. Polymer solutions of poor conductivity tend to form electro-sprays (i.e, droplets). The formation of beaded fibers due to electro-spraying can be avoided if a small amount of salt or polyelectrolyte is added to the polymer solution because electrical forces of the increased charge carried by the electrospinning jet causes the jet to elongate thereby producing uniform fibers[31]. It is generally observed that fiber

diameter decreases with increasing solution conductivity. Additionally, higher solution conductivity results in greater bending instability and creates a larger deposition area of collected fibers.

1.4.3 Flow Rate

The flow rate or feed rate of the polymer solution from the syringe is an important parameter that affects the jet velocity, Taylor cone formation and material transfer rate. It is important to have a balance between the applied voltage and the flow rate. A lower flow rate is more desirable as the solvent will get enough time for evaporation, and result in a smaller and more consistent fiber diameter. Increasing the flow rate of the solution increases the fiber diameter[32].

1.4.4 Surface Tension

Surface tension is caused by the attraction between the molecules in a liquid, which is created by a number of intermolecular forces. In the bulk of the liquid, each molecule is pulled equally in all directions by neighboring liquid molecules, resulting in a net force of zero. At the surface of the liquid, the molecules are subjected to an inward force that is balanced only by the resistance of the liquid to compression. The net effect causes the surface area to diminish until it possesses the lowest ratio possible of surface area to volume i.e, spherical. In electrospinning, the charges on the polymer solution and consequently the electrostatic repulsive force on the solution must be high enough to overcome the surface tension of the solution. As the liquid accelerates from the tip of the needle to the target, the polymer jet is stretched, and if the surface tension of the solution is high it may cause the jet to break up into droplets, resulting in electro-spraying.

1.4.5 Applied Voltage Gradient

The electrospinning process produces fibers only if the applied voltage between the electrodes is above a given limiting value required to overcome the surface tension of the solution. The electrical field is defined as the applied voltage divided by the distance between electrodes i.e, between the tip and the collector. Higher electric field values are obtained either through the decrease in the distance between the tip and collector or by increasing the applied voltage. In electrospinning experiments the droplets or fibers transport charges across the gap between the charged needle and the

electrically grounded target. As the field strength is increased the fibers experience greater stretching which results in decreased fiber diameter[33].

1.4.6 Collector Material and Tip-collector Distance

The type of material chosen for the grounded collector determines the degree of surface charge build up during the electrospinning process. It has been demonstrated that polymer fiber deposition during electrospinning is inversely proportional to the surface charge accumulation on the collector. Therefore a highly conducting collector plate is chosen to increase the density of the deposited electrospun fibers.

Tip-collector distance has a direct influence on jet flight time and electric field strength. Shortening the distance between the two electrodes causes an increase in the electrical strength between the needle and the collector, and accelerates the electrospinning process, thus reducing the time available for evaporation. Therefore, the resultant fibers may fuse due to presence of excess solvent to become an interconnected fiber mesh. Generally in the electrospinning process, increasing the collector distance decreases the fiber diameter. It has also been reported that increasing distance between the electrodes increases the average fiber diameter due to the reduced strength of the electric field[34].

1.4.7 Temperature and Humidity

Very few studies have been reported on the effect of temperature on electrospinning process and on fiber morphology. Increase in temperature causes the evaporation rate to increase[35]. Also increasing temperature lowers the viscosity of the solution thus producing higher stretching rate and thinner fibers.

The humidity of the electrospinning environment may have an influence on the polymer jet during electrospinning. Moisture may condense on the surface of the fiber when the process is carried out in a very humid environment. Condensation may significantly influence the fiber morphology; for example, circular pores can form on the fiber surfaces especially when polymers dissolved in volatile solvents are used. Researchers have reported that the size and depth of the circular pores increase with increasing humidity.

1.5 Morphologies of Electrospun Fibers

Electrospinning provides a possibility to produce nanofibers with different sizes and morphologies. A number of methods have been employed in different contexts to fabricate polymeric nanofibers with beaded, ribbon, porous, smooth and core-shell morphologies. A summary of different morphologies is given below.

1.5.1 Aligned Fibers

Electrospun fibers can be aligned by using a rotating cylinder as a collector plate. Fiber alignment depends upon the rotating speed of the collector relative to the rate of deposition[36,37]. Figure 1.4 B and C shows an example of aligned fibers of Nylon11 prepared from 20wt/vol% solution at the applied voltage of 20 kV and 10 cm between the electrodes.

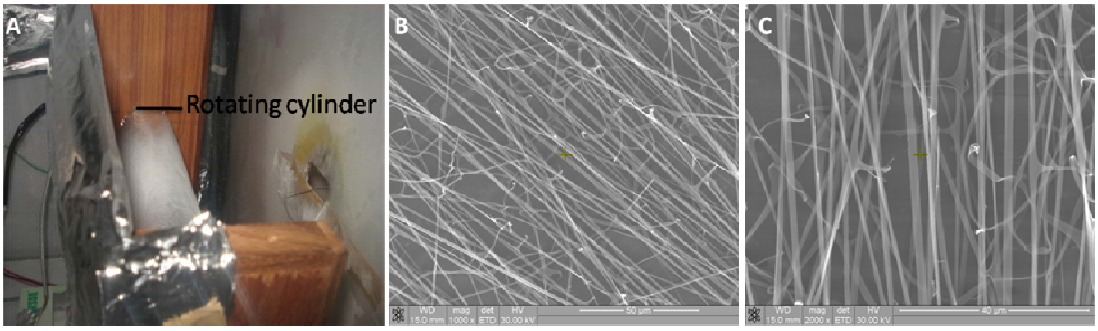

Figure 1.4 Rotating cylinder (A), Aligned electrospun fibers of Nylon11 at rotating speed of 1200 rpm (B and C) (M. Dhanalakshmi et al, unpublished work)

1.5.2 Porous Nanofibers

Fabrication of porous nanofibers through electrospinning increases the specific surface area of the fibers. Such porous nanofibers are in demand for a wide range of applications. Figure 1.5 shows porous electrospun fibers of polyhydroxybutyrate and polystyrene. The mechanism for the formation of porous fibers is phase separation. Highly porous nanofibers can be fabricated by rapid phase separation during the electrospinning process using a highly volatile solvent. The solvent vapor pressure has a critical influence on the process of pore formation. It has been reported that decreasing the vapour pressure of the solvent effectively reduces the pore formation[38]. Furthermore, porous nanofibers can be prepared by spinning of a blend of two different polymers. One of the polymers could be removed after fiber formation by selective dissolution in a solvent in which the other polymer is insoluble.

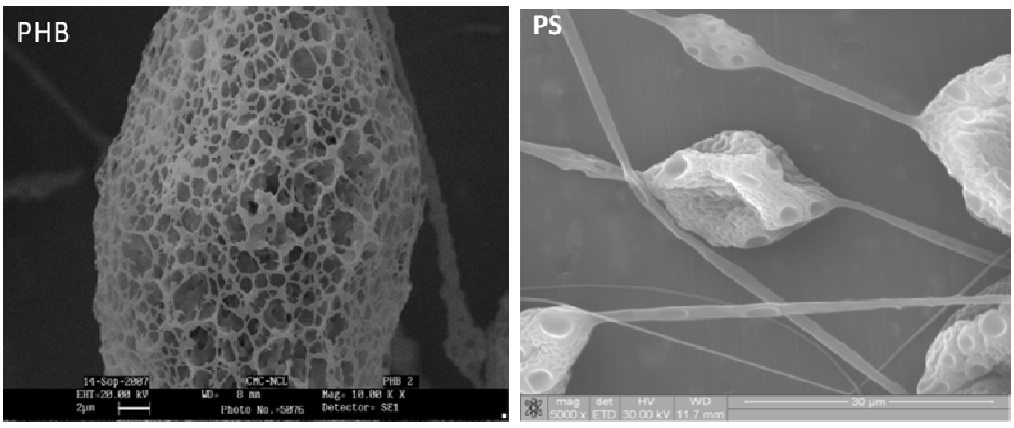

Figure 1.5 Electrospun porous fibers of polyhydroxybutyrate (PHB) prepared from 5wt/vol% solution in chloroform at the applied voltage of 15 kV and 10 cm collector distance (A). Polystyrene (PS) electrospun fiber was prepared from 10wt/vol% solution in tetrahydrofuran (THF) at the applied voltage of 20 kV and 10 cm distance between the electrodes (Prashant et al, unpublished work).

1.5.3 Branched Fibers

In electrospinning process, the charge per unit area carried by the jet can be changed by solvent evaporation and elongation of the jet during electrospinning. Difference between the surface tension and the electrical forces causes the shape of the jet to become unstable. This instability of the jet reduces its local charge per unit surface area by ejecting a smaller jet from the surface of the primary jet or by splitting apart into two smaller jets[39]. This results in the formation of branched fibers.

1.5.4 Nanofibers with Ribbon-like Morphology

Ribbon-like fibers can be obtained from several polymers under certain processing conditions. Figure 1.6 shows Nylon11 electrospun ribbon fibers. The mechanism of formation of ribbon-like fibers is related to the solvent evaporation at the jet surface during electrospinning process[40]. A thin polymer skin is formed on the surface of the electrospun jet with a liquid core. Thereafter, the skin undergoes an elastic buckling due to the critical pressure differential inside the ribbon. The circular cross section becomes elliptical and then flat, forming ribbon-like or flattened fibers. Recently, different polymers and composites have been used to create flattened or ribbon-like fibers using electrospinning technique with water and organic solvents.

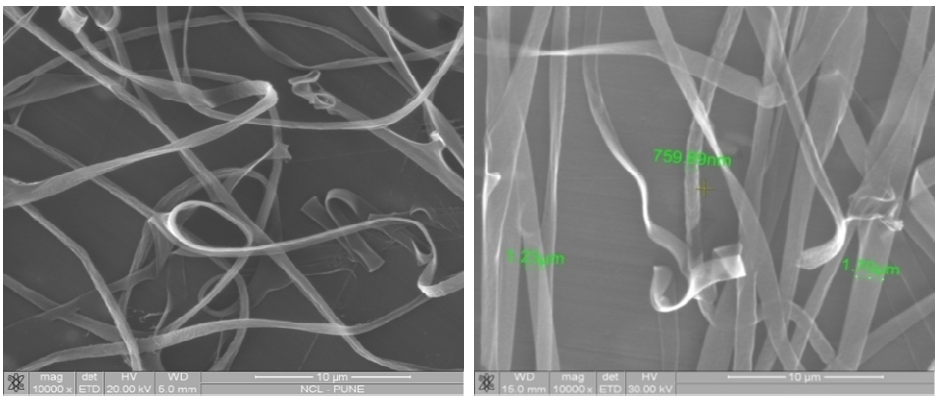

Figure 1.6 Nylon11 electrospun nanofibers with ribbon (flat) morphology prepared from 20wt/vol% at the applied voltage of 20 kV and 10 cm distance (M.Dhanalakshmi et al[41]; Reproduced with permission from Elsevier).

1.5.5 Core-shell Nanofibers

Core-shell fibers can be fabricated using two different polymeric components[42,43]. The co-axial electrospinning consists of a coaxial nozzle with a central tube surrounded by a concentric circular tube. The different polymer solutions are separately fed into the co-axial nozzle and ejected simultaneously. Core-shell structured fibers could enhance the material properties for various applications such microelectronics, optics and medicine. In addition, co-axial electrospinning offers the fabrication of hollow fibers and nanotubes using mineral oil as a core material and polymer or ceramic as a sheath material. After electrospinning, the mineral oil is removed to create hollow fibers or nanotubes.

1.5.6 Beaded Nanofibers

The formation of beads during electrospinning reduces the large surface area per unit mass of the obtained fibers. Therefore, beads are considered as a defect in the electrospinning process[44]. The mechanism of bead formation is related to the viscosity and surface tension of the polymer solution, and the net charge density carried by the polymer jet. The competition between surface tension, viscoelastic forces and electrical forces is the main reason of the bead formation. Basically, the surface tension of the polymer jet tries to decrease the surface area per unit volume, while the electric force tries to increase it. Higher surface tension leads to contraction of the radius of the jet and drives the jet towards the formation of beads. Decreasing solution viscosity and net charge density favors the formation of fibers having beads.

1.6 Applications of Electrospun Fibers

Electrospun fiber mats have wide applications in water filters, textiles, sound absorbing materials, and sensors for gas and other chemicals[45,46]. Figure 1.7 shows the diverse applications of electrospun fibers. The use of electrospun nanofibrous mats has also attracted a great deal of attention in biomedical applications. The most important feature of these nanofibrous mats which is exploited in biomedical applications is their ability to mimic extracellular mass (ECM). As a result, the mats are found suitable for biomedical applications such as wound dressing, scaffolds for artificial blood vessels, drug delivery carriers, cosmetics and skin masks.

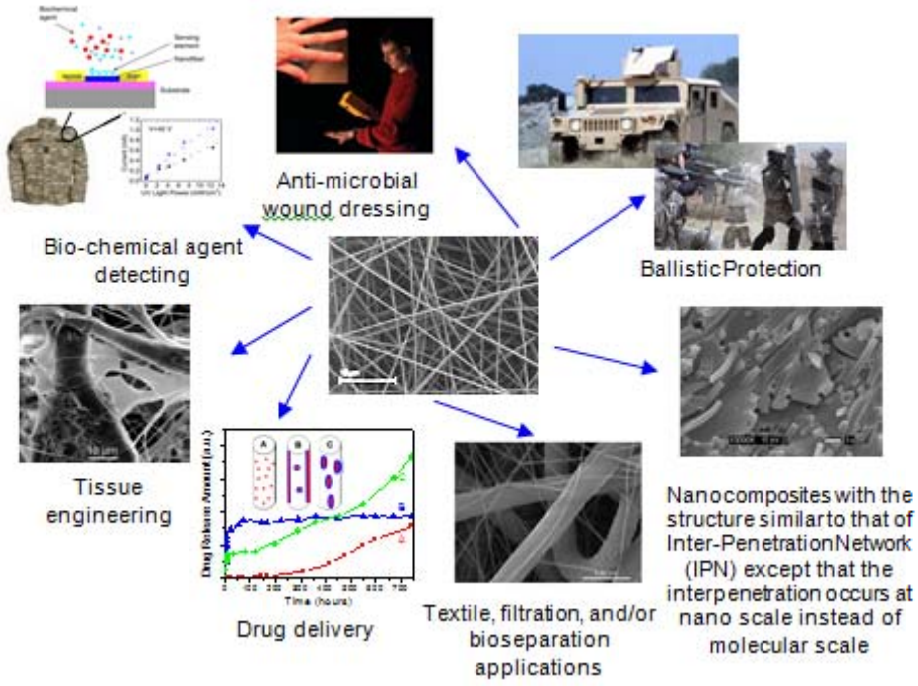

Figure 1.7 Various applications of electrospun fibers (source: http://webpages.sdsmt.edu/~hfong/research.htm).

1.7 Electrospinning of Nylon11

As mentioned earlier, a large number of natural and synthetic polymers have been used to prepare non-woven fibrous mats using the electrospinning process. However, one polymer that has not been tried extensively for this process is Nylon11. Nylon11 is biocompatible polymer prepared from (ω-amino undecanoic acid), which is obtained from castor bean oil. It is a polar polymer and exhibits piezoelectric and pyroelectric properties, low water absorption, good chemical resistance, high impact

strength at room and low temperatures and has the ability to accept high filler loadings[47]. It forms a crystalline phase in which the aliphatic chains are aligned in parallel, while the amide group dipoles are oriented perpendicular to the chain direction. Nylon11 is used in high-performance applications such as automotive fuel lines, pneumatic airbrake tubing, electrical anti-termite cable sheathing, oil and gas flexible pipes, sports shoes, electronic device components and catheters. In the present work we have extensively investigated the electrospinning of Nylon11.

1.7.1 Previous Work Done on Electrospinning of Nylon11

The electrospinning of Nylon11 was first demonstrated by Kris Beher etal in 2007. They used mixed solvent of formic acid and dichloro methane (DCM) in 1:1 ratio[48]. The electrospinning processing conditions were 20 kV applied voltage and distance of 10 cm between the electrodes. The concentrations were varied from 2-10 %. For 2 % concentration fibers, cylinder shaped fibers with 130 nm diameter were formed. Solutions of concentration less than 2 % could not form fibers. By increasing the polymer concentration to 5 %, ribbons were formed. The width of the ribbons was approximately 1 μm. Further increasing the concentration to 10 % resulted in formation of larger size ribbons of 2-20 μm width. The crystallinity of Nylon11 electrospun mats was found to be higher than the Nylon11 pellets. Raman spectra showed no significant difference in bulk and electrospun fibers.

M. Dhanalakshmi and Jog in 2008 reported electrospinning of Nylon11[49]. Formic acid was used as a solvent for Nylon11 electrospinning. Solution of 10 and 20wt/vol% concentrations were used for electrospinning and corresponding solution cast films also prepared for comparative study. SEM images showed that the solution of 10wt/vol% concentration formed circular fibers with diameter of around 200 nm. At higher concentration (20wt/vol%) ribbons were formed having width of 800 nm. XRD study showed that Nylon11 pellets and solution cast films have α crystalline structure, whereas Nylon11 electrospun mat exhibited γ crystalline structure. Thus the electrospinning process changed the crystalline structure of Nylon11. The electrospun mats were found to have lower crystallinity than the corresponding solution cast films.

Recently, structure-induced enhancement of thermal conductivities in Nylon11 electrospun mats was studied by Zhenxin etal[50]. 1,1,1,3,3,3-hexafluoro-2-propanol (HFIP) was used as a solvent for Nylon11 electrospinning. Concentration was varied

from 2- 12.5 %. A novel high – sensitivity micro-device platform was employed to determine the axial thermal conductivity of individual Nylon11 nanofibers fabricated by electrospinning and post stretching. Their thermal conductivity showed a correlation with the crystalline morphology measured by high resolution wide angle X-ray scattering.

1.7.2 Previous Work Done on Nylon11 Blends

Nylon11/Polypropylene melt blends[51] were studied by K.K Seth and C.J.E Kempster in 1977. They showed that addition of small amounts of Nylon11 produces bimodal crystal texture in polypropylene with most crystallites having either their c-axis or a-axis oriented parallel to the fiber axis. Maleic anhydride (MA) modified PP copolymer with Nylon11 blends were investigated by Bing Lu and T.C. Chung in 1999. They found that higher MA concentration results in poor blend morphologies[52]. Mechanical properties and morphologies of Nylon11/Ethylene-Octene copolymer blends were investigated by Qi Fang Li etal in 2003. The Ethylene-Octene copolymer (POE) was grafted with maleic anhydride (MAH) to increase the compatibility with Nylon11[53]. The mechanical properties and morphology of Nylon11 blended with POE depended on the MAH ratio. The tensile strength of the blends was lower than the pure Nylon11.

Crystallization of Nylon11/ Poly (vinylidene fluoride) blends was studied by Qiong and Scheinbeim in 2003. The existence of separate melting and crystallization temperature over the whole composition range showed that these two polymers did not co-crystallize[54]. However blending affected the crystallization behavior of each component. In 2003 another report on Nylon11/ Poly (vinylidene fluoride) blends was published by Yongjin Li and Akira Kaito. Blends were prepared by uniaxially stretching the melt blends[55].

Guosheng etal in 2004 investigated effect of the maleated ethylene – propylene-diene copolymer (EPDM-MAH) as a compatibilizer on Nylon11/Polyethylene blends[56]. They studied the morphology and mechanical properties of the blends. Ping-Chung Kuo etal in 2006 studied properties and biodegradability of Chitosan/Nylon11 blends[57]. Different ratios of Nylon11/chitosan blending films were prepared by solution casting method. The strength of the hydrogen bonds in the blended film weakened after addition of chitosan, and

spherulite growth was restricted as the ratio of chitosan increased. Biodegradability of Nylon11/Chitosan blended films was strongly affected by the addition of Chitosan.

Nylon11/Ethylene-vinyl alcohol (EVOH)/Dicumyl peroxide (DCP) melt blends were reported by Biaobing etal in 2008[58]. The melting behavior and crystallization kinetics were investigated using DSC. In 2012 Guo Yunxia et al reported Nylon11/Polyethylene-octene melt blends. Maleic anhydride was grafted with polyethylene-octene to increase the compatibility of blends[59]. In 2013 Wenyong etal studied melt compounded Poly(L-lactide) (PLLA)/ Nylon11 blends with small amount of rubber, ethylene glycidyl methacrylate-graft- styrene- co- acrylonitrile[60]. Brittle–to tough transition was observed on increasing the rubber sub–inclusion concentration in the PLLA phase.

1.8. References

1. Lai, K., Jiang, W., Tang, T. Z., Wu, Y., He, B., Wang, G. and Gu, Z. Superparamagnetic nano-composites scaffolds for promoting bone cell proliferation and defect reparation without a magnetic field. RSC Advances 2, 13007–13017 (2012).

2. Jun, F., Gwan, T. and Sung, D. A facile preparation of highly interconnected macroporous poly (D, L -lactic acid- co -glycolic acid) (PLGA) scaffolds by liquid – liquid phase separation of a PLGA – dioxane – water ternary system. Polymer 44, 1911–1920 (2003).

3. Yang, X., Chen, X. and Wang, H. Acceleration of osteogenic differentiation of preosteoblastic cells by chitosan containing canofibrous scaffolds. Biomacromolecules 10, 2772–2778 (2009).

4. Li, X., Zhang, Y. and Chen, G. Biomaterials nanofibrous polyhydroxyalkanoate matrices as cell growth supporting materials. Biomaterials 29, 3720–3728 (2008).

5. Taylor, P., Duan, Y., Wang, Z., Yan, W. and Wang, S. Preparation of collagen-coated electrospun nanofibers by remote plasma treatment and their biological properties. Journal of Biomaterials Science Polymer Edition 18, 1153–1164 (2012).

6. Zhou, Y., Yang, D., Chen, X., Xu, Q. and Lu, F. Electrospun water-soluble carboxyethyl chitosan/Poly (vinyl alcohol) nanofibrous membrane as potential wound dressing for skin regeneration. Biomacromolecules 9, 349–354 (2008).

7. Taboas, J. M., Maddox, R. D., Krebsbach, P. H. and Hollister, S. J., Indirect solid free form fabrication of local and global porous, biomimetic and composite 3D polymer-ceramic scaffolds. Biomaterials 24, 181–194 (2003).

8. Sin, D., Miao, X., Liu, G., Wei, F., Chadwick, G. Yan, C. and Friis, T. Polyurethane (PU) scaffolds prepared by solvent casting/particulate leaching (SCPL) combined with centrifugation. Materials Science and Engineering 30, 1-11 (2010).

9. Suzuki, A. and Hayashi, H. Ethylene tetrafluoroethylene nanofibers prepared by CO_2 laser supersonic drawing. eXPRESS Polymer Letter 7, 519–527 (2013).

10. Hulteen, J. C. and Martin, C. R. A general template-based method for the preparation of nanomaterials. Journal of Materials Chemistry 7, 1075–1087 (1997).

11. Do, H., Hee, E., Chan, I., Ramsurat, R., Do, J. and Lee, D.S. Effect of PEG – PLLA diblock copolymer on macroporous PLLA scaffolds by thermally induced phase separation. Biomaterials 25, 2319–2329 (2004).

12. Zhang, S., Gelain, F. and Zhao, X. Designer self-assembling peptide nanofiber scaffolds for 3D tissue cell cultures. Seminars in Cancer Biology 15, 413–420 (2005).

13. Lv, Q. and Feng, Q. Preparation of 3-D regenerated fibroin scaffolds with freeze drying method and freeze drying/foaming technique. Journal of Materials Science: Materials in Medicine 17, 1349–1356 (2006).

14. Fong, H., Liu, W., Wang, C. and Vaia, R. A. Generation of electrospun fibers of nylon 6 and nylon 6-montmorillonite nanocomposite. Polymer 43, 775–780 (2002).

15. Huang, Z., Zhang, Y., Kotaki, M. and Ramakrishna, S. A review on polymer nanofibers by electrospinning and their applications in nanocomposites. Composites Science and Technology 63, 2223–2253 (2003).

16. Yeo, M., Lee, H. and Kim, G. Three-dimensional hierarchical composite scaffolds consisting of polycaprolactone, β-tricalcium phosphate, and collagen nanofibers : fabrication, Physical properties, and in vitro cell activity for bone tissue regeneration. Biomacromolecules 12, 502–510 (2011).

17. Alvarez-perez, M. A., Guarino, V., Cirillo, V. and Ambrosio, L. Influence of gelatin cues in PCL electrospun membranes on nerve outgrowth. Biomacromolecules 11, 2238–2246 (2010).

18. Xie, J., Macewan, M. R., Schwartz, A. G. and Xia, Y. Electrospun nanofibers for neural tissue engineering. Nanoscale 2, 35–44 (2010).

19. Wang, W., Itoh, S., Konno, K., Kikkawa, T., Ichinose, S., Sakai, K., Ohkuma, T. and Watabe, K. Effects of Schwann cell alignment along the oriented electrospun chitosan nanofibers on nerve regeneration. Journal of Biomedical Materials Research Part A 994–1005 (2008).

20. Bhattarai, N., Edmondson, D., Veiseh, O., Matsen, F. A. and Zhang, M. Electrospun chitosan-based nanofibers and their cellular compatibility. Biomaterials 26, 6176–6184 (2005).

21. Antoine, J. and Nollet, A. Investigations on the causes for the ebullition of liquids. Journal of Membrane Science 100, 1–3 (1995).

22. J.F.Cooley. Apparatus for electrically dispersing fluids. Patent, US 692631 A (1902).

23. W.J.Morton. Methos of dispersing fluids. Patent No.705, 691 (1902).

24. Taylor, G. Disintegration of water drops in an electric field. Proceeding of the Royal Society of London. Series A, Mathematical and Physical Sciences 280, 383–397 (1964).

25. Luo, C. J., Stoyanov, S. D., Stride, E., Pelan, E. and Edirisinghe, M. Electrospinning versus fibre production methods: From specifics to technological convergence. Chemical Society Reviews 41, 4708–35 (2012).

26. Rutledge, G. C. and Fridrikh, S. V. Formation of fibers by electrospinning. Advanced Drug Delivery Reviews 59, 1384–1391 (2007).

27 Ziabari, M., Mottaghitalab, V. and Haghi, A. K. Application of direct tracking method for measuring electrospun nanofiber diameter. Brazilian Journal of Chemical Engineering 26, 53-62 (2009).

28. Chowdhury, M. and Stylios, G. Effect of experimental parameters on the morphology of electrospun Nylon6 fibres. International Journal of Basic and Applied Sciences 10, 70–78 (2010).

29. Tan, S.-H., Inai, R., Kotaki, M. and Ramakrishna, S. Systematic parameter study for ultra-fine fiber fabrication via electrospinning process. Polymer 46, 6128–6134 (2005).

30. Zong, X., Kim, K., Fang, D., Ran, S, Hsiao, B.S. and Chu, B. Structure and process relationship of electrospun bioabsorbable nanofiber membranes. Polymer 43, 4403–4412 (2002).

31. Du, J., Shintay, S. and Zhang, X. Diameter control of electrospun polyacrylonitrile/Iron acetylacetonate ultrafine nanofibers. Journal of Polymer Science: Part B: Polymer Physics 46, 1611–1618 (2008).

32. Milleret, V., Simona, B., Neuenschwander, P. and Hall, H. Tuning electrospinning parameters for production of 3D-fiber-fleeces with increased porosity for soft tissue engineering applications. European Cells and Materials 21, 286–303 (2011).

33. Deitzel, J. M., Kleinmeyer, J., Harris, D. and Tan, N. C. B. Processing variables on the morphology of electrospun nanofibers and textiles. Polymer 42, 261–272 (2001).

34. Henriques, C., Vidinha, R., Botequim, D., Borges, J. P. and Silva, J. A. M. C. A systematic study of solution and processing parameters on nanofiber morphology using a new electrospinning apparatus. Journal of Nanoscience and Nanotechnology 8, 1–11 (2008).

35. Camp, T. Van, Nelvig, A., B.Hagstrom, P.Westbroek and Clerck, K. D. The effect of temperature and humidity on electrospinning. Journal of Materials Science 44, 1357–1362 (2009).

36 Milleret, V., Simona, B., Neuenschwander, P. and Hall, H. Tuning electrospinning parameters for production of 3D-fiber-fleeces with increased

porosity for soft tissue engineering applications. European Cells and Materials 21, 286–303 (2011).

37 Chem, J. M., Zhong, W., Li, F., Chen, L. and Wei, Y. A novel approach to electrospinning of pristine and aligned MEH-PPV using. Journal of Materials Chemistry 22, 5523–5530 (2012).

38 Lu, P. and Xia, Y. Maneuvering the internal porosity and surface morphology of electrospun polystyrene yarns by controlling the solvent and relative humidity. Langmuir 29, 7070–7078 (2013).

39. Yarin, A. L., Kataphinan, W. and Reneker, D. H. Branching in electrospinning of nanofibers Branching in electrospinning of nanofibers. Journal of Applied Physics 98, 6501–6512 (2006).

40 Koombhongse, S., Liu, W. and Reneker, D. H. Flat polymer ribbons and other shapes by electrospinning. Journal of Polymer Science: Part B: Polymer Physics 39, 2598–2606 (2001).

41. Dhanalakshmi, M., Lele A. K. and Jog, J. P. Electrospinning of Nylon11: Effect of processing parameters on morphology and microstructure. Materials Today Communications (2015). DOI: 10.016/j. mtcomm. 2015.01. 002.

42. Wang, C., Yan, K., Lin, Y. and Hsieh, P. C. H. Biodegradable core/shell fibers by coaxial electrospinning□: Processing, fiber characterization, and Its application insustained drug release. Macromolecules 43, 6389–6397 (2010).

43. Li, S., Sun, B., Li, X. and Yuan, X. Characterization of electrospun core/shell poly (vinyl pyrrolidone)/poly(L-lactide-co- ε-caprolactone) fibrous membranes and their cytocompatibility in vitro. Journal of Biomaterials Science Polymer Edition 19, 245–258 (2008).

44 Cheng, M., Lin, C., Su, H., Chen, P. and Sun, Y. Processing and characterization of electrospun nanofibrous membranes. Polymer 49, 546–553 (2008).

45. Kadir, R.A., Li, Z., Sadek, A.Z., Rani, R.A., Field, M.R., Ou, J.Z., Chrimes, A.F. and Kalantar-Zadeh, K. Electrospun granular hollow SnO_2 nano fibers hydrogen gas sensors operating at low temperatures. The Journal of Physical Chemistry C 118, 3129–3139 (2014).

46. Hogan, C. J., Matsubayashi, Y., Kawabe, M., Iskandar, F. and Okuyama, K. Nanoparticle filtration by electrospun polymer fibers. Chemical Engineering Science 62, 4751–4759 (2007).

47. Kuo, P., Sahu, D. and Her, H. Properties and biodegradability of chitosan/nylon11 blending films. Polymer Degradation and Stability 91, 3097–3102 (2006).

48. Behler, K., Havel, M. and Gogotsi, Y. New solvent for polyamides and its application to the electrospinning of polyamides11 and 12. Polymer 48, 6617–6621 (2007).

49. Dhanalakshmi, M. and Jog, J. P. Preparation and characterization of electrospun fibers of Nylon11. eXPRESS Polymer Letter 2, 540–545 (2008).

50. Zhong, Z., Wingert, M. C., Strzalka, J. and Wang, H. Structure-induced enhancement of thermal conductivities in electrospun polymer nano fibers. Nanoscale 6, 8283–8291 (2014).

51. Seth, K. K. and Kempster, C. J. E. Observations of trimodal crystal texture in Polypropylene blended with Nylon11. Journal of Polymer Science: Polymer Symposium 310, 297–310 (1977).

52. Lu, B. and Chung, T. C. New maleic anhydride modified PP copolymers with block structure□: synthesis and application in PP/polyamide reactive blends. Macromolecules 32, 2525–2533 (1999).

53. Li, Q. F., Kim, D. G., Wu, D. Z., Lu, K. and Jin, R. G. Effect of maleic anhydride graft ratio on mechanical properties and morphology of Nylon Il/Ethylene-octene copolymer blends. Polymer Engineering and Science 41, 2155–2161 (2001).

54. Gao, Q. and Cheinbeim, J. S. Crystallization studies of polymer blends of Nylon-11/poly (vinylidene fluoride). Polymer Journal 35, 345–352 (2003).

55. Li, Y. and Kaito, A. Crystallization and orientation behaviors of poly (vinylidene fluoride) in the oriented blend with nylon 11. Polymer 44, 8167–8176 (2003).

56. Hu, G., Wang, B. and Zhou, X. Effect of EPDM-MAH compatibilizer on the mechanical properties and morphology of nylon11/PE blends. Materials Letters 58, 3457–3460 (2004).

57. Kuo, P., Sahu, D. and Her, H. Properties and biodegradability of chitosan/nylon11 blending films. Polymer Degradation and Stability 91, 3097–3102 (2006).

58. Wang, B., Ding, Z. and Hu, G. Melting behavior and isothermal crystallization kinetics of Nylon 11/ EVOH / Dicumyl peroxide blends. Polymer Engineering and Science 2354–2361 (2008).

59. Yunxia, G. U. O., Guosheng, H. U., Zhiqiang, W., Yingchun, L. I. and Yunfeng, Y. Isothermal crystallization kinetics and melting behavior of POE-g-MAH compatibilized PA11/POE blends. Journal of Wuhan University of Technology Mater. Sci. Ed. 27, 702–707

60. Dong, W., Cao, X. and Li, Y. High-performance biosourced poly (lactic acid)/ polyamide11 blends with controlled salami structure. Polymer International 63, 1094–1100 (2013).

Chapter 2

Objectives

2 Objectives

As mentioned in chapter 1, Nylon11 is a commercially available biocompatible polymer; but it has not been explored much for making scaffolds for cell culture and tissue engineering. In this work we have investigated the electrospinning of Nylon11 into non-woven mats which could be used for cell culture. Literature review summarized in chapter 1 has revealed that electrospinning of Nylon11 has not been studied in detail. Further, no research has been conducted for modifying the electrospun Nylon11 mats so as to make them suitable for cell culture application. Based on these facts, there are three main research objectives of the present work listed below.

1. The first objective was to prepare nonwoven electrospun mats of Nylon11 and study the effect of processing variables on the fiber diameter and morphology of mats.
2. The second objective was surface modification of Nylon11 electrospun mat, so as to make the mat hydrophilic and suitable for cell culture.
3. The third objective was to explore the electrospinning of Nylon11/PHB blends and nanocomposites.

2.1 Study of Electrospinning of Nylon11

The purpose of this part of the work is to study the effect of electrospinning process variables on the size of the nanofibers, their properties and the morphology of the mat. A potential utility of such a study would be to optimize process parameters to make mats of desired morphology and porosity.

2.2. Surface modification of Nylon11 electrospun mat

Nylon11 is a hydrophobic polymer. In order to use the Nylon11 electrospun mats in cell culture studies, it is required to make them hydrophilic and suitable for growing cells. In this work, two surface modification techniques have been used to convert hydrophobic Nylon11 electrospun mats to hydrophilic mats. The first surface modification was plasma treatment, which is a conventional surface treatment method that also creates surface roughness. In the second method, the plasma treatment method was followed by attachment of gold nanoparticles on the electrospun mat. A further objective of this study was to measure the longevity of the surface treatment methods by measuring contact angle as a function of aging time.

2.3. Nylon11 blends and nanocomposites

The third objective of this study was to explore the electrospinning of Nylon11 blends and nanocomposites, especially using biodegradable and /or biocompatible polymers and nanoparticles. A potential utility of such mats would be control on biodegradability time and mechanical properties, both of which are useful properties of scaffolds. Accordingly, electrospun mats of Nylon11/polyhydroxybutyrate and Nylon11/Zinc Oxide nanoparticles were prepared and their structure and properties were studied using a variety of characterization techniques.

Chapter 3

Electrospinning of Nylon11: Effect of Process Parameters on Morphology and Structure of Mats

In this chapter we have described the processing, characterization and cell culture application of electrospun non-woven nanofibers mats of Nylon11. Among the electrospinning process parameters, we have investigated the effects of solution concentration, applied voltage and distance between the electrodes on the diameter and shape of the nanofibers. The Nylon11 electrospun mats were further characterized using Scanning Electron Microscopy (SEM), X-Ray Diffraction (XRD), Dynamic Mechanical Analysis (DMTA), Dielectric Relaxation Spectroscopy (DERS), Differential Scanning Calorimetry (DSC) and Contact Angle Measurement (CA). The properties of these mats were compared with those of melt pressed and solution cast films of Nylon11. We have also carried out comparative cell culture studies using the HEK293 cells on these films and electrospun mats.

3.1 Introduction

In chapter 1 the electrospinning process was described in detail. We provide below a brief summary of the process before describing in detail the work done on electrospinning of Nylon11.

Electrospinning is a cost effective approach for fabrication of polymer fiber mats. It provides a simple route to fabricate fibers with diameters ranging from nanometer to micrometers. The advantage of these fibers is the huge increase in the surface area to volume ratio. A wide variety of polymers, ceramics and metal oxides have been electrospun. Electrospinning results in sub-micron polymer fibers that are produced using an electro-statically driven jet of polymer solution or polymer melt. Processing parameters affect the fiber formation and consequently the fiber diameter. Several researchers have studied the effect of electrospinning process variables for different polymers dissolved in different solvents[1–3]. Parameters such as concentration, viscosity and conductivity of the solution, applied voltage, flow rate and distance between the two electrodes affect the fiber morphology. In general, an increase in the concentration of the solution increases the fiber size[4,5], an increase in the applied voltage decreases the size of the fiber[6] and an increase in the distance between the electrodes reduces the fiber size[7]. Temperature, humidity and surface tension of the solution also play an important role in the electrospinning process. Electrospun fibrous mats find wide applications in water filters[8], textiles, sound absorbing materials[9], sensing of gas and other chemicals[10] and more recently as scaffolds in tissue engineering applications[11,12].

Tissue engineering is an interesting and emerging field. The main requirements of scaffold used for tissue engineering applications are biocompatibility, biodegradability, 3-dimensional structure, mechanical strength and interconnected porosity. Several different fabrication methods such as solution casting[13], freeze drying[14] and template synthesis[15] can be used to fabricate polymer scaffolds. Scaffolds made from electrospun non-woven mats have many advantages compared to scaffolds made from these fabrication methods. Some of the important advantages are high surface area, porosity and 3-D environment[16]. These characteristics are important for cells to adhere and grow. Process parameters of electrospinning can be easily tuned to make nonwoven mats with structural features similar to that of the native tissue.

Natural polymers such as collagen, chitosan, gelatin and silk fibroin have been used as scaffolds for tissue engineering application due to their biocompatibility and

biodegradability. The main drawbacks of natural polymeric scaffolds are poor mechanical strength and batch-to-batch variation. To overcome this problem, biocompatible and biodegradable synthetic polymers like polylactic acid (PLA), polyhydroxybutyrate (PHB), polycaprolactone (PCL), polyvinyl alcohol (PVA) and polyurethane (PU) have been used[17–21].

As mentioned in chapter 1, Nylon11 is a bioderived and biocompatible high performance semicrystalline polymer. The crystalline structure and polymorphism of Nylon11 have been studied by several researchers[22-25]. Nylon11 has low water absorption compared to other Nylons.

Inspite of these advantages, there is limited evidence for use of Nylon11 electrospun mats for biomedical applications. Thus, it is an objective of this work to fabricate electrospun mats using a solution of Nylon11 in formic acid and correlate the morphology of these electrospun mats with the parameters used in the electrospinning process. A second objective of this work is to compare the physical properties of Nylon11 electrospun mats with melt pressed and solution cast Nylon11 films. Finally the electrospun mats have been evaluated for cell culture studies.

3.2 Materials and Methods

3.2.1 Materials

Nylon11 pellets were purchased from Sigma Aldrich Chemicals. Formic acid was procured from Merck, India. MTT assay kit, Dulbecco's Modified Eagle Medium (DMEM), Fetal Bovine Serum (FBS) and Trypsin were purchased from Sigma Aldrich Chemicals. All chemicals were used as received without any further purification.

3.2.2 Preparation of Nylon11 Solution Cast and Melt Pressed Films

Solution cast films were prepared by slow evaporation of the solvent at room temperature for 24 hrs. For comparative study, melt pressed film were also prepared from Nylon11 pellets. A laboratory compression press was used for making Nylon11 melt pressed film. The temperature was set at 220 °C and the applied pressure was 150 psi (holding time 5 min). After hot pressing, the film was cooled slowly. The approximate thickness of the Nylon11 solution cast and melt pressed films were 0.5 mm. These Nylon11 films were used for the further characterization.

3.2.3 Electrospinning Process

5-20 wt/vol% solutions of Nylon11 in formic acid were used for electrospinning. The solutions were prepared in a constant temperature bath at 70 °C under constant stirring for 2 hr. A custom-built horizontal laboratory scale electrospinning apparatus was used for all electrospinning experiments. The set-up consists of a high voltage supply (0-40 kV) from Gamma Corporation, USA, a syringe pump from Sage Instruments (Model 351, flow rate capacity of 0.0015 to 60 ml/min) and a ground collector located inside a closed chamber. A 10 ml plastic syringe and a stainless needle of 0.8 mm diameter bore were used. The electrospinning setup and the envelope cone obtained in electrospinning of Nylon11 are shown in Figure 3.1.A and Figure 3.1.B.

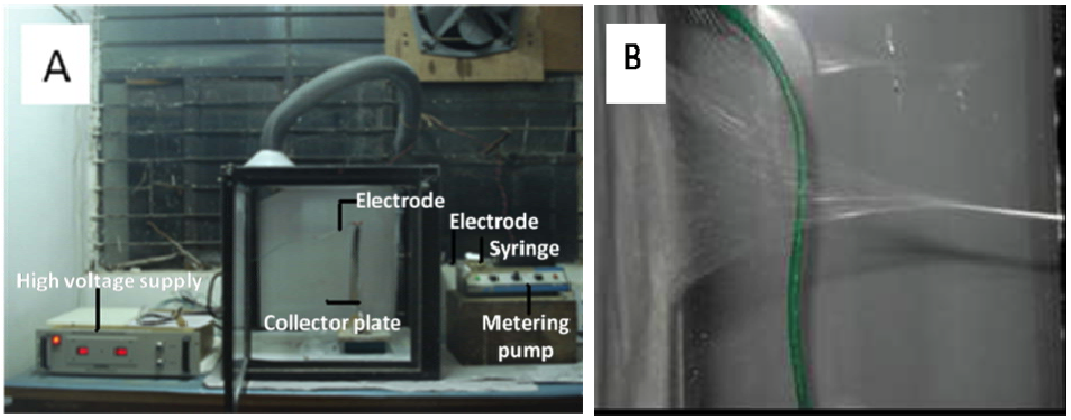

Figure 3.1 Electrospinning setup (A) and envelope cone (B) of Nylon11 during electrospinning process.

For cell culture and water contact angle studies, 20 mm diameter circular cover slips were pasted on the collector plate. Fibers were collected on the glass cover slips. Once electrospinning was done, the cover slips were removed from the collector plate and used for further studies.

Electrospinning was done at the following conditions:

Concentration =5-20 wt/vol%

Voltage = 5-20 kV.

Flow rate = 0.1 ml/min.

Distance between the electrodes = 5-15 cm.

Electrospinning process was carried out at room temperature. The approximate thickness of the electrospun mat was 0.1 mm.

3.2.4 Scanning Electron Microscopy Analysis (SEM)

The morphology of Nylon11 electrospun fibers was studied by using Leica-440 Scanning Electron Microscope operated at 20 kV. Electrospun mats were directly mounted on the SEM sample holder and the micrographs of representative areas were recorded at different magnifications. The sample surfaces were coated with gold to avoid specimen charging.

3.2.5 Measurement of Fiber Diameter

The detail protocol used for measuring fiber diameter is described below for a representative electrospinning experiment in which a Nylon11 20wt/vol% solution was electrospun at an applied voltage of 20 kV, with the distance between the electrodes maintained at 10 cm and a flow rate of 0.1 ml/min.

Electrospinning was performed at least thrice per concentration. Each time a fresh 20wt/vol% solution was prepared. SEM micrographs were obtained at different locations on the mats. The diameters of approximately 300 fibers were measured using Image J software for each process parameter study. Figure 3.2 A shows a representative SEM image opened in Image J along with diameters of several fibers marked on it. The histogram produced after measurement of about 300 such fibers from multiple SEM images is also shown in Figure 3.2 B.

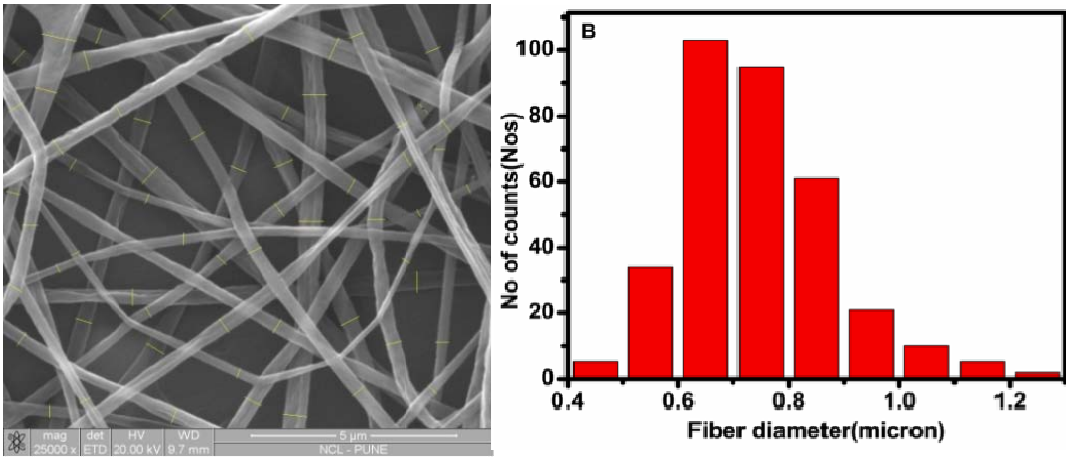

Figure 3.2 Electrospun fiber diameter (A) and histogram (B) of Nylon11 20wt/vol% electrospun mat measured using Image J (Scale bar = 5 microns). The average fiber diameter was 730±17 nm.

3.2.6 Measurement of Viscosity and Conductivity

Viscosity measurements were performed with MCR 301 Rheometer (Anton Paar, Austria) using a cup and bob fixture inserted in a Peltier environmental system maintained at 25 °C. A shear rate ramp experiment was carried out over the shear rate range of 1 to 1000 s^{-1}. Conductivities of formic acid and Nylon11 solutions were measured using Mettler Toledo conductivity meter at room temperature.

3.2.7 X-Ray Diffraction Analysis (XRD)

Crystalline structures of the Nylon11 samples were characterized using a Rigaku Model Dmax 2500 X-ray diffractometer with Cu/K_α radiation, operating at 40 kV and 100 mA. The samples were scanned over the 2θ range of 10-40 °. Nylon11 melt pressed films, solution cast films made from 5-20wt/vol% solutions and electrospun mats prepared from 5-20wt/vol% solution at applied voltage of 20 kV and 10 cm distance between the electrodes were used for XRD.

3.2.8 Differential Scanning Calorimetry (DSC)

DSC studies of Nylon11 melt pressed film, solution cast film and electrospun fibers (20 kV, 10 cm, 0.1 ml/min) were performed on Differential Scanning Calorimeter (DSC-Q100, TA Instrument) with temperature ranging from 0-230 °C and at heating and cooling rates of 10 °C/min. The tests were carried out in Nitrogen atmosphere. The melting point of polymer (T_m), crystallization temperature (T_c) and % crystallinity of electrospun polymer were determined from the first heating and cooling respectively.

3.2.9 Dynamic Mechanical Thermal Analysis (DMTA)

The viscoelastic properties of Nylon11 samples were measured using Dynamic Mechanical Thermal Analysis (Rheometric Scientific Inc. model IIIE). Rectangular tension-compression geometry was used. The test was carried out in linear viscoelastic region over the temperature range of -100 °C to 120 °C at a constant frequency of 10 rad/s with 0.02 % strain. Nylon11 melt pressed film, solution cast films (20wt/vol%) and electrospun mats (prepared from 20wt/vol% solution, applied voltage 20 kV, distance 10 cm and flow rate 0.1 ml/min) were used for DMTA studies.

3.2.10 Dielectric Relaxation Spectroscopy Analysis (DERS)

Dielectric frequency response measurement of Nylon11 samples were done using Nova control broad band dielectric spectrometer with the ZGS active sample cell equipped with a temperature controller. The tan delta response of the material in the frequency range of 10^{-4} Hz to 10^{4} Hz and temperature range of 30 to165 °C was measured by placing a 20 mm disk sample between two 20 mm gold plated electrodes. Quick drying silver paste was applied to ensure good electrical contact. In case of Nylon11 electrospun mats and solution cast films, an aluminum foil was used for ensuring good electrical contact. Nylon11 20wt/vol% electrospun mats for DERS measurement were prepared using a voltage of 20 kV, distance of 10 cm between the electrode and flow rate of 0.1 ml/min.

3.2.11 Contact Angle Measurement (CA)

Water contact angle measurement was performed by using contact angle instrument (Digidrop Instrument- Rame-Hart 100 Goniometer GBX). Deionized water was used to measure the contact angle of the Nylon11 scaffolds. Water contact angle measurement results reported here are the averages of 6 independent measurements. Nylon11 melt pressed film and electrospun fibrous mats were used for contact angle measurement analysis.

3.2.12 Cell Culture Study

A) Morphological Study

Nylon11 melt pressed film and Nylon11 20wt/vol% electrospun mats were sterilized by autoclaving for 2 hrs at 120 °C at a pressure of 15 psi. After sterilization, Nylon11 scaffolds were placed in a 24 well plate in 1 ml DMEM media with 10 % FBS. Approximately $3x10^{4}$ HEK293 cells were inoculated on each Nylon11 scaffold and the cell culture plate was used as control. Cells were incubated at 37 °C at 5% CO_2 for 5 days. HEK293 cells on the Nylon11 scaffolds were observed under a Leica-440 Scanning Electron Microscope after fixation with 2 % formaldehyde and 0.2 % gluteraldehyde in phosphate buffered saline (PBS). The microscope was operated at 20 kV and the micrographs were recorded at different magnifications.

B) Cell Proliferation Assay (MTT assay)

An MTT assay was performed on the Nylon11 cultured scaffolds at regular intervals to monitor cell proliferation. After 2 days of cell inoculation on Nylon11 scaffolds, the substrates were removed and shifted to a new well and washed with PBS to remove non adherent cells and spent media. 600 µl of fresh medium without phenol red and 60 µl of MTT [3-(4,5-dimethylthiazoyl-2-yl)-2,5-diphenyltetrazolium bromide were added to the Nylon11 scaffolds and incubated for 4 hrs at 37 °C under 5% CO_2. The mitochondrial succinate dehydrogenase converts MTT into a deep purple colored formazan compound, and the amount of formazone produced directly correlates with the number of viable cells present. Formazone was dissolved in 600 µl DMSO (dimethyl sulfoxide). The absorbance at 550 nm was measured. The same procedure was repeated on 3^{rd}, 5^{th}, 8^{th} and 10^{th}day after inoculation of cells on the Nylon11 scaffolds. All experiments were carried out in triplicate.

3.3 Results and Discussion

3.3.1 Viscosity of the Nylon11 Solution

Nylon11 solutions in formic acid were prepared at varying concentrations for the electrospinning experiments. These solutions were characterized for their viscosity and conductivity. Figure 3.3 A depicts the change in viscosity for change in concentration of Nylon11 formic acid solutions. Viscosity increases from 0.009 Pa.s at 5wt/vo% to 0.29 Pa.s at 20wt/vol%. The data show a scaling of $\eta \propto c^{2.4}$ as shown in Figure 3.3 B. This exponent suggests that the polymer solution is in the semi-dilute regime[26].

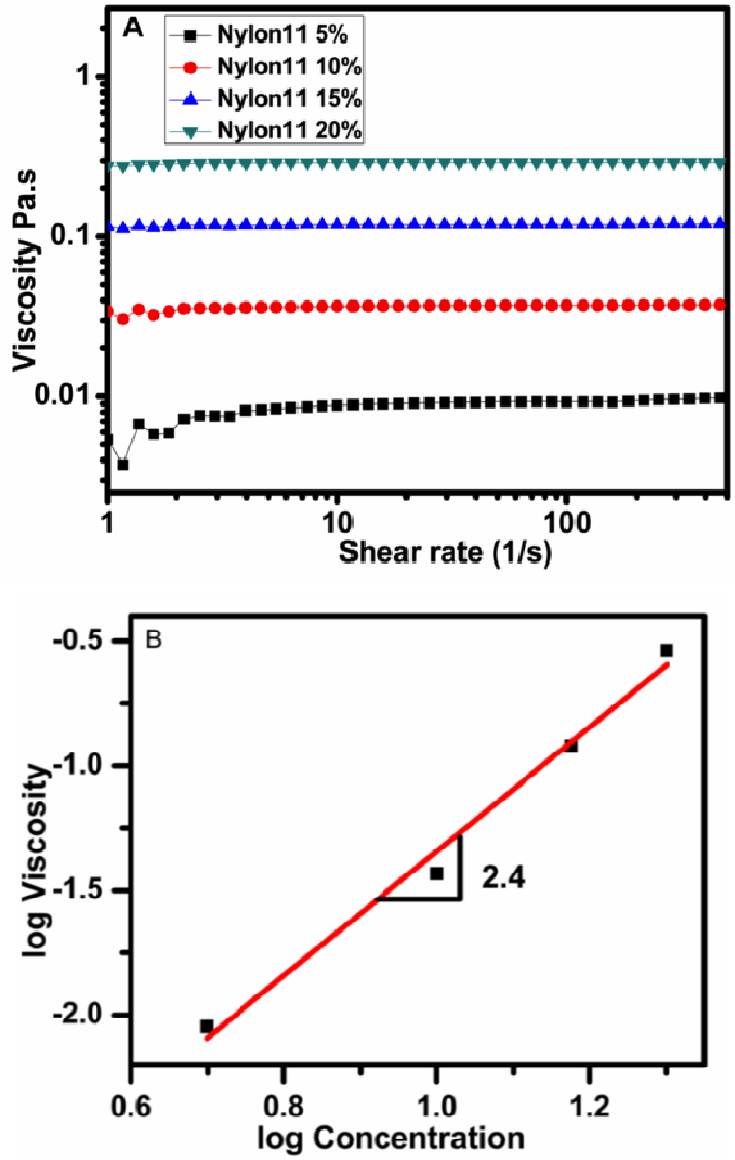

Figure 3.3 Viscosity of Nylon11 solutions with increasing concentration.

3.3.2 Electrical Conductivity of Nylon11 Solutions

Figure 3.4 shows the conductivity of the Nylon11 solutions as a function of concentration. It can be clearly seen that conductivity increases as the concentration of Nylon11 in solution is increased. The dependence of conductivity on concentration is weaker than that of viscosity.

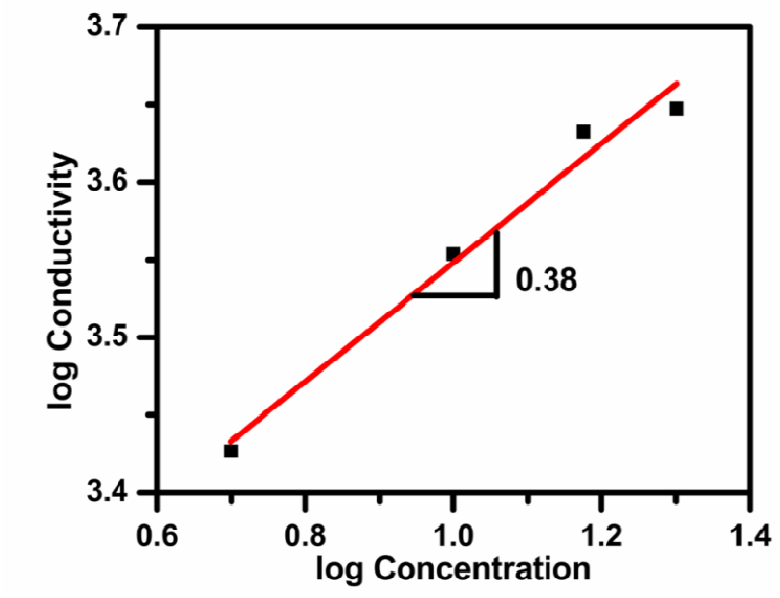

Figure 3.4 Conductivity of Nylon11 solutions with increasing concentration.

3.3.3 Electrospinning of Nylon11 by Varying Processing Parameters

In electrospinning process, the fiber morphology and fiber diameter depend on the electrospinning processing conditions and polymer solution properties such as viscosity, conductivity and surface tension. The main electrospinning processing parameters are applied voltage, flow rate and distance between the two electrodes. In some cases, environmental conditions such as temperature and humidity also affect the fiber morphology.

In the present study, the three key parameters namely concentration, voltage and distance between the two electrodes were varied during electrospinning of Nylon11 solutions. This section summarizes the effect of these parameters on the morphology of electrospun mats. The main data is presented in Table 3.1.

Table 3.1 Average fiber diameter of Nylon11 electrospun fibers with varying concentration, applied voltage and distance between the two electrodes.

Concentration (wt/vol%)	**Electrode distance (cm)**	**Fiber diameter (nm) with standard deviation**			
		5 kV	**10 kV**	**15 kV**	**20 kV**
5	10	-	69±9	73±11	113±20
10	5	132±20	211±40	251±40	312±60
	10	148±10	209±30	255±40	258±41
	15	-	177±43	222±60	241±41
15	5	246±46	369±56	468±102	308±57
	10	237±52	338±73	353±76	375±75
	15	-	363±96	262±86	392±86
20	5	468±54	741±136	736±145	822±209
	10	615±152	730±175	770±156	742±136
	15	686±233	750±174	897±212	905±197

A) Effect of Concentration

As observed in the earlier section, a change in concentration of Nylon11 in formic acid results in significant changes in the viscosity and conductivity of the solution. In order to obtain a stable jet, solutions of appropriate concentration were required. If the concentration of the solution is too low, a continuous stream of the charged liquid (charged jet) cannot be formed. For such solutions, the charged jet undergoes a flow instability leading to the formation of droplets (electro spraying). A critical solution concentration needs to be exceeded to form a stable continuous charged jet. Similarly, conductivity of the solution also affects spinnability. Repulsion of charges at the surface of the electrospinning jet causes the solution to stretch and form nanofibers. A significant reduction in the diameter of the electrospun nanofibers can therefore be observed when the electrical conductivity of the solution is increased because the jet carries more charges. Formation of beaded fibers can be avoided if a small amount of

salt or polyelectrolyte is added to the polymer solution. This is because the electrical forces of the increased charge carried by the electrospinning jet cause the jet to elongate thereby producing uniform fibers[27]. It is also impossible to form fibers if the solution has no conductivity.

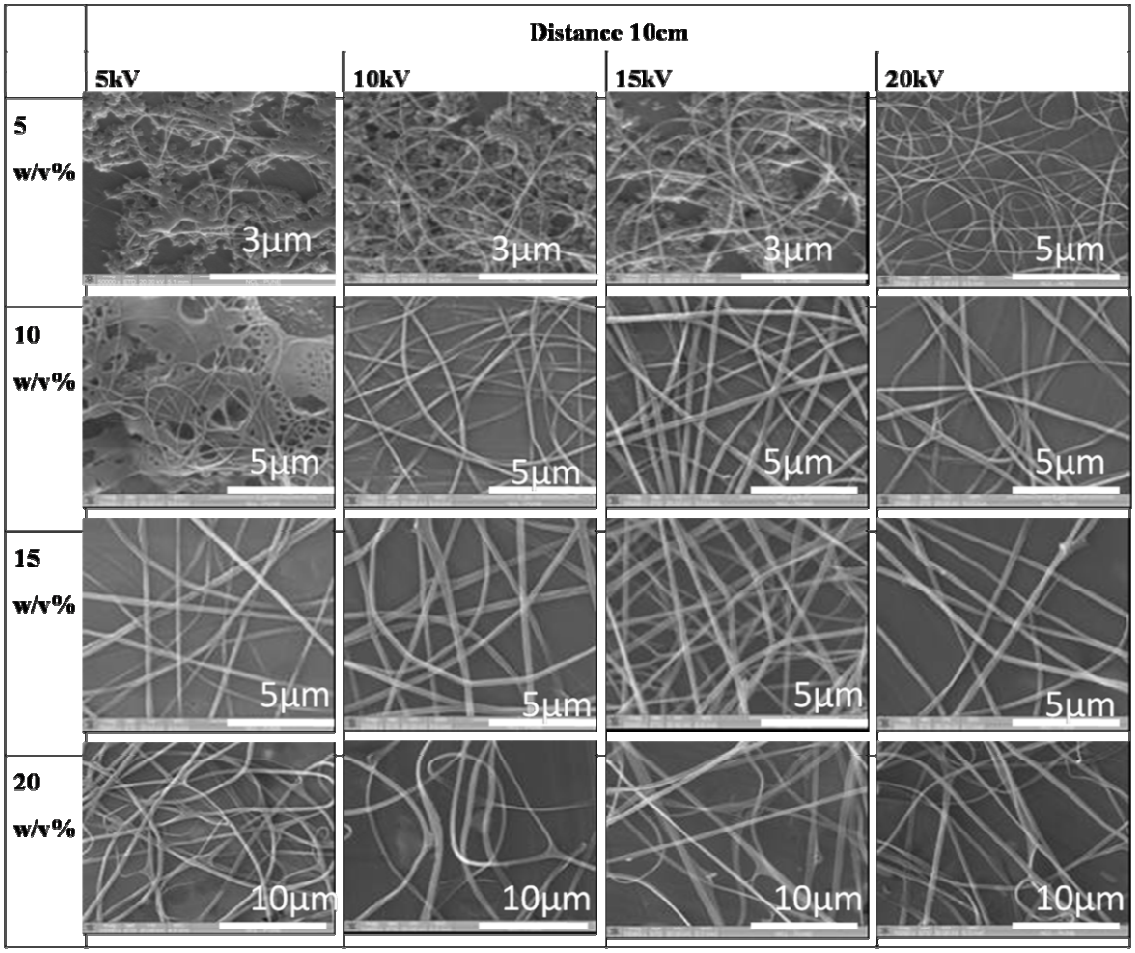

Figure 3.5 SEM images of Nylon11 electrospun mats showing the effect of concentrations on fiber diameter.

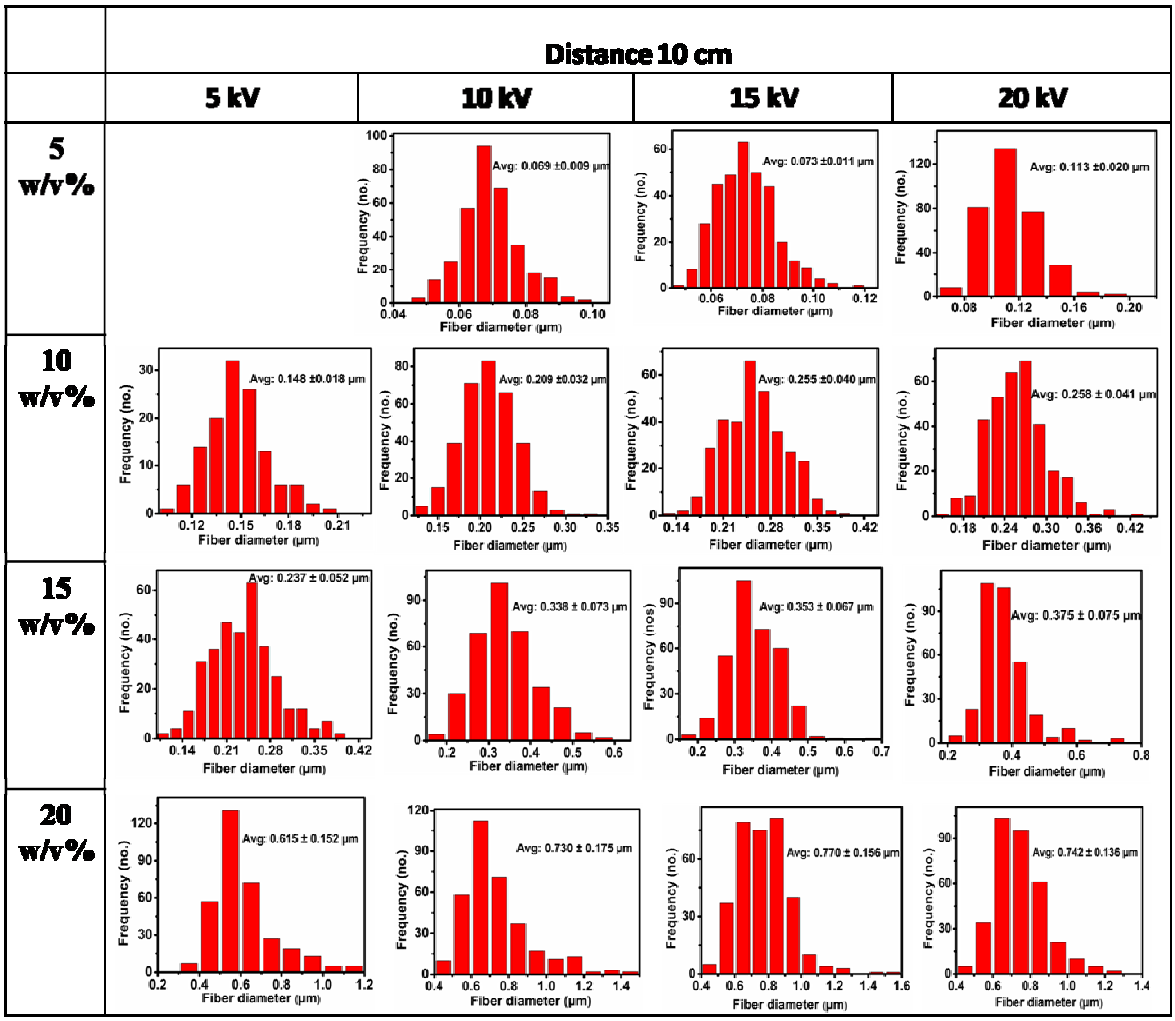

Figure 3.6 Fiber size distribution study of Nylon11 electrospun mats produced using different concentrations, different applied voltage and at constant distance of 10 cm between electrodes.

Figure 3.5 shows the SEM images of Nylon11 electrospun fibers with varying concentration. SEM images show that both bead and fiber morphologies were formed at 5wt/vol% solution because of low concentration of polymer solution. However, as the applied voltage was increased to 20 kV the bead formation was reduced and uniform fibers with diameters ranging from 150-200 nm were formed. As the concentration was increased to 10wt/vol%, beads and fibers were obtained at lower applied voltage (5 kV). On applying higher voltage, beads disappeared and smooth electrospun fibers were obtained. Increasing the solution concentration to 15 and 20wt/vol% resulted in the formation of ribbons of about 700-800 nm width. The formation of ribbon like nanofibers is due to rapid solvent vaporization from the surface of the jet. Ribbons or flat fibers have been observed for several polymer-

solvent systems[28]. The approximate thickness of these ribbons, as measured from SEM images, was in the range of 90-95 nm. Thus SEM images reveal that increasing the concentration of Nylon11 affects the fiber morphology and fibers diameter. At lower concentrations, the average fiber diameters were in the range of 150-200 nm, while at higher concentration the diameters increased to 700-800 nm.

We also investigated the effect of concentration on fiber diameter with varying applied voltage and distance between the two electrodes (needle and collector plate). Figure 3.7 (A-C) shows that as the solution concentration was increased from 5 to 20wt/vol% the fiber size increased gradually for all operating voltages and for all distances between electrodes.

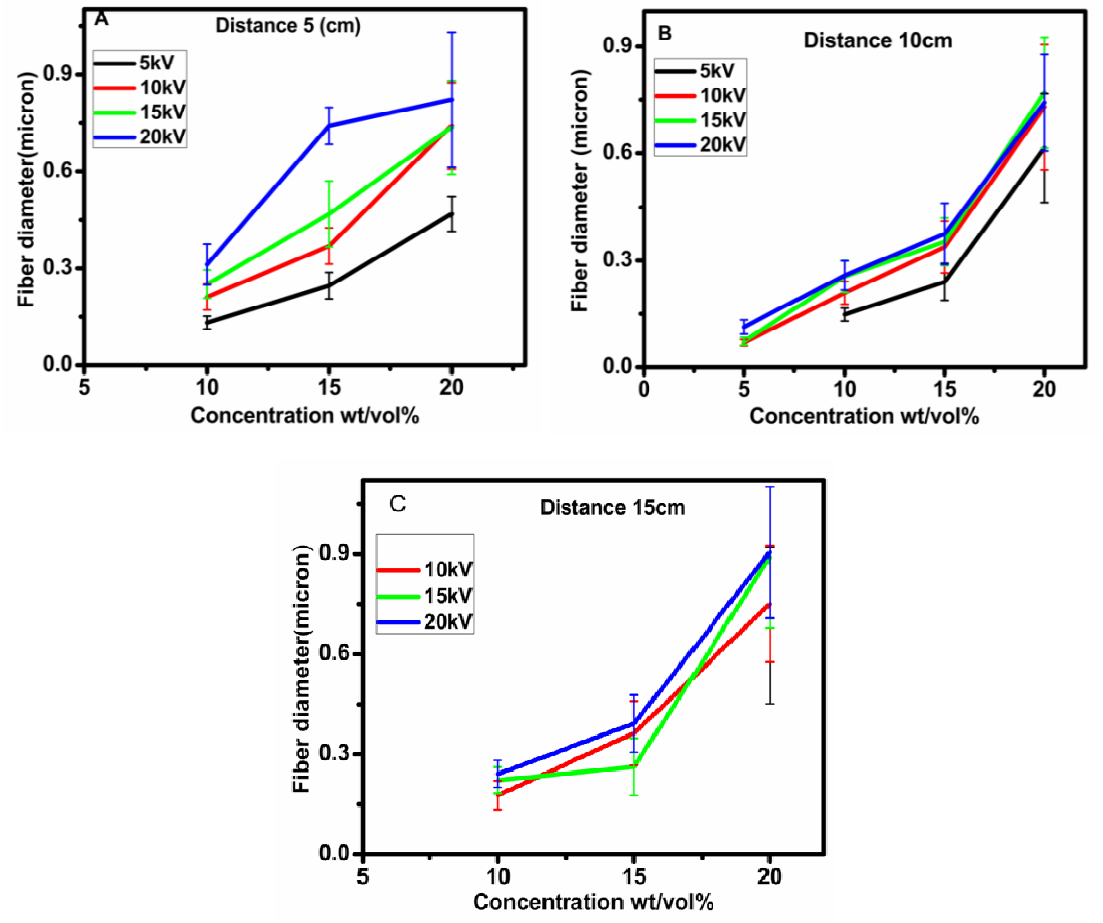

Figure 3.7 Effect of concentraion on fiber diameter (A-C).

Increasing concentration could have two opposing effects on fiber size. With increase in concentration since the solution viscosity increases, the jet can be expected to stretch to a lesser extent. However increase in concentration also increases the conductivity, which would tend to reduce the fiber size. From the results shown in

Figure 3.7 it is apparent that the effect of conductivity is not dominant. This could be because the increase in viscosity was more significant (exponent of 2.4) compared to the increase in conductivity (exponent of 0.38) for the same increase in concentration. Our results are in agreement with those reported earlier for various polymer systems[29].

B) Effect of Voltage on Fiber Diameter

In the electrospinning process, a continuous spinning fiber jet can only be obtained if the applied voltage is above a given critical value. This voltage is required to overcome the surface tension forces of the electrospinning solution.

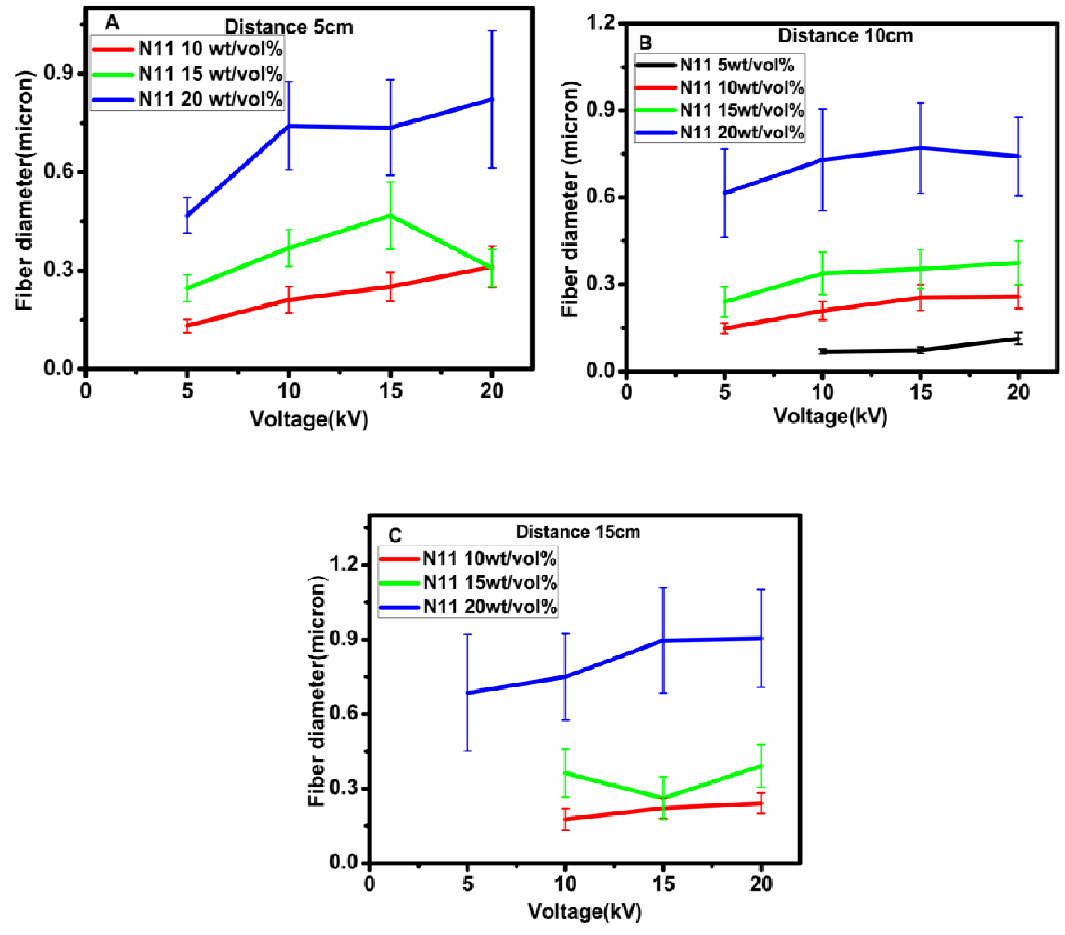

Figure 3.8 Effect of voltage on fiber diameter (A-C).

Figure 3.8 shows the relationships between fiber diameter and the applied voltage. As seen in the figure, an increase in voltage did not significantly affect the fiber diameter. In most causes the fiber diameter increased slightly with applied

voltage. An increase in voltage at constant distance between electrodes can be expected to increase the voltage gradient for spinning, which would tend to decrease fiber diameter[30]. However, if the applied voltage is higher, the fibers travel to the collector plate at higher velocity and hence in a shorter residence time. Upon reaching the collector plate, there is no more elongation of the fiber. The total stretch experienced by the fiber is the product of stretch rate and flight time. Since these two parameters vary in opposing manner with increase in voltage, therefore effectively the fibers may not end up stretching very much. As a result, our experiments show that the fiber diameter is not strongly dependent on the applied voltage.

C) Effect of Varying Distance

Figure 3.9 shows the morphology of Nylon11 10wt/vol% electrospun mats with varying collector distances ranging from 5-15 cm. Both fibers and bead formation were observed for Nylon11 10wt/vol% solution spun at an applied voltage of 5 kV and at collector distance of 5 cm. Upon increasing the distance to 10 cm and 15 cm, uniform fiber formation was observed and the fiber diameters slightly decreased. As shown in Figure 3.10 A for Nylon11 10wt/vol%, it was observed that the average fiber diameter decreased with increasing distance. This may be because with increasing distance the flying time is higher, and this allows enough time for jet to elongate and thin down. However for Nylon11 fibers electrospun from 15 and 20wt/vol% solutions, the fiber diameter increased with increasing the collector distance (Figure 3.10 B and C). This is likely due to decreased strength of electric field gradient. For these solutions of higher concentrations, the increased viscosity does not assist in thinning during the larger flight times.

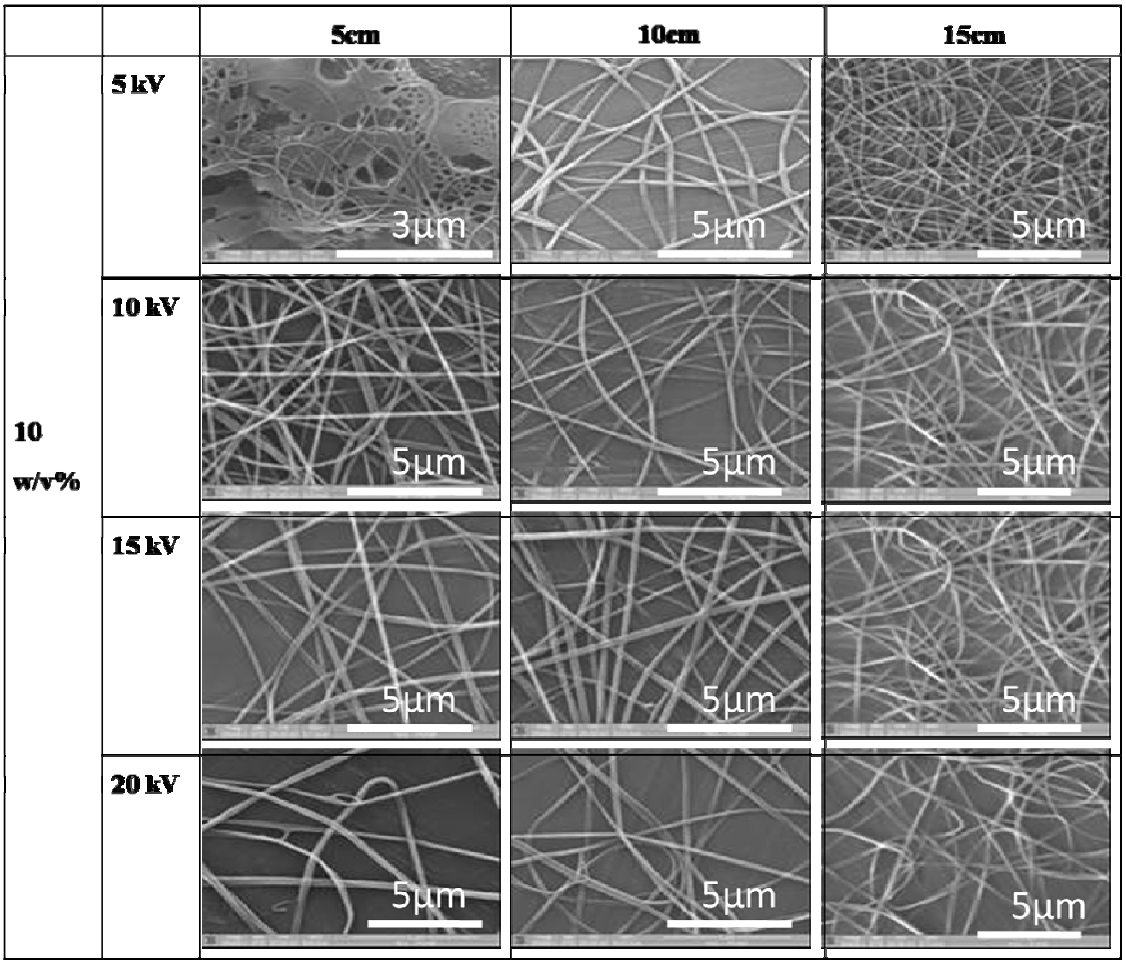

Figure 3.9 SEM images of Nylon11 electrospun mats of 10 wt/vol%.

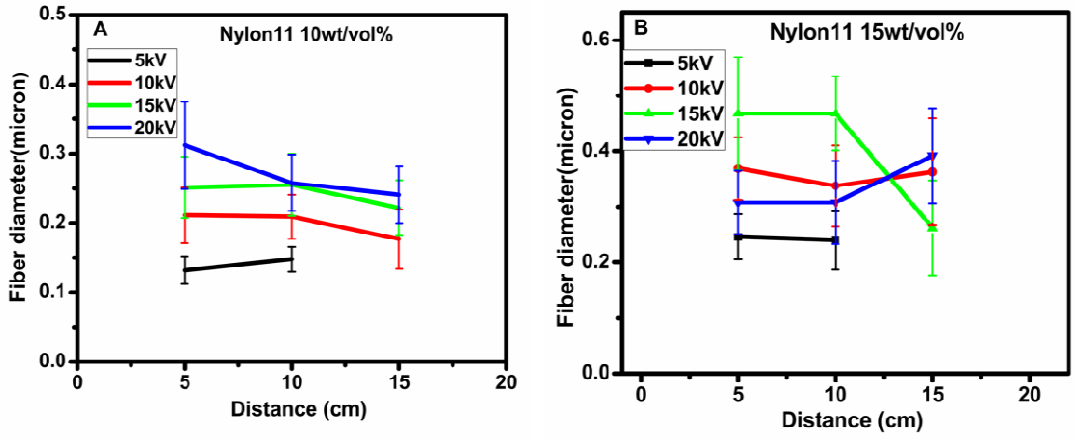

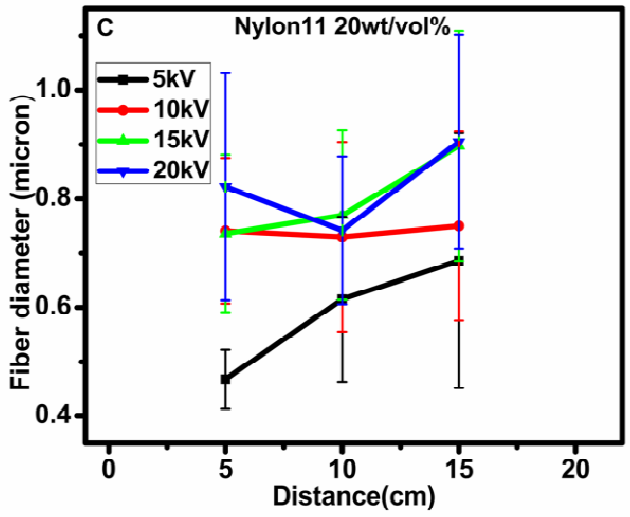

Figure 3.10 Effect of fiber diameter with increasing distance between the two electrodes (A-C).

3.3.4 Micro-structural Analysis Using Wide Angle X-ray Diffraction

Crystalline structure of Nylon polymers has been an area of extensive research for several decades[31,32]. Nylon exhibits different crystalline phases when subjected to thermal and chemical treatments. In general, Nylon11 crystallizes into a three dimensional ordered structure of hydrogen-bonded sheets with high degree of coupling between adjacent amide groups.

Nylon11 has been shown to exhibit crystalline modifications such as α, α′, γ, δ and δ′. The stable α phase, which has a triclinic unit cell, is formed during annealing of the quenched polymer[33]. It is also known to form during solution casting from m-cresol[34]. The α′ phase is the predominant structure obtained upon crystallization from melt. A pseudohexagonal phase also called γ phase, can be obtained above room temperature by heating the α′ phase. The γ phase is also shown to form during solution casting from trifluoro acetic acid (TFA)[35]. The smectic, or δ′ phase is obtained upon melt quenching[36]. The diffraction angles of the various polymorphs are given in Table 3.2. The structure of Nylon11 however has not been studied much in electrospun mats. In the following, we present results on crystalline structure of electrospun Nylon11.

Table 3.2 Different crystalline forms of Nylon11.

Nylon11 crystalline forms	Methods	XRD 2 theta values (°)
α	Stretching, or melting Solution casting m-cresol	7.54, 20.39, 23.06
α′	Melt crystallization	6.93, 20.17, 23.13
γ	Solution casting from trifluoro acetic acid	21.60
δ′	Melt quenching	7.11, 21.40

Figure 3.11 shows the diffraction patterns of Nylon11 melt pressed film, solution cast film and electrospun non-woven mat. The melt pressed film exhibited two strong reflections (100) and (110, 010) at the diffraction angles of 2θ=20.32 ° and 23.17 °, which correspond to the α and α' crystalline phase of Nylon11. Solution cast films of 5 to 20wt/vol% showed characteristic reflections of 21.6 ° and 23.03 ° indicating the coexistence of gamma and alpha crystalline form respectively[37]. The electrospun mats show a broad reflection at 21.6 °, which indicates weakly ordered hexagonal gamma crystalline form of Nylon11[38]. This may be because in electrospinning process the structure of the fiber is formed under the influence of two simultaneous processes namely the evaporation of the solvent and the elongation of the fibers.

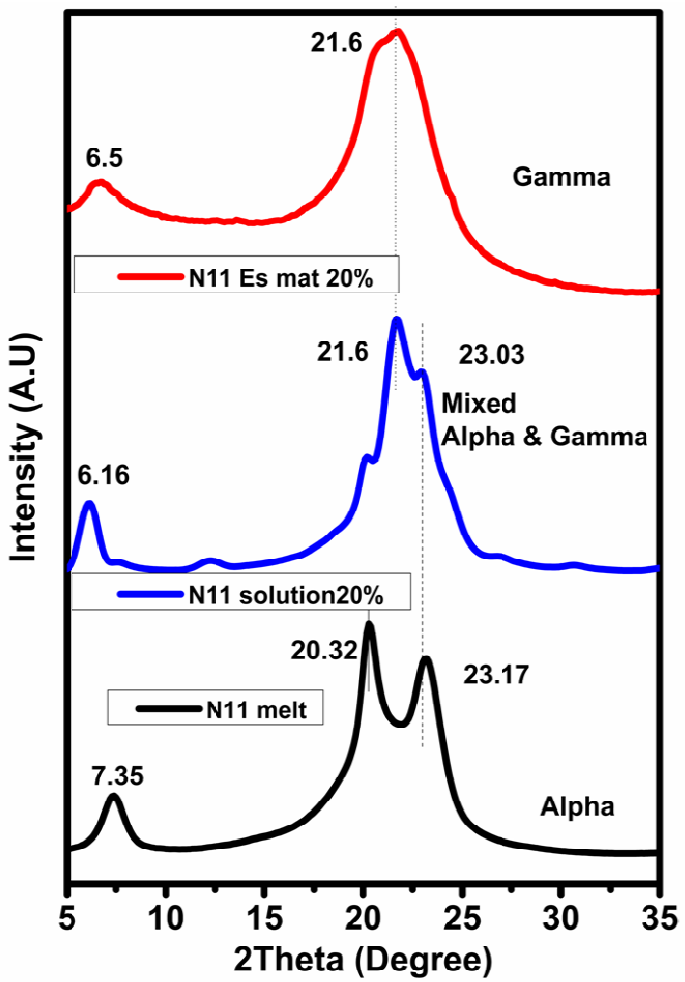

Figure 3.11 XRD analysis of Nylon11 melt pressed film, 20wt/vol% solution cast film and 20wt/vol% electrospun mats.

3.3.5 Differential Scanning Calorimetry (DSC)

Differential Scanning Calorimetry (DSC) is an important technique to understand the microstructure of Nylon11[39]. The technique can be used to complement the results obtained using WAXD. Nylon11 melt pressed film, solution cast film and electrospun mats were subjected to thermal analysis using DSC. The melting and crystallization parameters are presented in Table 3.3.

Table 3.3 Heat of fusion (ΔH_f), melting temperature, crystallization temperature and % crystallinity of melt pressed, solution cast and electrospun mats of Nylon11.

Sample coding	First heating			% Crystallinity
	Heat of fusion (ΔH_f) J/g	Crystallization temperature Tc (^oC)	Melting temperature (^oC)	
N11 melt pressed film	55.4	163.5	189.8	26.9
N11 solution cast film 5wt/vol%	96.7	165.2	189.5	47.4
N11 solution cast film10wt/vol%	95.9	164.4	190.1	46.5
N11 solution film 15wt/vol%	86.7	166.1	188.3	41.7
N11 solution cast film 20wt/vol%	94.3	163.5	189.5	45.7
N11 ES 10wt/vol%	68.1	166.4	186.7	33.1
N11 ES 15wt/vol%	62.8	164.4	186.3	30.4
N11 ES 20wt/vol%	61.0	165.5	186.7	29.6

Figure 3.12 shows first heating and cooling scans of Nylon11 melt pressed film, solution cast film and electrospun mats. The crystallinity of samples was calculated by dividing the heat of fusion of polymer samples by the heat of fusion of 100 % crystalline Nylon11. The heat of fusion for 100 % crystalline Nylon11 is 206 J/g.

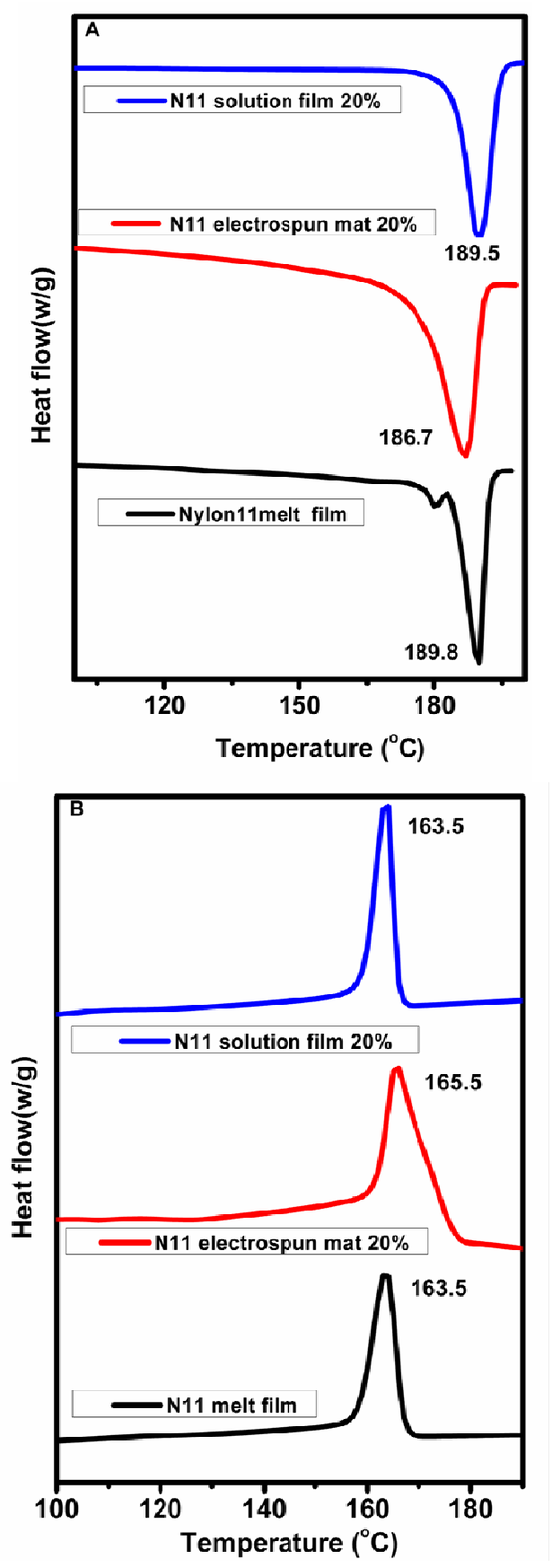

Figure 3.12 First heating and cooling scans of Nylon11 melt pressed film, solution cast film and electrospun mats of 20wt/vol%.

The electrospun fibers showed higher crystallinity than melt pressed film, whereas the solution cast film showed the highest crystallinity. The melting temperature for the electrospun fibers is lower, while the crystallization temperature is higher as compared to melt pressed film. Interestingly, the electrospun mats has a broad crystallization peak. This could be because of residual orientation of nanofibers left after first heating. The lower crystallinity of the electrospun mats agreed with the weak crystalline order observed in wide angle diffraction results.

Structure formation during electrospinning is governed by the simultaneous processes of rapid evaporation of the solvent and elongation of the solidifying fiber. In crystalline polymers, solidification is accompanied with formation of crystals. The shorter time for crystallization is expected to result in small crystallites with defects and thus lower melting point and lower degree of crystallinity compare to the slow solvent evaporation process. The stretching of the fibers during electrospinning can offset the rapid solvent evaporation leading to rapid crystallization. However the results shown in Table 3.3 show that the effect of rapid solvent evaporation dominates crystallization during electrospinning. In contrast, during the preparation of solution cast film by slow evaporation of the solvent, the macromolecular chains have sufficient time to crystallize thereby forming relative high crystalline order. Similar results were reported by Behler et al[40].

3.3.6 Dynamic Mechanical Analysis

In the present investigation, the differences in viscoelasticity as measured in terms of storage modulus (E′), loss modulus (E″) and damping factor (tan δ) between Nylon11 melt pressed film, solution cast film and electrospun mat were studied. The absolute values of E’ should not be compared since the dimensions of the sample are not identical. Rather, it is only important to note the alpha transition in the samples, which is seen as the decrease in E’ over a range of 50-100 °C (Figure 3.13 A), or a peak in tanδ (Figure 3.13 B) over the same temperature range.

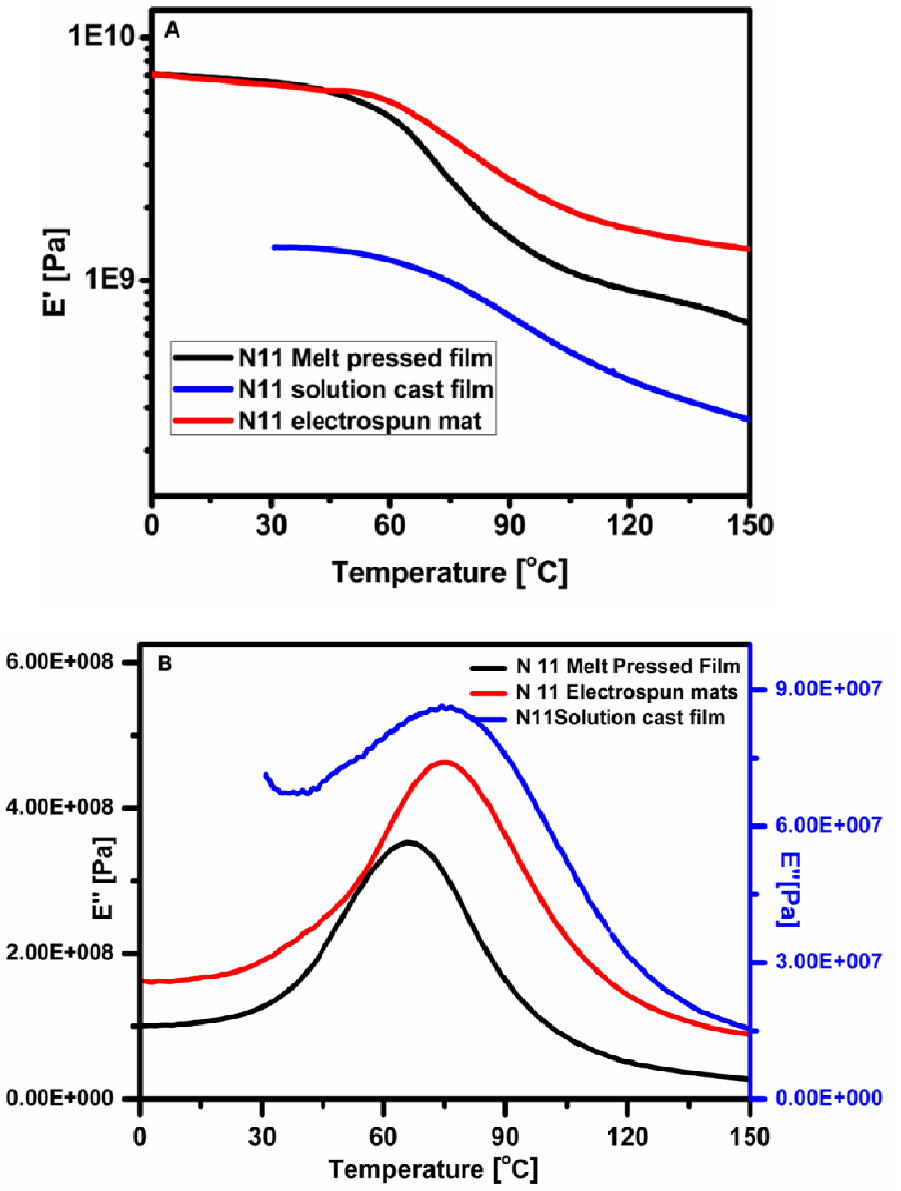

Figure 3.13 Storage modules (A) and loss modules (B) of Nylon11 melt pressed film, solution cast film and electrospun mat.

Figure 3.13 exhibits DMA results of Nylon11 melt pressed film, solution cast film and electrospun mat. The α relaxation temperature of electrospun mat is seen to be shifted to higher temperature compared to melt pressed film. The α relaxation of Nylon11 electrospun mat was 76 °C, that of solution cast film was 75 °C, while that of the melt pressed film is around 66 °C[41] and is narrower than solution cast film and electrospun mat. The increase of α relaxation of electrospun fibers is likely to be due to the presence of oriented rigid amorphous phase.

3.3.7 Dielectric Relaxation Spectroscopy Analysis (DERS)

Dielectric analysis was used to measure the activation energy of the α transitions of Nylon11 films and electrospun mat. Specifically, DERS experiments were performed at various frequencies and the temperature dependence of the α relaxation was measured. In our experiments we observed that tan delta maximum shifted to higher temperatures with increasing frequency shown in Figure 3.14. The α relaxation is typically known to follow Arrhenius dependence[42,43]. Accordingly, the graph of ln (frequency) versus reciprocal temperature was used to calculate the activation energy of α relaxation. Nylon11 melt pressed film showed activation energy of Ea= 137.7 kJ/mol, whereas the activation energy of Nylon11 solution cast film was observed to be 152 kJ/ mol.

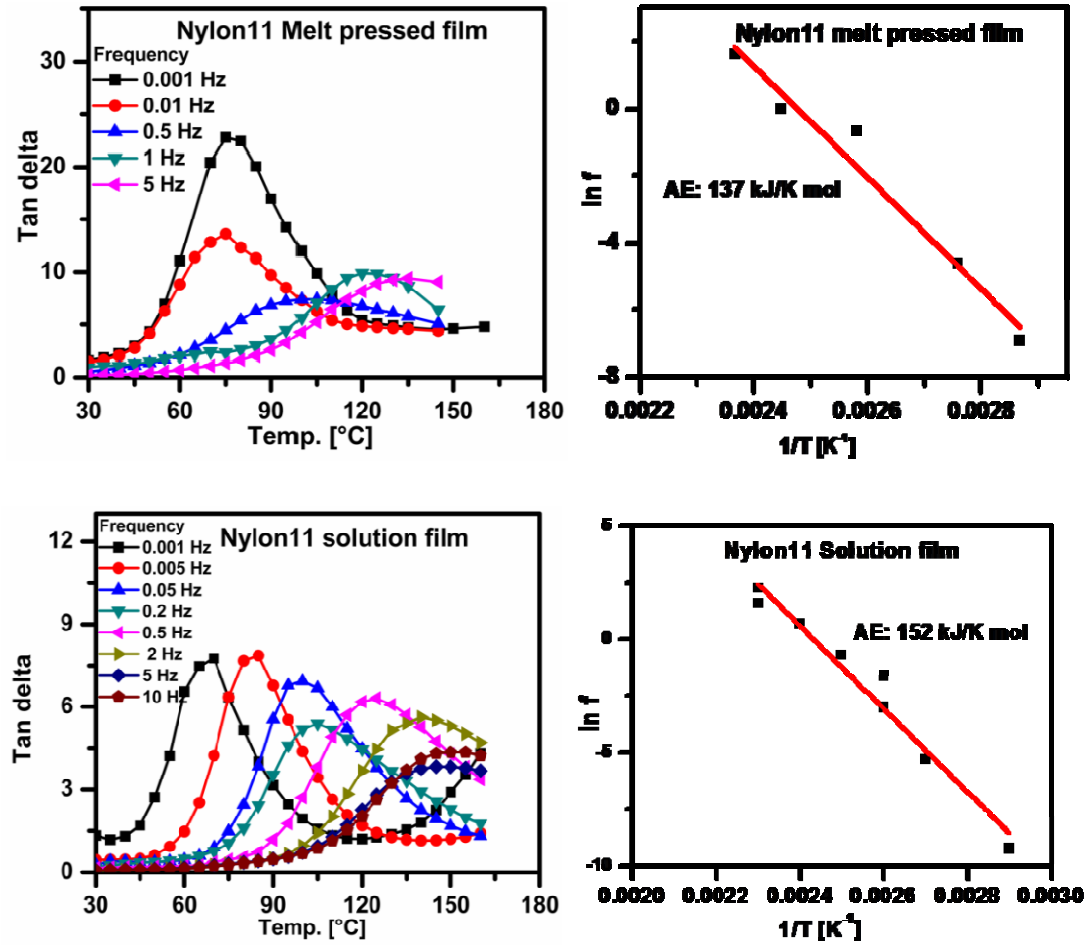

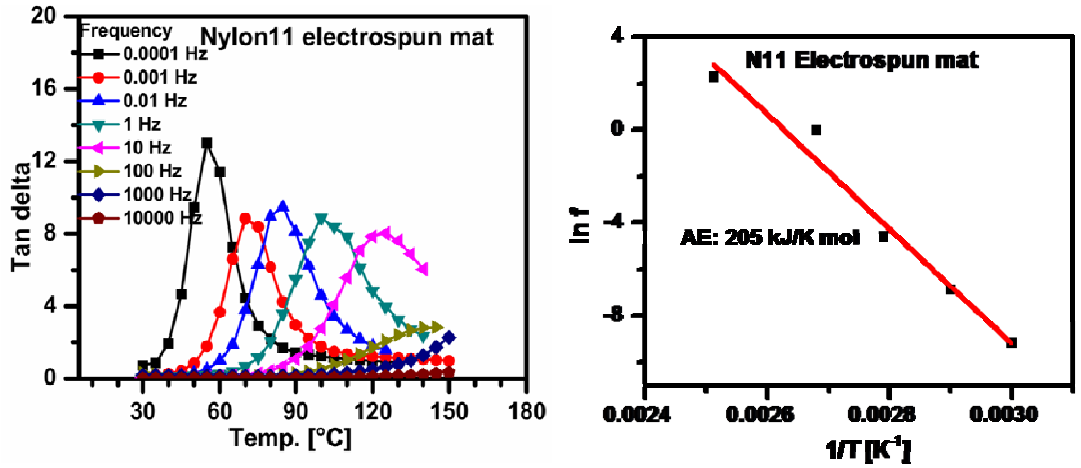

Figure 3.14 Tan delta Vs temperature by varying frequency and corresponding slope of Nylon11melt pressed film, solution cast film and electrospun mat.

In case of Nylon11 electrospun mat prepared from 20wt/vol% solution, the activation energy was seen to be 205 kJ/mol, which was higher than Nylon11 melt pressed film and solution cast film. The higher activation energy of Nylon11 electrospun mat may also be due to the presence of oriented rigid amorphous phase.

3.3.8 Contact Angle Measurement

Hydrophilicity of the polymeric surface is important for adhesion and proliferation of cells. Wettability of Nylon11 films and electrospun mats was determined by measuring the contact angle of a deionized water droplet on the specimen surfaces. The contact angle is defined as the angle between the substrate support surface and the tangent line at the liquid droplet with the substrate.

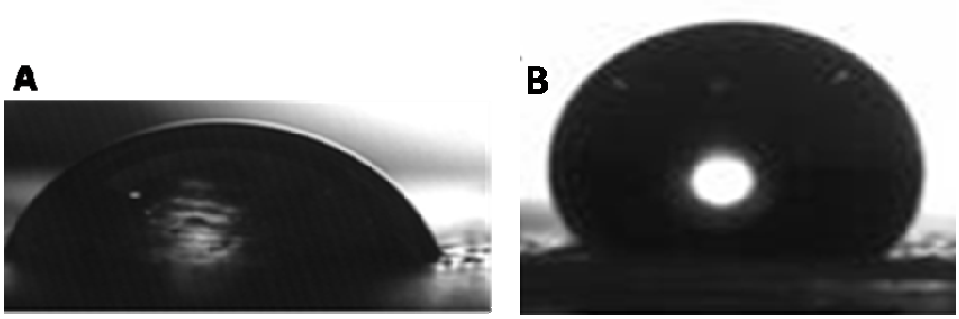

Figure 3.15 Water contact angle images of Nylon11 melt pressed film (A) and Nylon11 20wt/vol% electrospun mat (B).

Nylon11 melt pressed film exhibited contact angle value of 79±2 ° (Figure 3.15 A). Nylon11 electrospun mats of 20wt/vol% electrospun fiber exhibited contact

angle of ~ 131±2 ° to 135.5±2 ° (Figure 3.15 B). Thus Nylon11 electrospun fiber showed higher contact angle values, and this is mainly because of air pockets and multiple contact points on the electrospun mats[44,45], which resist the instantaneous spreading of the water droplet.

3.3.9 Cell Culture Studies

A) Morphological Studies of HEK293 Cells on Nylon11 Scaffolds

HEK293 cells were cultured on the Nylon11 melt pressed film and electrospun mats. Figure 3.16 shows representative SEM micrographs after cell culture. SEM images show that HEK293 cells had adhered and spread over the Nylon11 melt pressed film and Nylon11 20wt/vol% electrospun mats. Similar results for other polymers such as polylactic acid and polyvinyl alcohol were reported by other researchers[46,47].

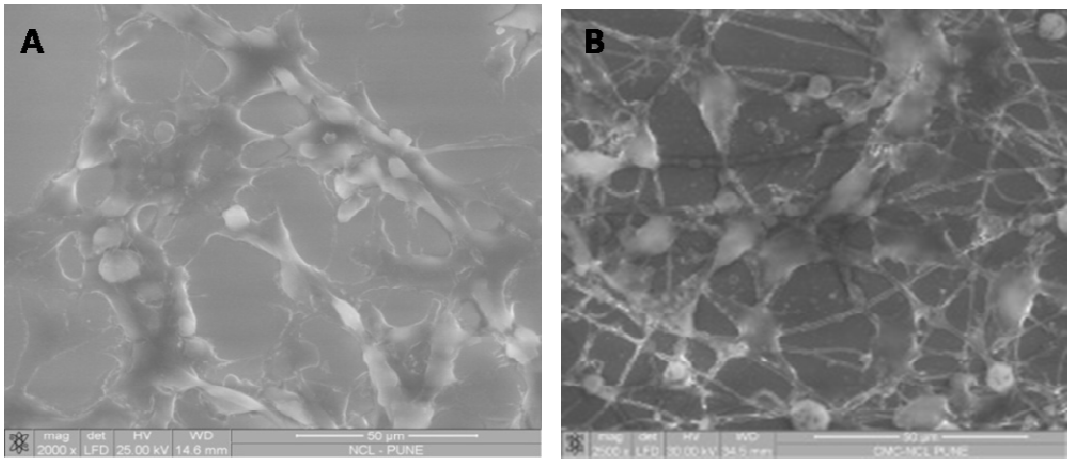

Figure 3.16 SEM images of HEK 293 cells on Nylon11 melt pressed film (A) and electrospun mats (B).

However, the HEK293 cells do not appear to have penetrated through the Nylon11 nanofibers network possibly due to the small pore size between the fibers. From the shape of the HEK293 cells, they seems to be healthier in Nylon11 electrospun mat surfaces. Further optimization is necessary if penetration of cells within the fibrous network is desired.

B) Cell Proliferation Assay (MTT assay)

Cell proliferation over a period of 10 days was measured using the MTT assay. The MTT assay measures the number of metabolically active cells on the scaffold and this can be tracked by monitoring the absorbance at 550 nm. Figure 3.17 shows the compiled results of the MTT assay experiment on Nylon11 melt pressed film and electrospun mats.

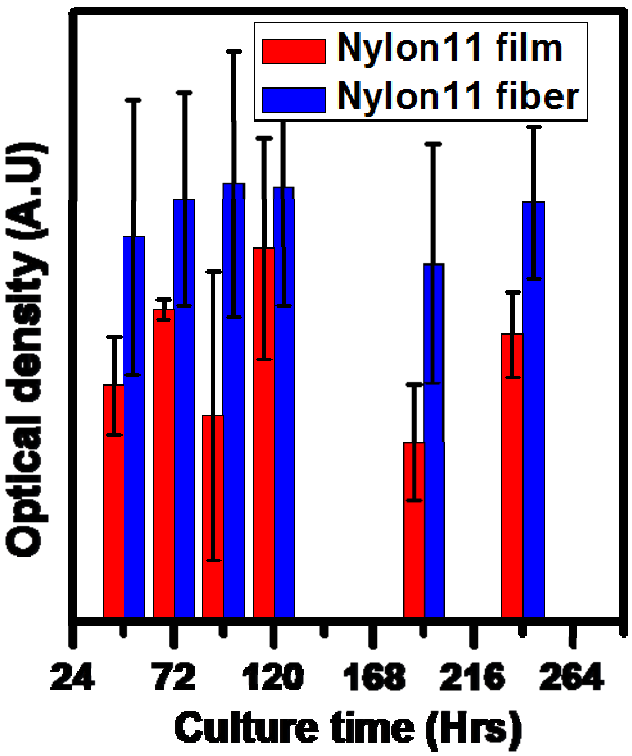

Figure 3.17 Cell proliferation study on melt pressed film and electrospun mats of Nylon11.

Following the inoculation of $3x10^4$ cells on the scaffold, cells continue to grow for 10 days, after which the absorbance reached a plateau. MTT assay study shows that cell proliferation rate was higher in Nylon11 electrospun mat, when compared to Nylon11 melt pressed film. We may expect the Nylon11 electrospun mat to respond better because of 3-D porous structure and higher surface area[48–50].

3.4. Conclusions

Following are salient findings of the work reported in this chapter

Viscosity and conductivity of the solutions increased with Nylon11 concentration in solution. Increasing Nylon11 solution concentration increased the fiber diameter. Other process variables did not have much effect on fiber diameter.

XRD results showed that Nylon11 melt pressed film exhibits alpha crystalline structure, whereas solution cast film results in coexistence of alpha and gamma crystalline structure. However Nylon11 electrospun mats show gamma crystalline structure. The formation of gamma crystals is attributed to the possible high rate of elongation experienced by the polymer during electrospinning.

The thermal properties of nanofibers show increase in crystallinity as compared to the melt crystallized film but lower crystallinity than solution crystallized samples. DMA study shows that Tg of Nylon11 electrospun mat is shifted to higher temperature when compared to melt pressed film. Nylon11 electrospun mat exhibits higher activation energy for chain mobility than melt pressed and solution cast films. Nylon11 melt pressed film exhibit hydrophilic nature, whereas electrospun mats were hydrophobic.

SEM images of cultured Nylon11 scaffolds show that HEK293 cells adhere well on both the melt pressed film and fibrous surfaces. MTT assay showed that the cell proliferation rate on the Nylon11 electrospun mat was higher than for melt pressed films.

3.5 References

1. Henriques, C., Vidinha, R., Botequim, D., Borges, J. P. and Silva, J. A. M. C. A systematic study of solution and processing parameters on nanofiber morphology using a new electrospinning apparatus. Journal of Nanoscience and Nanotechnology 8, 1–11 (2008).

2. Theron, S. A., Zussman, E. and Yarin, A. L. Experimental investigation of the governing parameters in the electrospinning of polymer solutions. Polymer 45, 2017–2030 (2004).

3. Shenoy, S. L., Bates, W. D., Frisch, H. L. and Wnek, G. E. Role of chain entanglements on fiber formation during electrospinning of polymer solutions□: good solvent, non-specific polymer – polymer interaction limit. Polymer 46, 3372–3384 (2005).

4. Deitzel, J. M., Kleinmeyer, J., Harris, D. and Tan, N. C. B. The effect of processing variables on the morphology of electrospun nanofibers and textiles. Polymer 42, 261–272 (2001).

5. Mit-uppatham, C., Nithitanakul, M. and Supaphol, P. Ultrafine electrospun polyamide-6 fibers□: Effect of solution conditions on morphology and average fiber diameter. Macromolecular Chemistry and Physics 6, 2327–2338 (2004).

6. Liu, Y., Dong, L., Fan, J., Wang, R. and Yu, J. Effect of applied voltage on diameter and morphology of ultrafine fibers in bubble electrospinning. Journal of Applied Polymer Science 120, 592–598 (2010).

7. Du, J., Shintay, S. and Zhang, X. Diameter control of electrospun polyacrylonitrile / Iron acetylacetonate ultrafine nanofibers. Journal of Polymer Science: Part B: Polymer Physics 1611–1618 (2008).

8. Yoon, K., Kim, K., Wang, X., Fang, D. and Hsiao, B. S. High flux ultrafiltration membranes based on electrospun nanofibrous PAN scaffolds and chitosan coating. Polymer 47, 2434–2441 (2006).

9. Mohrova, J. and Kalinova, K. Different structures of PVA nanofibrous membrane for sound absorption application. Journal of Nanomaterials, 1-4 (2012).

10. Kadir, R.A., Li, Z., Sadek, A.Z., Rani, R.A., Field, M.R., Ou, J.Z., Chrimes, A.F. and Kalantar-Zadeh, K. Electrospun granular hollow SnO_2 nano fibers hydrogen gas sensors operating at low temperatures. The Journal of Physical Chemistry C 118, 3129–3139 (2014).

11. Lai, K., Jiang, W., Wu, Y., He, B., Wang, G. and Gu, K. Superparamagnetic nano-composites scaffolds for promoting bone cell proliferation and defect reparation without a magnetic field. RSC Advances 2, 13007–13017 (2012).

12. Chem, J.M., He, L., Shi, Y., Han,Q., Zuo, Q., Ramakrishna, S. and Zhou, L. Surface modification of electrospun nanofibrous scaffolds via polysaccharide – protein assembly multilayer for neurite outgrowth. Journal of Materials Chemistry 22, 13187–13196 (2012).

13. Chang, H. M., Wang, Z. H., Luo, H. N., Xu, M., Ren, X. Y., Zheng, G. X., Wu, B. J., Zhang, X. H., Lu, X. Y., Chen, F., Jing, X. H. and Wang, L. Poly (3-

hydroxybutyrate-co-3 hydroxyheannnoate)-based scaffolds for tissue engineering. Brazilan Journal of Medical and Biological Research 47, 533–539 (2014).

14. Lv, Q. and Feng, Q. Preparation of 3-D regenerated fibroin scaffolds with freeze drying method and freeze drying/foaming technique. Journal of Materials Science: Materials in Medicine 17, 1349–1356 (2006).

15. Wang, Y., Bansal, V., Zelikin, A. N. and Caruso, F. Templated synthesis of single-component polymer capsules and their application in drug delivery 2008. Nano Letters 6, 1741–1745 (2008).

16. Li, X., Zhang, Y. and Chen, G. Biomaterials nanofibrous polyhydroxyalkanoate matrices as cell growth supporting materials. Biomaterials 29, 3720–3728 (2008).

17. Yang, F., Xu, C. Y., Kotaki, M., Wang, S. and Ramakrishna, S. Characterization of neural stem cells on electrospun poly (L-lactic acid) nanofibrous scaffold poly (L - lactic acid) nanofibrous scaffold. Journal of Biomaterials Science Polymer Edition 15, 1483–1497 (2004).

18. Chen, F., Li, X., Mo, X. and He, C. Electrospun chitosan-P(LLA- CL) nanofibers for biomimetic extracellular matrix. Journal of Biomaterials Science Polymer Edition 19, 677–691 (2008).

19. Cheng, M., Lin, C., Su, H., Chen, P. and Sun, Y. Processing and characterization of electrospun nanofibrous membranes. Polymer 49, 546–553 (2008).

20. Zhang, Y., Ouyang, H., Lim, C. T., Ramakrishna, S. and Huang, Z.-M. Electrospinning of gelatin fibers and gelatin/PCL composite fibrous scaffolds. Journal of Biomedical Materials Research. Part B, Applied Biomaterials 72, 156–65 (2005).

21. Li, S., Sun, B., Li, X. and Yuan, X. Characterization of electrospun core/shell poly (vinyl pyrrolidone)/poly (L-lactide-co-ε-caprolactone) fibrous membranes and their cytocompatibility in vitro. Journal of Biomaterials Science Polymer Edition 19, 245–258 (2008).

22. Zhang, Q., Mo, Z., Zhang, H., Liu, S. and Cheng, S. Z. D. Crystal transitions of Nylon11 under drawing and annealing. Polymer 42, 5543–5547 (2001).

23. Wu, M., Yang, G., Wang, M., Wang, W., Zhang, W., Feng, J. and Liu, T. Nonisothermal crystallization kinetics of ZnO nanorod filled polyamide11 composites. Materials Chemistry and Physics 109, 547–555 (2008).

24. Nair, S. S., Ramesh, C. and Tashiro, K. Crystalline phases in Nylon-11□: Studies using HTWAXS and HTFTIR. Macromolecules 39, 2841–2848 (2006).

25. Liu, T., Lim, K. P., Tjiu, W. C., Pramoda, K. P. and Chen, Z. Preparation and characterization of nylon11/organoclay nanocomposites. Polymer 44, 3529–3535 (2003).

26. M.Rubinstein and R.H.Colby. Polymer Physics Book, 3th Edition. Oxford publication. (2003).

27. Uyar, T. and Besenbacher, F. Electrospinning of uniform polystyrene fibers□: The effect of solvent conductivity. Polymer 49, 5336–5343 (2008).

28. Koombhongse, S., Liu, W. and Reneker, D. H. Flat polymer ribbons and other shapes by electrospinning. Journal of Polymer Science: Part B: Polymer Physics 39, 2598–2606 (2001).

29. Ki, C.S., Baek, D.H., Gang, K.D., Lee, K.H., Um, I.C. and Park, Y.H. Characterization of gelatin nanofiber prepared from gelatin – formic acid solution. Polymer 46, 5094–5102 (2005).

30. Chowdhury, M. and Stylios, G. Effect of experimental parameters on the morphology of electrospun Nylon6 fibres. International Journal of Basic and Applied Sciences 10, 70–78 (2010).

31. Scheinbeim, J. I. and Newman, B. A. Ferroelectric polarization mechanisms in Nylon11. Macromolecules 25, 3729–3732 (1992).

32. Prevorsek, D. C., Butler, R. H. and Reimschuessel, H. K. Mechanical Relaxations in Polyamides. Journal of Polymer Science: Part A-29, 867–886 (1971).

33. Gogolewski, S. Effect of annealing on thermal properties and crystalline structure of polyamides . Nylon11 (polyundecaneamide). Colloid and Polymer Science 257, 811–819 (1979).

34. Kim, K. G., Newman, B. A. and Scheinbeim, J. I. Temperature dependence of the crystal structures of Nylon11. Journal of Polymer Science: Polymer Physics Edition 23, 2477–2482 (1985).

35. Sasaki, T. Notes on the polymorphism in Nylon11. Polymer Letters 3, 557–560 (1965).

36. Balizer, E., Fedderly, J., Haught, D., Dickens, B. and Dereggi, A. S. FTlR and X-ray study of polymorphs of Nylon11 and relation to ferroelectricity. Journal of Polymer Science: Part B: Polymer Physics 32, 365–369 (1994).

37. Jacobs, E. W., Hicks, J. C., Jacobs, E. W. and Hicks, J. C. Electric field induced morphological changes in Nylon11. Applied Physics Letters 44, 402–403 (1984).

38. Nair, S. S., Ramesh, C. and Tashiro, K. Polymorphism in Nylon-11□: Characterization using HTWAXS and HTFTIR. Macromolecular Symposia 242, 216–226 (2006).

39. Zhang, X., Xie, T. and Yang, G. Isothermal crystallization and melting behaviors of Nylon11/Nylon 66 alloys by in situ polymerization. Polymer 47, 2116–2126 (2006).

40. Behler, K., Havel, M. and Gogotsi, Y. New solvent for polyamides and its application to the electrospinning of polyamides11 and 12. Polymer 48, 6617–6621 (2007).

41. Frubing, P., Kremmer, A., Gerhard-multhaupt, R., Spanoudaki, A. and Pissis, P. Relaxation processes at the glass transition in polyamide11□: From rigidity to viscoelasticity. The Journal of Chemical Physics 125, 214701 (2006).

42. Arroyo, M. and Lo, M. A. Thermal and dynamic mechanical properties of polypropylene and short organic fiber composites. Polymer 41, 7761–7767 (2000).

43. Nunez, L., Gomez-Barreiro, S., Gracia-Fernandez, C. A. and Nunez, M.R. Use of the dielectric analysis to complement previous thermoanalytical studies on the system diglycidyl ether of bisphenol A/1,2 diamine cyclohexane. Polymer 45, 1167–1175 (2004).

44. Il, Y., Sik, H., Seok, W., Seung, T. and Ho, W. Superhydrophobicity of PHBV fibrous surface with bead-on-string structure. Journal of Colloid and Interface Science 320, 91–95 (2008).

45. Ma, M., Hill, R. M. and Rutledge, G. C. A review of recent results on superhydrophobic materials based on micro- and nanofibers. Journal of Adhesion Science and Technology 22, 1799–1817 (2008).

46. Yang, F., Murugan, R., Wang, S. and Ramakrishna, S. Electrospinning of nano/micro scale poly (L-lactic acid) aligned fibers and their potential in neural tissue engineering. Biomaterials 26, 2603–2610 (2005).

47. Zhou, Y., Yang, D., Chen, X., Xu, Q. and Lu, F. Electrospun water-soluble carboxyethyl chitosan/Poly(vinyl alcohol) nanofibrous membrane as potential wound dressing for skin regeneration. Biomacromolecules 9, 349–354 (2008).

48. Areias, A. C., Ribeiro, C., Sencadas, V. and Garcia-giralt, N. Influence of crystallinity and fiber orientation on hydrophobicity and biological response of poly (L -lactide) electrospun mats. Soft Matter 8, 5818–5825 (2012).

49. Chuysinuan, P., Pavasant, P. and Supaphol, P. Preparation and characterization of caffeic acid-grafted electrospun poly(L-Lactic acid) fiber mats for biomedical applications. Applied Materials and Interfaces 4, 3031–3040 (2012).

50. Alvarez-perez, M. A., Guarino, V., Cirillo, V. and Ambrosio, L. Influence of gelatin cues in PCL electrospun membranes on nerve outgrowth. Biomacromolecules 11, 2238–2246 (2010).

Chapter 4

Surface Modification of Nylon11 Electrospun Mats

The main objective of this chapter was to convert the hydrophobic Nylon11 mats to hydrophilic mats in order to facilitate cell growth. The novel method used to modify Nylon11 electrospun mats also ensured that the hydrophilicity is retained for long time.

4.1 Introduction

As mentioned in chapter 3, Nylon11 electrospun mats exhibit hydrophobic nature with the water contact angle value of 135 °. In order to use Nylon11 electrospun mats for growing cells, it is necessary to make them hydrophilic and thereby facilitate cell growth. D'brotto etal[1] have proposed a novel method for converting hydrophobic polymeric surfaces to hydrophilic surfaces using gold nanoparticles (GNPs). In the present work we have used D'brotto's surface modification method to convert the Nylon11 hydrophobic electrospun mats to hydrophilic mats.

Polymer surfaces are usually modified to increase or decrease the surface hydrophilicity (wettability), roughness, ionic charge or pH, and impurities[2-4]. Several methods are available to modify polymer surfaces. Some examples are acid etching and plasma treatment. Among these, plasma treatment is more widely used because it is a solvent free process and allows facile modification of the physical and chemical properties without affecting their bulk properties[5]. Plasma treatment can be used for incorporating desired functional groups on the surfaces. This is done by introducing various gases during plasma treatment such as O_2[6], H_2, N_2, NH_3[7], Argon[8] etc. The wetting behavior of a solid surface depends not only on surface chemistry but also on the surface roughness. Plasma treatment also induces surface roughness naturally.

D'brotto etal had demonstrated the surface modification of poly (etherimide) (PEI) film with plasma treatment followed by GNP and Lysin attachments. The initial water contact angle of the PEI film was 90 °. After the surface modification the water contact angle of the PEI film reduced to 25 °. They showed that PEI film treated with plasma and attached with GNPs and Lysin enhanced the cell proliferation rate.

In this work, two surface modification techniques are deployed to modify the surface of Nylon11 electrospun mats: Plasma treatment and plasma treatment followed by GNP attachment. Plasma treatment was done in presence of N_2 and H_2 so that primary amine groups are created on the mat surfaces. It is well known that GNPs have strong affinity to amine groups[9]. Thus it is anticipated that the GNPs will strong adsorb on the plasma treated mats because of the amine groups. The surface modified Nylon11 electrospun mats were characterized by using SEM, TEM and TGA. Furthermore, contact angle measurements were performed over an extended period of time to compare the longevity of the surface modification of just plasma treated mats and plasma treated mats with gold nanoparticles.

4.2 Materials and Methods

4.2.1 Materials and Electrospinning Process

Chloroloauric acid was procured from Sisco Research Laboratory. Electrospun mats were prepared from 20wt/vol% solution of Nylon11 in formic acid at an operating voltage of 20 kV, flow rate of 0.2 ml/min and distance between the electrodes 10 cm. These mats were further used for surface modification studies.

4.2.2 Plasma Treatment Process

The Nylon11 electrospun mats were exposed to plasma by using K1050 X Plasma Asher (power output 0-100 W, Radio frequency (RF) 13.56 MHz). Hydrogen and Nitrogen gases were introduced in the plasma chamber. Their presence is expected to result in the formation of amine (NH_2) groups on the Nylon11 electrospun mats. The Nylon11 electrospun mats were placed on the metal plate holder located inside the Plasma reactor. After the samples were loaded, the plasma reactor was first pumped to a base pressure of $6x10^{-1}$ mbar. Then the gas mixture N_2 and H_2 was introduced into the plasma reactor and the pressure was maintained at 5 bar. RF power of 70 W was applied to initiate and sustain plasma. The plasma ashing time was set to 15 min.

4.2.3 Synthesis of Gold Nanoparticles

Gold nanoparticles were synthesized by using chloroauric acid ($HAucl_4$) of 0.1 mM solution. 100 µl of chloroauric acid and 100 ml of deionized (DI) water were kept in a constant temperature bath at 70 °C for 10 min. 1 g of citric acid was added to the hot solution. Within 1-2 min the color of the solution changed to purple, which indicated that the gold nanoparticles were formed.

UV- Spectroscopic measurements of gold solution was carried out using a Perkin Elmer Lambda 950 UV-Vis spectrophotometer operated at a resolution of 2 nm. Figure 4.1 shows the UV–visible data for the aqueous gold solution. The spectrum exhibits an absorption band at 530 nm, indicating that gold nano particles 10-20 nm[10] size was formed.

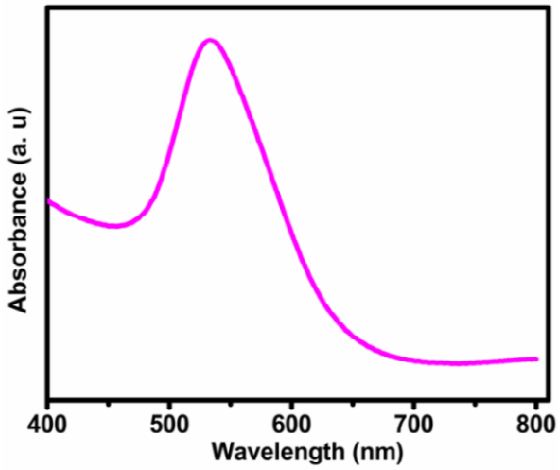

Figure 4.1 UV-visible spectroscopy of gold solution.

In the next step, the plasma treated Nylon11 electrospun mats were immersed in the gold sol for 12 hrs at room temperature. After 12 hrs, the electrospun mats were removed and kept under vacuum for 2 hrs. The change in colour of the electrospun mats confirms the attachment of gold nanoparticles; this is shown in Figure 4.2. In the next step, 50 mg of L-Lysin was dissolved in the deionized (DI) water. The GNP containing electrospun mats were immersed in the Lysin solution for 12 hrs.

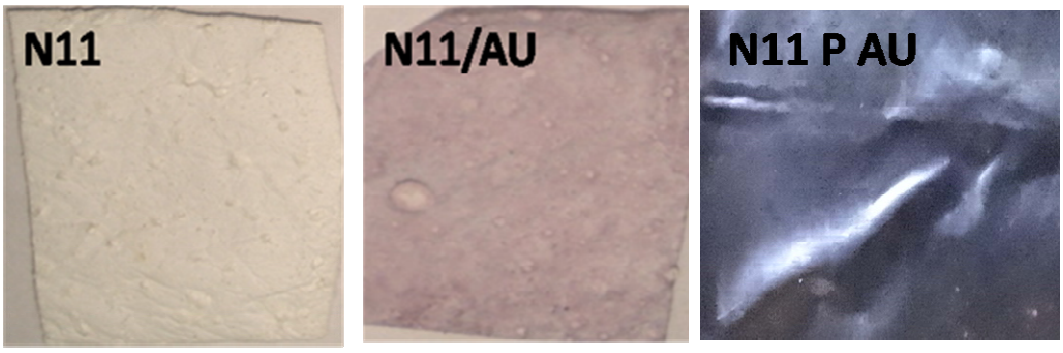

Figure 4.2 Nylon11 electrospun mats, Nylon11 electrospun mats with gold nanoparticles and plasma treated Nylon11 electrospun mats with gold nanoparticles.

4.2.4 Characterization

The morphology of Nylon11 surface modified electrospun mats were studied by using Leica-440 Scanning Electron Microscope (SEM) operated at 20 kV. Electrospun mats were directly mounted on the SEM sample holder and the micrographs of representative areas were recorded at different magnifications. The sample surfaces were coated with gold to avoid specimen charging. Gold nanoparticles and surface

modified Nylon11 electrospun mats were also characterized using Transmission Electron Microscopy (JEOL–JEM-2010 UHR) at accelerating voltage of 200 kV and 80 kV. TEM sample of as-synthesized GNPs were prepared by placing drops of dispersion containing GNPs on the carbon coated copper grids. Surface modified electrospun mats were cut into small pieces and allowed to float on water. Fibers were collected on copper grids.

Crystalline structures of the samples were characterized using a Rigaku Model Dmax 2500 X-ray diffractometer with Cu/K_α radiation, operating at 40 kV and 100 mA. The samples were scanned over the 2 θ range of 10-50 °. FTIR studies were carried out using Perkin Elmer Spectrophotometer in ATR mode. Spectra were recorded over the frequency range of 3500-500 cm^{-1} and resolution of 4 cm^{-1}. Thermal stability of Nylon11 and surface modified Nylon11 electrospun mats was studied using Perkin Elmer Simultaneous Thermal Analyzer 6000 (STA 6000) over the temperature range of 30 to 550 °C at a heating rate of 20 °C/min. The test was carried out in Nitrogen atmosphere. The percent weight loss of sample was measured as a function of temperature.

4.2.5 Water Contact Angle Study

The hydrophilicity of the Nylon11 electrospun mats was measured in terms of contact angle of water drops. Electrospun mats were placed on the sample holder stage of contact angle instrument (Digidrop Instrument- Rame-Hart 100 Goniometer GBX). A drop of deionized water (1-3 µl) was placed on the sample surfaces. Images of the water droplet were recorded using a video camera. It was observed that for hydrophilic surfaces the water droplet spread immediately, whereas with gradual decrease in hydrophilic nature of the substrate the water droplet took a finite measurable time to spread. The time required for the droplet to spread on the surface was measured and was considered as a measure of the hydrophilicity of the surface. The water droplet spreads quickly on hydrophilic surfaces, whereas it takes a longer time to spread on partially hydrophobic surfaces. Electrospun mats modified with plasma and plasma plus GNPs were preserved in a closed container at ambient conditions for upto 100 days and contact angle measurements were done every 10 days. Electrospun mats were dried in a vacuum oven at 70 °C for 4 hrs before performing the water contact angle measurement.

4.3 Results and Discussion

4.3.1 Scanning Electron Microscopy

Figure 4.3 shows SEM micrographs of plasma treated electrospun mats, plasma treated mats having attached gold nanoparticles, and EDAX mapping of surface modified Nylon11 electrospun mats. The SEM image (Figure 4.3 A) of plasma treated electrospun mats is similar to the image of untreated Nylon11 mats given in chapter 3 (Figure 3.5). The diameter of electrospun fibers was in the range of 700-800 nm. The average fiber diameter of the plasma treated electrospun mats was also 700-800 nm, from which it is clear that plasma treatment does not affect the morphology of the Nylon11 electrospun mat surface.

The SEM image of mat immersed in GNP solution (Figure 4.3 B) shows that gold nanoparticles are adhered to the mat surface. This was also confirmed by EDAX mapping (Figure 4.3 C) of the surface of Nylon11 electrospun mats.

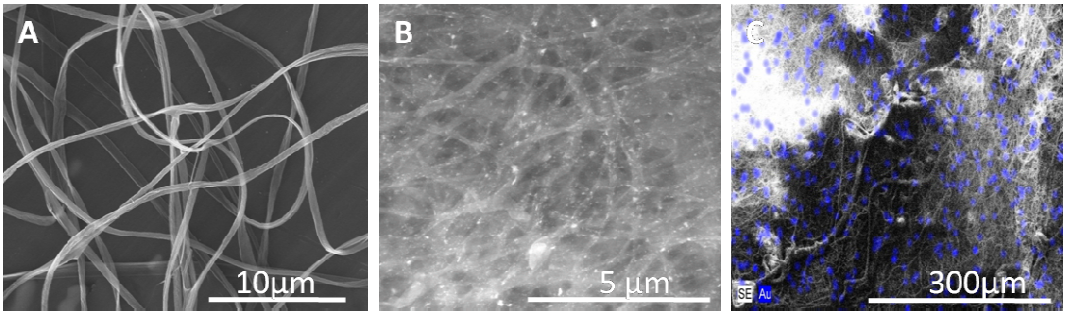

Figure 4.3 (A) SEM images of Nylon11 plasma treated electrospun mats, (B) Plasma treated followed by GNP attachement, (C) EDAX mapping of mat shown in B.

4.3.2 TEM of Nylon11 Surface Modified Electrospun Mats

Figure 4.4 shows TEM images of gold nanoparticles and electrospun mats whose surface is modified by GNPs (Figure 4.4 A and B). TEM images show that gold nanoparticles are polyhedral[11]. The size of the gold nano particles was measured using Image J. Approximately 150 particles were used for the analysis. The average size of the gold nanoparticles was found to be 15±5 nm. TEM images of surface modified electrospun mat show that the gold nanoparticles are attached to the mat surfaces[12-14] (Figure 4.4 D, E and F).

Upon sonication for 4 hrs, the gold nanoparticles still remained adhered to the electrospun mat (Figure 4.4 G, H and I). This indicates that the gold nanoparticles

were strongly adsorbed on the mats. The strong adsorption could be due to the interaction of GNPs with amine functional groups on the mats which are created by the plasma treatment method. Thus it is likely that the GNPs are chemi-sorbed on the mats. As a control, we also immersed Nylon11 electrospun mats, which are not plasma treated, in GNP solution. The surface of these mats also show GNPs adhered the fibers. However, these mats were not as hydrophilic as those treated with plasma.

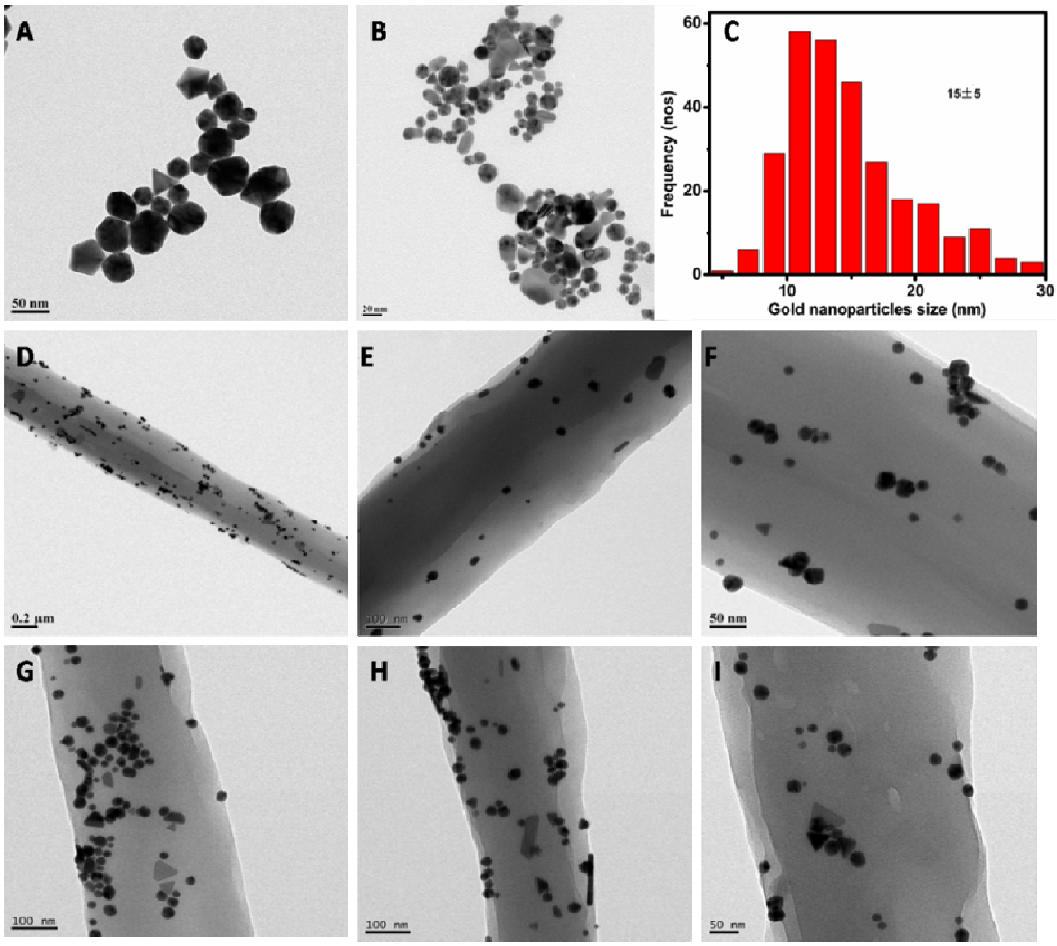

Figure 4.4 TEM image of gold nanoparticles (A and B), Gold nanopraticles size distribution (C), surface modified Nylon11 mats (D, E and F), surface modified Nylon11 mats after 4 hrs sonication (G, H and I).

4.3.3 X-ray Diffraction and Fourier Transforms Infrared Spectroscopy (FTIR) Studies

XRD studies revealed that Nylon11 electrospun mats and surface modified mats exhibit gamma crystalline structure. The diffraction peaks were discussed in Chapter 3. In addition, the surface modified electrospun mats also show 2θ reflections at 37 °,

45 °, 65 ° and 78 °, which corresponds to the characteristic of (111), (200), (220) and (311) plane[15] of face centered cubic GNPs.

In FTIR scans Amide I and Amide II bands were observed at 1636 cm^{-1} and 1539 cm^{-1} for Nylon11 mats and at 1638 cm^{-1} and 1545 cm^{-1} for Nylon11 surface modified mats. The asymmetric and symmetric CH_2 appeared at 2920 cm^{-1} and 2049 cm^{-1} for both the Nylon11 and surface modified Nylon11 mats[16]. The amide band (N-H stretch) was seen at 3304 cm^{-1} for Nylon11 mats and 3306 cm^{-1} for surface modified mats. Plasma treatment is expected to produce primary amine groups on the surface modified mats but since secondary amine groups are already present in the Nylon11, it was not possible to detect the primary amines by FTIR.

4.3.4 Thermo Gravimetric Analysis (TGA)

Figure 4.5 shows the weight loss % as a function of temperature for Nylon11 electrospun mat and Nylon11 surface modified electrospun mat. The degradation of Nylon11 starts at 401 °C, whereas the degradation of Nylon11 surface modified electrospun mats begin at 425 °C. The decomposition temperatures (first derivative peak temperatures) of Nylon11 and surface modified electrospun mats were 453 °C and 470 °C. Thus the incorporation of gold nanoparticles enhanced the thermal stability[17] of Nylon11 electrospun mats.

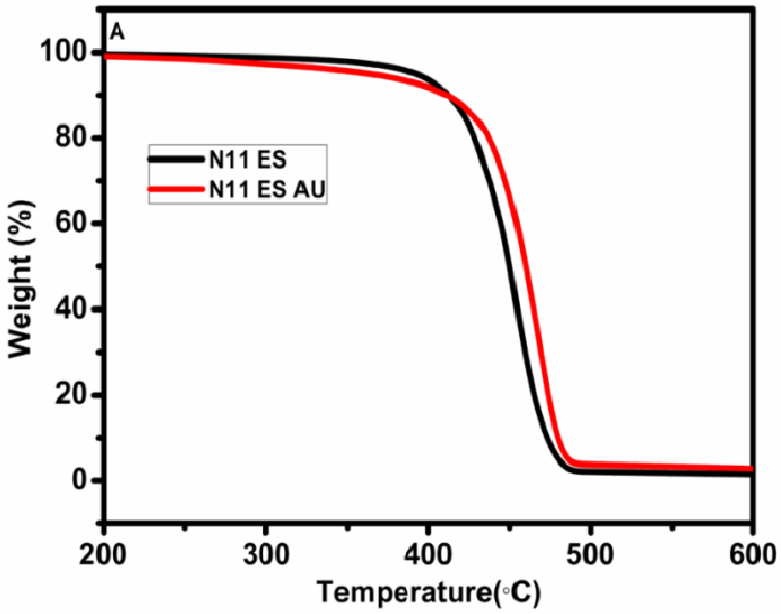

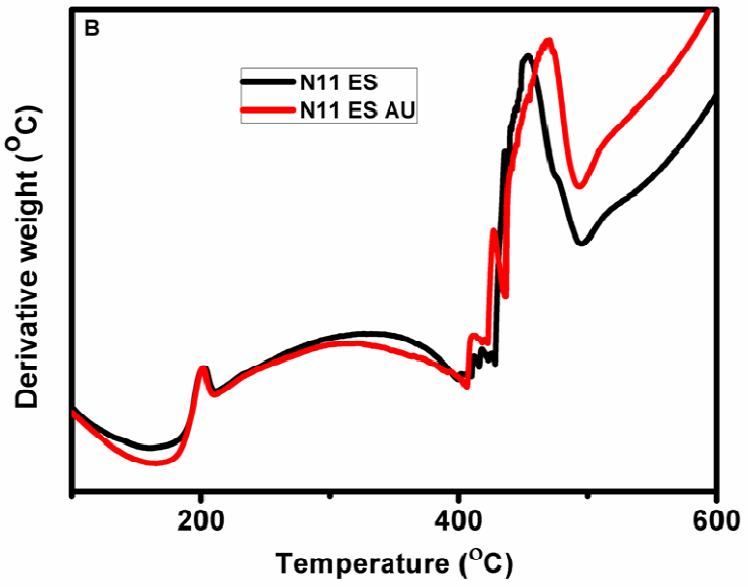

Figure 4.5 Weight percent with respect to temperature of Nylon11 and Nylon11 surface modified electrospun mats (A), first derivative peak of Nylon11 and surface modified Nylon11 elelctrospun mats (B).

The residue was calculated at 700 °C for Nylon11 electrospun mats and Nylon11 surface modified electrospun mats. The Nylon11 electrospun mats gave a residue of 1.0 % while the Nylon11 surface modified electrospun mats gave a residue of 1.8 %. This suggested that the surface modified mats had about 0.8 % by weight of GNPs on their surfaces.

4.3.5 Longevity Study of Surface Modified Mats

The contact angles of the Nylon11 mats after the two surface treatments were found to be much lower than that of the unmodified mats. As mentioned in chapter 3, the contact angle for the unmodified electrospun mat was 135 °. Immediately upon surface modification by plasma treatment and plasma treatment followed by GNP attachment, the initial contact angles of the modified mats were too small to be measured. The water drop essentially spread and wetted the mats rapidly.

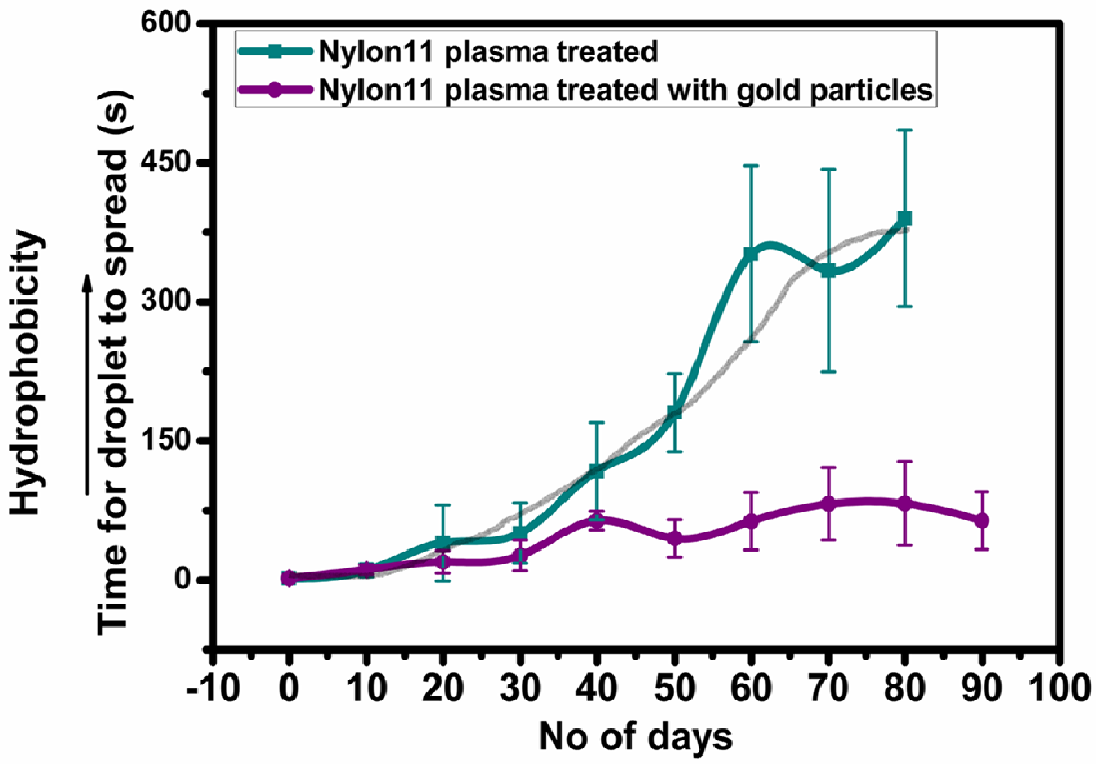

Figure 4.6 Longevity study of the surface modification of plasma treated mat and plasma treated mat with gold nanoparticles. Lines through the data are guides for the eye.

The longevity of the surface modification achieved by the two methodologies was assessed through contact angle measurements as a function of aging time. Upon aging, the initial contact angle of the drop increased to 30-45 °. However, the drop eventually spread out within a finite measurable time. As mentioned earlier, the time it took for the drop to spread and wet the mats was considered as being indicative of the extent of hydrophilicity of the mat. An increase in spreading time suggests loss of hydrophilicity. Note that for an untreated Nylon11 mat, a water drop on its surface does not spread for more than 500 s. Thus as evident from Figure 4.6, the plasma treated mat lost its hydrophilicity with time[18,19]. This was attributed to the segmental motion of surface polymer chains which causes the hydrophilic amine groups to be buried in the bulk[20] where it is thermodynamically more stable compared to being exposed to the hydrophobic polymer-air interface. Hence the plasma treated mat lost its hydrophilicity with time. On the other hand the amine groups attached to the gold nanoparticles cannot be buried in the bulk because of the large size of the gold nanoparticles. As a result, the electrospun mat retained its hydrophilicity for longer time. This is schematically shown in Figure 4.7.

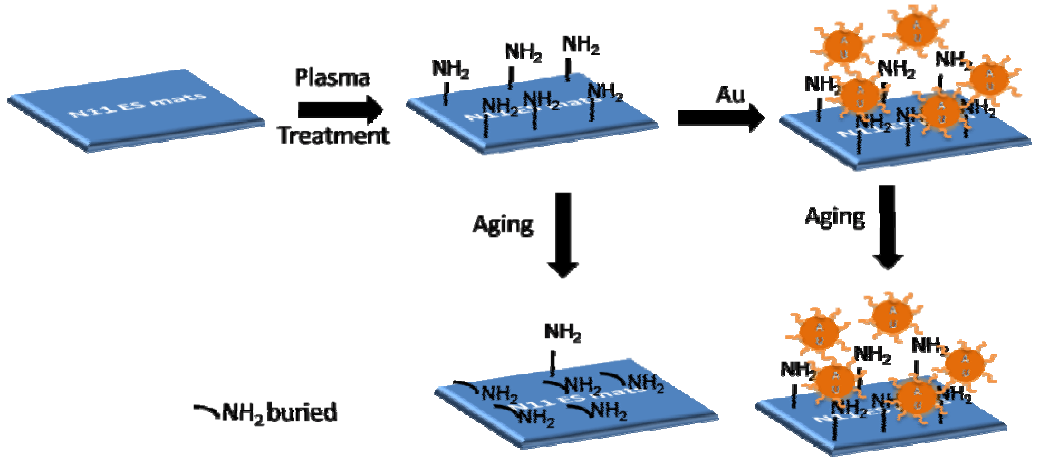

Figure 4.7 A schematic representation of the Nylon11 surface modification process.

4.3.6 Cell Culture Study

Cell culture procedure was the same as that described in the chapter 3. MTT assay results of 2nd and 5th day are shown in Figure 4.8. Interestingly, the Nylon11 electrospun mats exhibit higher cell proliferation rate compared to Nylon11 electrospun mat treated with plasma and GNPs. A likely reason behind this could be that cells are negatively charged and the surface modified gold nanoparticle is also negatively charged. The zeta potential of the GNPs solution was -40. As a result, cells have low affinity towards the surface modified mats. Upon coupling Lysin on the GNPs, the surface change is rendered positive. As a result Lysin treatment again enhanced the cell proliferation rate. Cells are more attracted towards the positive charged Lysin.

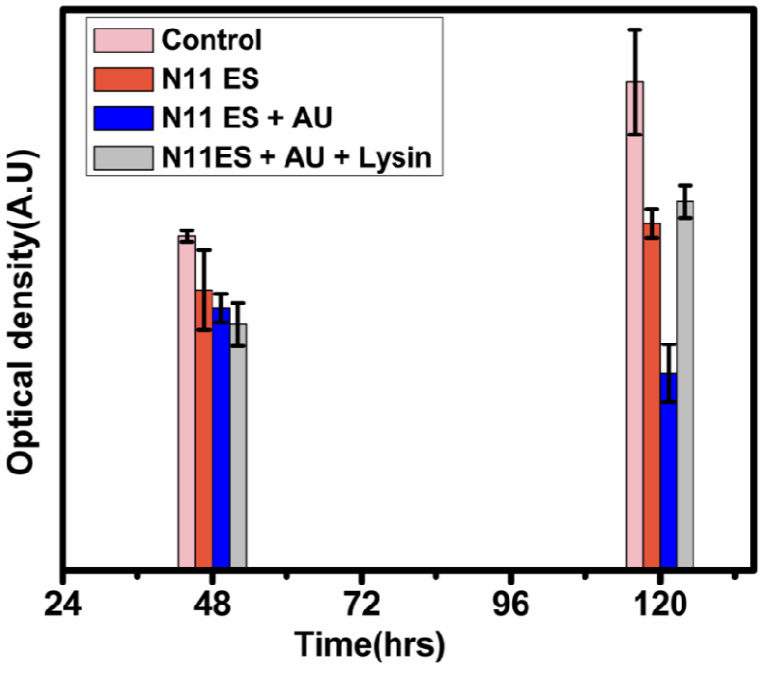

Figure 4.8 MTT assay of Nylon11 electrospun mat, Nylon11 electrospun mat with gold nanoparticles and Nylon11 electrospun mat with gold nanoparticles treated with Lysin

4.4 Conclusions

SEM and TEM images show that gold nanoparticles are attached on the Nylon11 electrospun mat. The thermal stability of surface modified electrospun mats were enhanced with the incorporation of gold nanoparticles. Water contact angle study shows that plasma treated electrospun mat loses its hydrophilicity with time whereas plasma treated electrospun mat with gold nanoparticles retains its hydrophilicity for a longer time.

4.5 References

1. Britto, V. D., Tiwari, S., Purohit, V., Wadgaonkar, P. P., Bhoraskar, S. V., Bhonde, R. R. and Prasad, B. L. V. Composites of plasma treated poly (etherimide) films with gold nanoparticles and lysine through layer by layer assembly□: A “friendly-rough” surface for cell adhesion and proliferation for tissue engineering applications. Journal of Materials Chemistry 19, 544–550 (2009).

2. Kang, E. T., Neohs, J. K. G., Tan, K. L., Y.Uyama., Morikawa, N. and Ikada, Y. Surface modifications of polyaniline films by graft copolymerization. Macromolecules 25, 1959–1965 (1992).

3. Gun, J., Rizkov, D., Lev, O., Abouzar, M. H., Poghossian, A. and Schoning, M. J. Oxygen plasma-treated gold nanoparticle-based field-effect devices as transducer structures for bio-chemical sensing. Microchim Acta 164, 395–404 (2009).

4. France, R. M. and Short, R. D. Plasma treatment of polymers□: Effects of energy transfer from an argon plasma on the surface chemistry of poly(styrene), low density poly(ethylene), poly(propylene) and poly(ethylene terephthalate). Journal of the Chemical Society, Faraday Transactions. 93, 3173–3178 (1997).

5. Yan, D., Jones, J. and Lee, J. C. Plasma treatment of random and aligned electrospun PCL nanofibers. Journal of Medical and Biological Engineering 33, 171–178 (2013).

6. Banik, I., Soo, K., Il, Y., Ho, D., Mo, C, Park, C. S., Sur, G. S. and Park, C. E. A closer look into the behavior of oxygen plasma-treated high-density polyethylene. Polymer 44, 1163–1170 (2003).

7. Li, S., Han, K., Rong, H., Li, X. and Yu, M. Surface modification of aramid fibers via Ammonia-Plasma treatment. Journal of Applied Polymer Science 40, 1–6 (2014).

8. Sajdl, P., Bla, O., Slepic, P., Sajdl, P., Blahova, O., Sutta, P. and Hantavicz, V. Gold Coating of poly (ethylene terephthalate) modified by Argon plasma. Plasma Processes and Polymers 4, 69–76 (2007).

9. Sainsbury, T., Ikuno, T., Okawa, D., Pacile, D., Fre, J. M. J. and Zettl, A. Self-assembly of gold nanoparticles at the surface of amine- and thiol-functionalized boron nitride nanotubes. Journal of Phys. Chem. C 111, 12992–12999 (2007).

10. Sugunan, A., Thanachayanont, C., Dutta, J. and Hilborn, J. G. Heavy-metal ion sensors using chitosan-capped gold nanoparticles. Science and Technology of Advanced Materials 6, 335–340 (2005).

11. Namazi, H., Mohammad, A. and Fard, P. Preparation of gold nanoparticles in the presence of citric acid-based dendrimers containing periphery hydroxyl groups. Materials Chemistry and Physics 129, 189–194 (2011).

12. Bai, J., Li, Y., Yang, S., Du, J., Wang, S., Zhang, J., Wang, Y., Yang, Q., Chen, X. and Jing, X. A simple and effective route for the preparation of poly (vinylalcohol) (PVA) nanofibers containing gold nanoparticles by electrospinning method. Solid State Communications 141, 292–295 (2007).

13. Ravichandran, R., Sridhar, R., Venugopal, J. R., Sundarrajan, S. and Ramakrishna, S. Gold nanoparticle loaded hybrid nanofibers for cardiogenic differentiation of stem cells for infarcted myocardium regeneration. Macromolecular Bioscience 1–11 (2013).

14. Dhakal, K. P., Lee, H., Lee, J., Lee, H. and Kim, J. Gold nanoparticles Hybridized rubrene nanofibers made by electrospinning: enhancement of optical and structural properties. Journal of Materials Chemistry C 2, 1830–1835 (2014).

15. Luong, N. D., Oh, J., Lee, Y., Yeon, J. H., Hur, J., Park, J. J., Kim, J. M. and Nam, J. D. Immobilization of gold nanoparticles on poly (methyl methacrylate) electrospun fibers exhibiting solid-state surface plasmon effect. Surface and Interface Analysis 44, 318–321 (2012).

16. Nair, S. S., Ramesh, C. and Tashiro, K. Polymorphism in Nylon-11□: Characterization using HTWAXS and HTFTIR. Macromolecular Symposia 242, 216–226 (2006).

17. Cohen-karni, T., Jeong, K. J., Tusi, J. H., Reznor, G., Mustata, M., Wanunu, M., graham, A., Marks, C., Bell, D. C., Langer, R. and Kohane, D. S. Nanocomposite gold-Silk nano fibers. Nano Letters 12, 5403–5406 (2012).

18. Yun, Y. O. I. L., Kim, K. S. O. O. and Uhm, S. Aging behavior of oxygen plasma-treated polypropylene with different crystallinities. Journal of Adhesion Science and Technology 18, 1279–1291 (2004).

19. Hyun, J. A new approach to characterize crystallinity by observing the mobility of plasma treated polymer surfaces. Polymer 42, 6473–6477 (2001).

20. Canal, C., Molina, R. and Bertran, E. Wettability, ageing and recovery process of plasma-treated polyamide6. Journal of Adhesion Science and Technology 18, 1077–1089 (2004).

Chapter 5

Electrospun Mats of Nylon11 Blends and Composites

Nylon11 can be blended with other polymers and inorganic fillers to enhance its properties. In this chapter we describe our work on Nylon11/PHB biocompatible blends prepared from different processing techniques such as melt blending, solution blending and electrospinning. We also describe the preparation and characterization of Nylon11/ZnO nano composites prepared by electrospinning.

5.1 Nylon11/PHB Blends

5.1.1 Introduction

A polymer blend is a mixture of two or more polymers blended together to create a new material with different physical properties. An effective blending methodology can be utilized to tailor-make morphology and performance of the material for a specific purpose[1]. Polymer blending is important because it allows facile preparation of polymers with desired properties, low cost and improved processability.

A miscible polymer system shows unlimited solubility and zero interfacial tension. Therefore a mixture of miscible components is expected to result in a homogenous blend with a single Tg[2,3]. Miscibility can be influenced by various factors such as crystallization, intermolecular interaction and surface tension. An immiscible system shows limited mutual solubility and a finite interfacial tension, resulting in a multi phase structure[4,5]. For low molecular weight materials, increasing temperature generally leads to increase miscibility. For high molecular weight polymers, miscibility is usually driven by specific attractive intermolecular interactions between the compounds. For such polymers, increasing temperature can decrease miscibility. Thus liquid-liquid and polymer-solvent mixtures (that have borderline miscibility) usually exhibit upper critical solution temperature (UCST), whereas polymer mixtures often exhibit lower critical solution temperature (LCST). The most common specific intermolecular interaction occurring between two different polymer chains are hydrogen bonding[6], ionic bonds[7], dipole–dipole interaction and donor-acceptor. Polymer blends can be prepared using various techniques such as melt blending, solution casting and powder mixing. Recently electrospinning has also been used as an efficient method to produce polymer blends[8–10].

Nylon11 is thermoplastic polyamide prepared from the renewable monomer ω-amino undecanoic acid, which is obtained from castor bean oil. It has excellent properties such as high mechanical strength, good ductility, excellent resistance to solvent, improved fatigue and abrasion resistance. Nylon11 has also been blended with other polymers to obtain materials with reduced moisture sensitivity, improved toughness and dimensional stability[11]. The amide group (C=ON-H) in Nylon results in strong hydrogen bonding and crystallinity. At the same time because of the polar nature and hydrogen bonded structure, polyamides are generally immiscible with

most other polymers[12]. In addition, the high degree of interfacial tension between polyamides and other class of polymers leads to highly phase separated blends.

Nylon11 is also a possible material for tissue engineering applications. In chapter 3 we have shown that HEK293 cells can be successfully cultured on Nylon11 melt pressed film and Nylon11 electrospun mats. It is now well known that cells can be grown in a facile manner on biocompatible and biodegradable polymers such as are polyhydroxybutyrate (PHB), chitosan, polylactic acid (PLLA) and silk. Thus blends of Nylon11 and a biodegradable polymer can result in interesting scaffolds that would have controlled degradability and a pore structure that can evolve with time as the components degrade from the blends. In this work, we explore blends of Nylon11 with PHB.

Polyhydroxyalkonates are a class of naturally occurring biodegradable[13] and biocompatible polymers. Various polymers in this class are polyhydroxybutyrate (PHB), polyhydroxyvalerate (PHV), poly(3-hydroxybutyrate-co-3-hydroxyvalerate) (PHBV), polyhydroxyoctanoate (PHO), polyhydroxyhexanoate (PHH). PHB is a thermoplastic polyester which is synthesized in the cytoplasm of bacteria as an energy reserve material[14]. The structures of Nylon11 and PHB are given below:

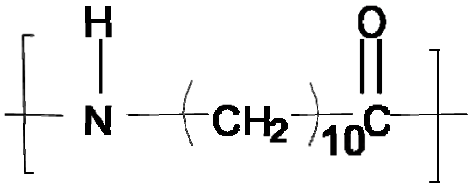

Structure of Nylon11

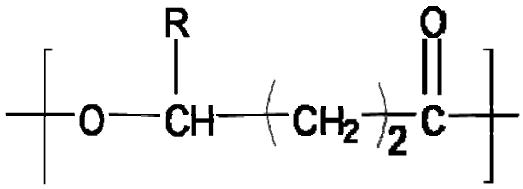

Structure of Polyhydroxybutyrate

The biocompatibility and biodegradability of PHB makes it an attractive choice for many applications such as in marine and medical applications[15]. PHB has an ability to degrade and resorb in the human body environment. This makes it a suitable candidate for implantable biomaterial that can guide tissue growth and be replaced eventually by newly formed tissues. Most properties of PHB are similar to polypropylene except that it exhibits low elongation at break and high density. The disadvantage of PHB is that it is thermally unstable, hence difficult to process. A significant number of studies on blends of PHB have been reported[16–18]. PHB has also been used to prepare non-woven mats by electrospinning for tissue engineering application. PHB by itself cannot form self-supporting electrospun mats. Peelability and mechanical strength of PHB electrospun mat are limiting issues.

The primary objective of this work was to study Nylon11 and PHB blends prepared using melt blending, solution blending and electrospinning. The effect of the processing conditions on the structure and morphology of the blends were studied. The blend compositions investigated here were Nylon11/PHB (30:70), Nylon11/PHB (50:50) and Nylon11/PHB (70:30). These blends were characterized using various techniques such as SEM, XRD, DSC, FTIR, DMA, TGA and water contact angle measurement. The electrospun mats were also characterized for their morphology and microstructure. Finally, the Nylon11, PHB and Nylon11/PHB (50:50) electrospun mats were tested in preliminary cell culture studies.

5.1.2 Materials and Methods

5.1.2.1 Materials

Nylon11 and PHB were purchased from Sigma Aldrich Chemicals and were used as is. Formic acid was procured from Merck.

5.1.2.2 Blend Preparation

Nylon11/PHB blends having composition of 30:70, 50:50 and 70:30 weight/fractions were prepared by using melt and solution blending. Melt blending was carried out using DSM co-rotating twin screw micro compounder. The polymer were blended at 200 °C using 60 rpm screw speed for 5 min. Films were prepared from the blends using a laboratory compression press at 220 °C at an applied pressure of 150 psi for 5 min. The thickness of the film was approximately 0.5 mm.

Solution blends were prepared at a fixed polymer concentration of 15 wt/vol% in formic acid which serves as the common solvent. Polymers were dissolved at constant temperature of 70 °C for 3 hrs. Solution-blended polymer films were prepared by slow evaporation of the solvent at room temperature for 48 hrs.

Blends of Nylon11 and PHB were also prepared by electrospinning from formic acid solution under the following conditions:

Solution concentration: 15 wt/vol%

Voltage: 20 kV

Flow rate: 0.2 ml/min

Distance between the electrodes: 10 cm

5.1.2.3 Characterization

Steady shear experiments were performed to measure the viscosity of Nylon11, PHB and their blend solutions. The experiments were performed on MCR 301 Rheometer (Anton Paar, Austria) using a cup and bob fixture inserted in a Peltier environmental system that was maintained at 25 ^{o}C. Conductivity of Nylon11, PHB and their blend solutions were measured using Mettler Toledo conductivity meter at room temperature. The viscosity of the melt blends were measured by using Rheometer (ARES G2). Parallel plate of 10 mm diameter was used at 200 °C and at a shear rate of 0.3 s^{-1}. The morphologies of electrospun Nylon11, PHB and their electrospun blends were studied by using Scanning Electron Microscope (SEM Leica-440) operated at 20 kV. Electrospun mats were directly mounted on the SEM sample holder and the micrographs of representative areas were recorded at different magnifications. The sample surfaces were coated with gold to avoid specimen charging. Crystalline structure of the samples was characterized using a Rigaku Model Dmax 2500 X-ray diffractometer with Cu/K_{α} radiation, operating at 40 kV and 100 mA. The samples were scanned over the 2 θ range of 10-50 °. DSC studies of Nylon11/PHB melt, solution and electrospun blends were performed on Differential Scanning Calorimeter (DSC-Q100, TA Instrument) over a temperature range of 0-220 °C and at heating and cooling rates of 10 °C/min. The tests were carried out in Nitrogen atmosphere. The melting point (T_m), crystallization temperature (T_c) and % crystallinity were determined from the first heating and cooling respectively. FTIR studies were carried out using Perkin Elmer Spectrophotometer in ATR mode. The spectra were recorded over the frequency range of 3500-500 cm^{-1} at resolution of 4 cm^{-1}. Thermal stability of Nylon11, PHB and their blends was studied using Perkin Elmer Simultaneous Thermal Analyzer 6000 (STA6000) over the temperature range of 30 to 550 °C at a heating rate of 20 ° C/min. The test was carried out in a Nitrogen atmosphere. The percent weight loss of sample was measured as a function of temperature. The viscoelastic properties of Nylon11, PHB and their melt blends were measured using Dynamic Mechanical Thermal Analyzer (RSA-3, TA Instruments). A rectangular tension-compression geometry was used. The test was carried out in linear viscoelastic region over the temperature range of -100 °C to 150 °C at a constant frequency of 10 rad/s with 0.02% strain. Water contact angle measurement was performed by using water contact angle meter (Digidrop instrument). Deionized water was used to measure the contact angle of the Nylon11 scaffolds. Water contact angle

measurement results reported here are the averages of 6 independent measurements. Nylon11 melt, solution and electrospun blends were used for contact angle measurement analysis. The cell culture procedure was same as described in the chapter 3.

5.1.3 Results and Discussion

5.1.3.1 Measurement of Viscosity and Conductivity of the Solution

15 wt/vol% solutions of Nylon11, PHB and their blends in formic acid were used for viscosity and conductivity measurements and this data is summarized in Table 5.1. The viscosity and conductivity of the Nylon11 solutions was higher than the PHB solution.

Table 5.1 Viscosity and conductivity values of Nylon11, PHB and their solution blends.

Composition	Viscosity Pa.s	Conductivity μS/cm
Formic Acid	0.0016	307
PHB	0.11	318
Nylon11/PHB (30-70)	0.08	1689
Nylon11/PHB (50-50)	0.09	2470
Nylon11/PHB (70-30)	0.10	3090
Nylon11	0.14	4310

The Figure 5.1 A and B shows viscosity and conductivity of Nylon11 solution, PHB solution and their solution mixtures. The viscosities of the blends were lower than the base polymers, which suggested an attractive interaction between the polymers. The conductivity increases as the concentration of the Nylon11 in solution is increased, as a result of which the spinnability improved with increasing Nylon11 content.

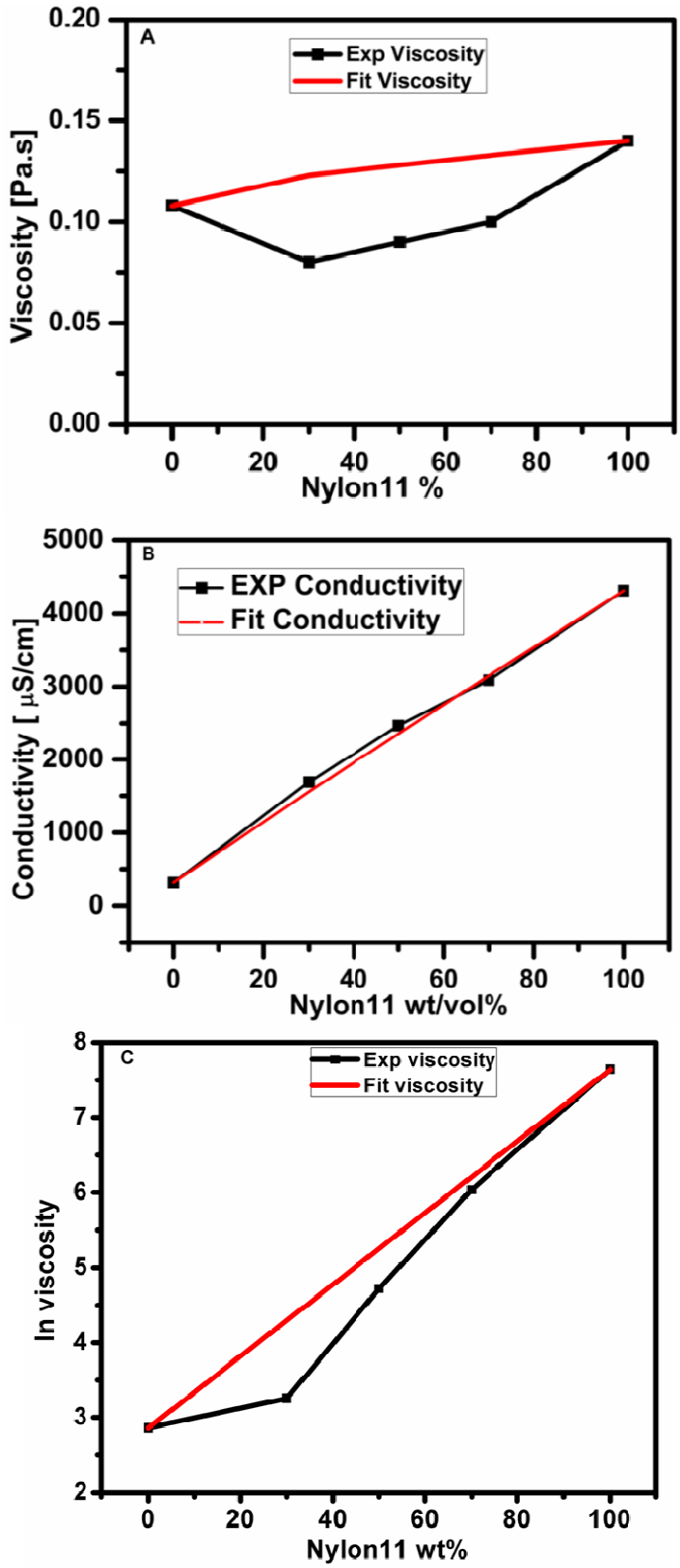

Figure 5.1 Experimentally determined and predicted values of viscosity and conductivity of Nylon11 solution**,** PHB solution and their solution blends (A and B). Experimental and predicted viscosity of Nylon11 melt, PHB melt and their melt blends at 200 °C and 0.3 shear rate (C).

The viscosity and conductivity of solutions containing Nylon11 and PHB can be estimated using the measured viscosities and conductivities of individual polymer solutions by using following equations.

$$\boldsymbol{\eta_{predicted}} = \left(\frac{\boldsymbol{\phi_{PHB}^{Blend}}}{\boldsymbol{\phi_{PHB\ solution}}}\right) * \boldsymbol{\eta_{PHB\ solution}} + \left(\frac{\boldsymbol{\phi_{N11}^{Blend}}}{\boldsymbol{\phi_{N11\ solution}}}\right) * \boldsymbol{\eta_{N11\ solution}}$$

$$\boldsymbol{\sigma_{predicted}} = \left(\frac{\boldsymbol{\phi_{PHB}^{Blend}}}{\boldsymbol{\phi_{PHB\ solution}}}\right) * \boldsymbol{\sigma_{PHB\ solution}} + \left(\frac{\boldsymbol{\phi_{N11}^{Blend}}}{\boldsymbol{\phi_{N11\ solution}}}\right) * \boldsymbol{\sigma_{N11\ solution}}$$

Where η is the viscosity, σ is the conductivity and φ is the volume fraction.

The above equation assumes validity of the law of additivity of mixtures. The predicted conductivity values of solution blends are in good agreement with experimental data. On the other hand, Nylon11/PHB solution blends exhibit negative deviation from the additive rule. It is likely because of small attractive interaction between Nylon11 and PHB.

In the case of melt blends the viscosity values increased with increasing concentration of the Nylon11 in blends. Assuming the validity of the rule of additivity,

$$ln\eta_{Blend} = W_{PHB} * ln\eta_{PHB} + W_{N11} * ln\eta_{N11}$$

Where η is the viscosity and W are the weight fractions of the two polymers. Here again the experimental values shows a negative deviation from the additivity rule (See Figure 5.1.C).

5.1.3.2 Morphological Studies of Electrospun Fibers of Nylon11, PHB and their Blends

Figure 5.2 shows SEM micrographs of PHB, Nylon11 and their electrospun blends. The SEM images show that PHB forms branched fibers along with some beads. Also, it was observed that the PHB solution could not form continuous fibers. This may be attributed to the low conductivity of PHB solutions, which results in restricted fiber

formation. By increasing concentration of Nylon11 in the solutions, the conductivity increased, which led to improved fiber formation[19]. Increasing the solution conductivity ultimately increased charge carried by the electrospinning jet, which resulted in formation of uniform fibers. Nylon11 electrospun mats exhibited ribbon or flat fiber morphology as discussed in chapter 3. The ribbons were found to be about 600-700 nm in width. The PHB rich blends showed branched fiber like morphology, while Nylon11 rich blends showed ribbon like morphology. However Nylon11/PHB (50/50) blends were observed to show circular uniform fiber formation.

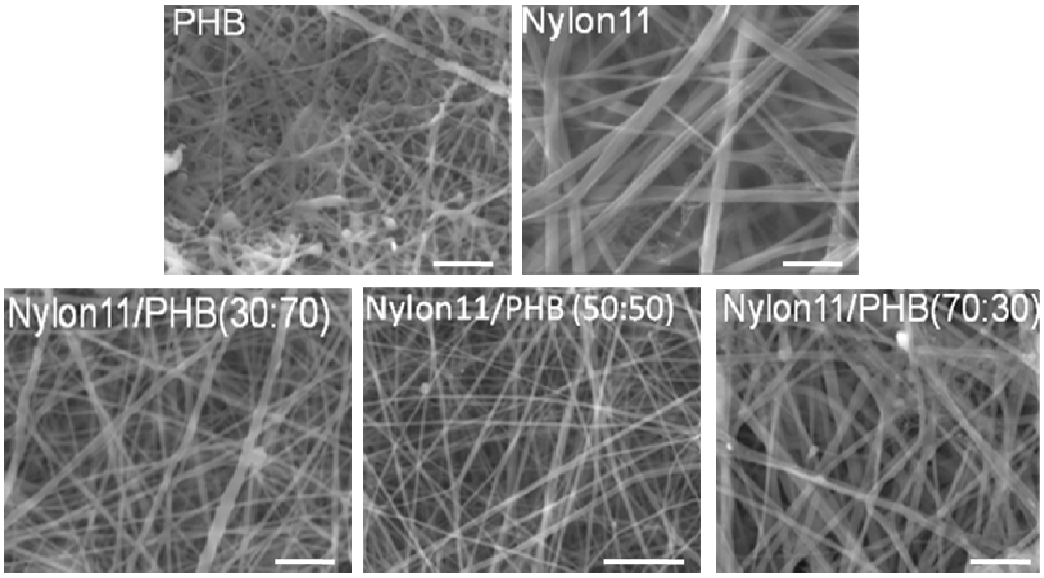

Figure 5.2 SEM micrographs of electrospun fibers of PHB, Nylon11 and their electrospun blends (scale bar = 2 microns).

5.1.3.3 X-Ray Diffraction Study

Figure 5.3 A shows wide- angle powder diffraction data for melt pressed Nylon11, PHB and their blends prepared by melt compounding. The helical alpha crystalline form of PHB show reflections at 13.40°, 17.0°, 25 ° and 27.0 °[20]. The planar zigzag beta form of PHB, which occurs because of stretching, shows reflection at 19.70 °. A coexistence of alpha and beta phase of PHB was observed in the melt compounded blends. Nylon11 in these blends exhibited alpha crystalline structure which shows characteristic reflections at the 2θ =7.20 °, 20.30 ° and 23.05 °[21].

Figure 5.3 B shows X-ray diffraction data for solution cast Nylon11, PHB and their blends. The 2 θ reflections at 6.18 °, 21.60 ° and 22.87 ° suggests Nylon11 exists in alpha and gamma crystalline structure in the solution blends. The crystalline

structure of PHB is found to be similar in melt and solution blended films. It shows the coexistence of alpha and beta crystalline form.

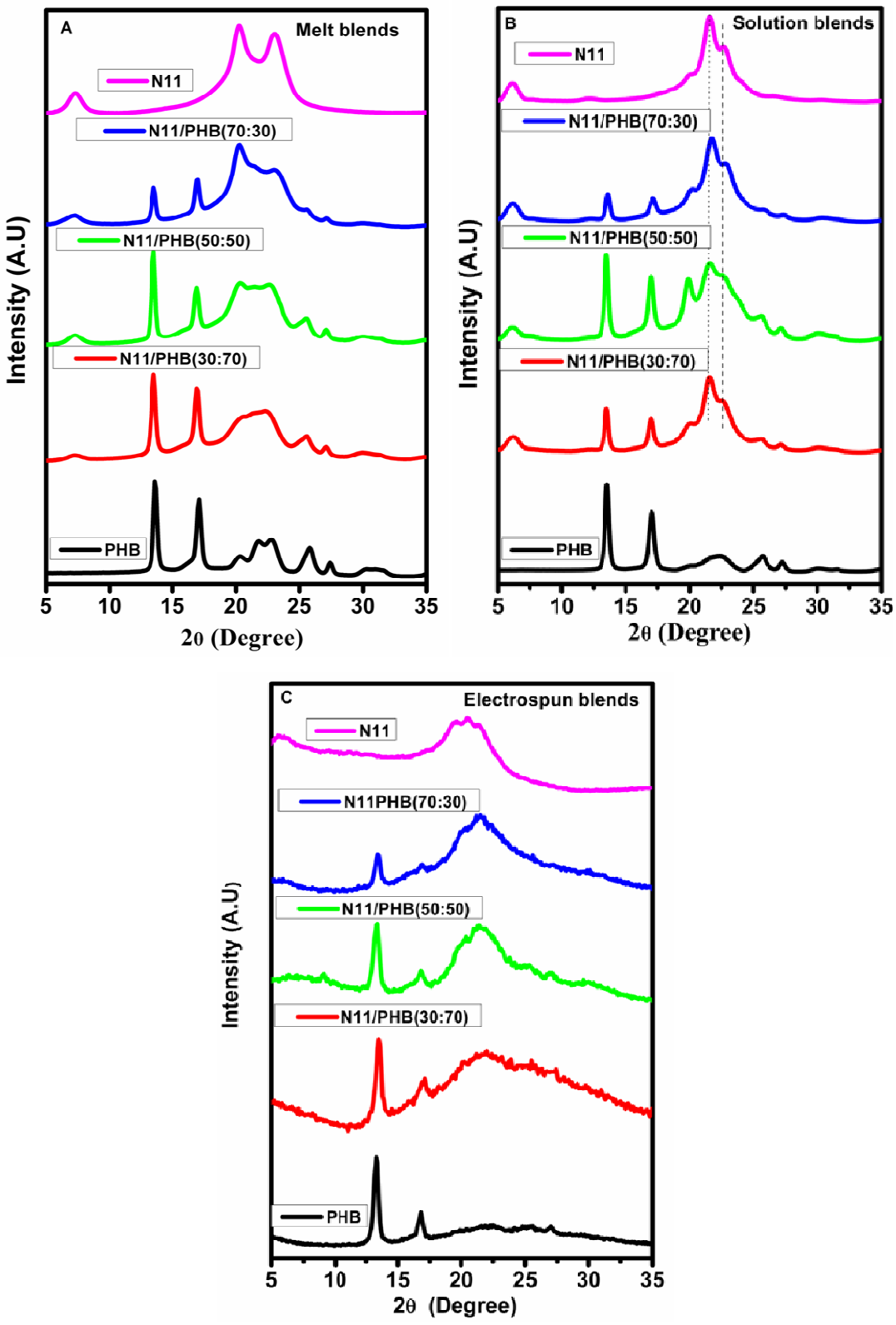

Figure 5.3 XRD studies of Nylon11, PHB and their melt, solution and electrospun blends (A-C).

Figure 5.3 C shows crystalline structures of electrospun fibers of Nylon11, PHB and their blends. Nylon11 electrospun mats exhibited weakly ordered gamma crystalline phase[22], which shows a reflection at 21.6 °. In the electrospinning process, the structure of the fibers is formed under the influence of two simultaneous processes namely the evaporation of the solvent and the elongation of the fibers. A coexistence of alpha and beta phase of PHB was observed in the electrospun blends and thus it can be concluded that PHB crystallizes to give the same microstructure irrespective of the processing techniques used here. However the long-range order of Nylon11 and PHB were found to be lower in electrospun mats.

5.1.3.4 Differential Scanning Calorimeter (DSC)

The DSC first heating and cooling curves for pure Nylon11, PHB and their electrospun blends are shown in Figure 5.4. The heating run shows endothermic temperature peaks at 189 °C and 164 °C corresponding to the melting transitions of pure Nylon11 and PHB. Nylon11/PHB blends exhibited two melting peaks in all the three blends shown in Figure 6.4 A-C. Similarly two melting peaks were observed in Nylon6/PHB blends[23]. This indicates Nylon11/PHB blends do not co-crystallize.

Cold crystallization peak of PHB was observed at 58 °C by Zhaobin Qiu etal[24]. In neat PHB we did not observe any cold crystallization peak. However, the Nylon11/PHB (70:30) melt blend, solution blends N11/PHB (50:50) and N11/PHB (70:30) exhibited cold crystallization peak at around 43°C. However Nylon11/PHB electrospun blends were observed to show cold crystallization for all compositions.

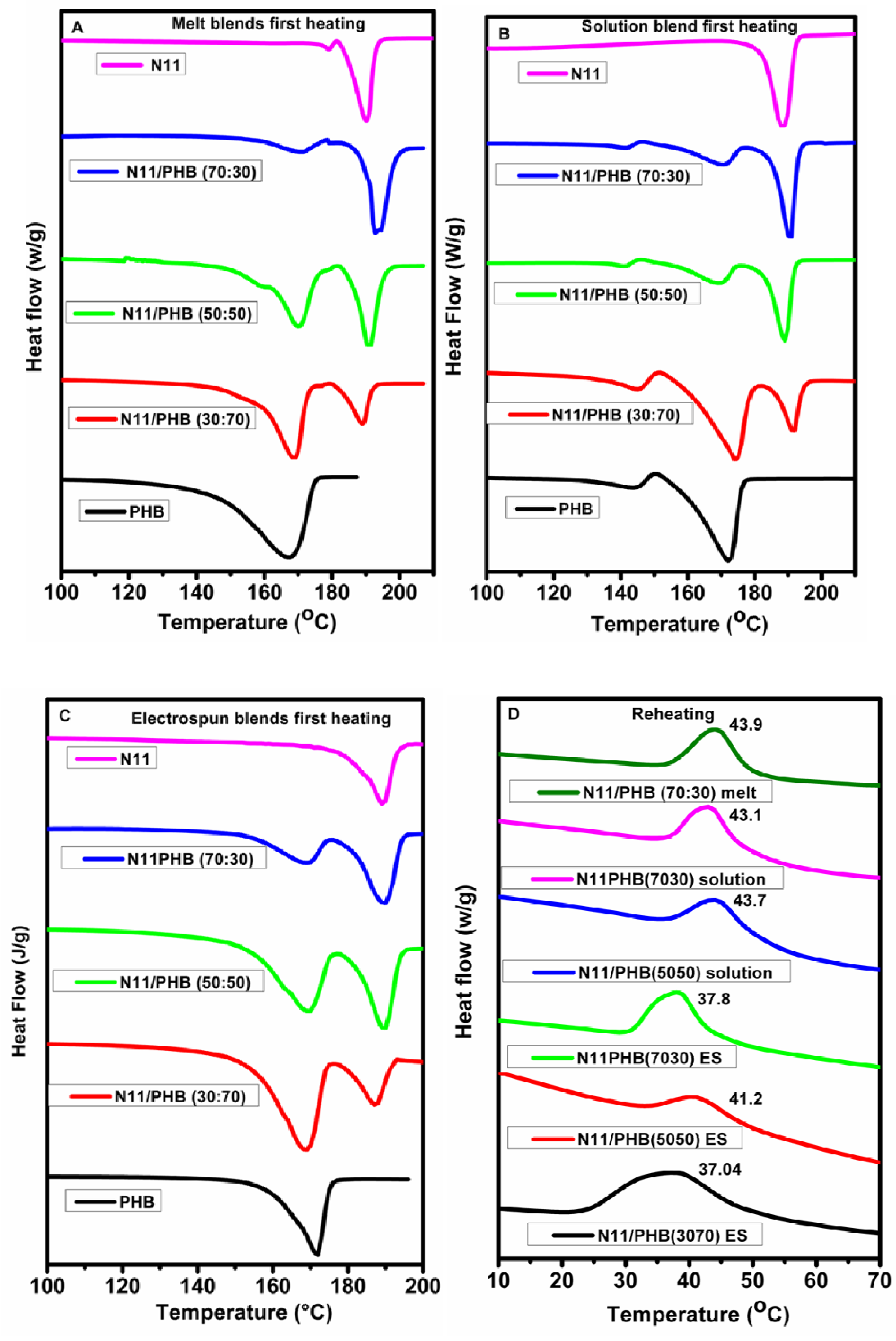

Figure 5.4 DSC first heating studies of Nylon11, PHB and their melt, solution and electrospun blends (A-C), cold crystallization peak of melt, solution and electrospun blends from DSC second heating (D).

Table 5.2 DSC first heating results of Nylon11, PHB and their melt, solution and electrospun blends.

Composition	Melt blend (First heating)						Tc (°C)	
	Tm (°C)		(ΔH_f) J/g		% Crystallinity			
	N11	PHB	N11	PHB	N11	PHB	N11	PHB
PHB	-	167.6	-	87.7	-	60.0	-	81.4
N11/PHB (30:70)	189.2	168.4	45.4	74.7	22.0	51.1	166.2	74.0
N11/PHB (50:50)	190.7	169.6	44.5	78.4	21.6	53.6	165.5	69.4
N11/PHB (70:30)	193.4	169.9	32.6	16.9	17.5	11.5	164.9	67.2
Nylon	190.3	-	55.3	-	24.4	-	163.5	-
Solution blend (First heating)								
	N11	PHB	N11	PHB	N11	PHB	N11	PHB
PHB	-	162.8		104.6		71.6	-	74.3
N11/PHB (30:70)	189.7	172.1	14.3	49.7	6.9	34.0	165.9	81.6
N11/PHB (50:50)	188.3	168.3	55.7	22.8	27.1	15.6	165.9	76.1
N11/PHB (70:30)	188.9	168.7	49.3	18.5	23.9	12.7	162.2	76.1
Nylon	189.0	-	47.1	-	44.8	-	164.5	-
Electrospun mats (First heating)								
	N11	PHB	N11	PHB	N11	PHB	N11	PHB
PHB	-	171.7	-	101.3	-	69.0	-	84.0
N11/PHB (30:70)	187.4	168.9	16.6	50.5	8.0	34.5	137.0	91.0
N11/PHB (50:50)	189.7	169.0	30.6	37.6	14.8	25.7	160.0	71.0
N11/PHB (70:30)	189.6	168.4	38.3	17.3	18.5	11.8	165.0	69.9
Nylon11	189.2	-	75.2	-	36.5	-	165.0	-

Table 5.2 shows the melting temperature and crystallinity values for both polymers in all three types of Nylon11/PHB blends. The ΔH_f values for both polymers in the blends have been calculated after accounting for the compositions. Thus, ΔH_f given in Table 5.2 is calculated as $\Delta H_{f,x}^{measured}/w_x$, where w_x is the weight fraction of the component x (x = PHB or Nylon11). Non-isothermal DSC data on Nylon11/PHB blends indicate reduced order and reduced degree of crystallinity of Nylon11 in all the three blends. The degree of crystallinity of PHB is aslo significantly reduced. For electrospun mats the rate of evaporation is high, which hinders crystal formation. However it is also accompanied by high stretching of the fiber, leading to some crystallinity in the fiber. The lower crystallinity of electrospun mat agrees with the weak order observed in the wide-angle data. The melting points of Nylon11 and PHB in blends did not show any depression relative to pure component value.

5.1.3.5 Fourier Transform Infrared Spectroscopy (FTIR)

The FTIR spectrum of Nylon11 melt pressed film is expected to show α crystalline form, whereas Nylon11 electrospun mats show spectrum corresponding to the γ crystalline form. Ramesh etal[25] have reported the FTIR bands for these two crystalline forms of Nylon11. These are documented in Table 5.3 [26-27]. The amide I band appears at 1634 cm^{-1} for α phase; for the γ phase it shifted to 1639 cm^{-1}. The amide II band appears at 1537 cm^{-1} for the α phase. It shifts to 1549 cm^{-1} for the γ phase. The amide II band arises mainly from the in-plane N-H bending and has contribution from ordered, disordered and free N-H groups. The amide band at about 3300 cm^{-1} is assigned to N-H vibration. In the Nylon11 α crystalline form this peak appears at 3302 cm^{-1} and for the γ crystalline form it is seen at 3298 cm^{-1}.

In Nylon11/PHB blends there is a likelihood of the formation of hydrogen bonding between the amide group of Nylon11 and the ester and hydroxyl groups of PHB leading some amount of miscibility. A shift in the NH and C=O stretching bands would reflect hydrogen bonding of amides groups. ATR spectra of Nylon11, PHB and their melt, solution and electrospun blends are shown in Figure 5.5. We observed that the FTIR spectra of the blends were the sum of the two individual components. This suggests that the Nylon11 and PHB do not show significant hydrogen bonding.

Table 5.3 FTIR assignments of Nylon11 and PHB.

Nylon11		**PHB**	
Peak Position (cm^{-1})	**Assignment**	**Peak position (cm^{-1})**	**Assignment**
3309 3297	NH Stretching (α) NH Stretching (γ)	1725	C=O Stretching, C=O amorphous carbonyly group
2924	Asymmetric CH_2	1453	C-H bending
2852	Symmetric CH_2	1379	Symmetric CH_3
1640 1639	Amide I (α) Amide I (γ)	1279	Asymmetric C-O-C Stretching
1537 1555	Amide II (α) Amide II (γ)	1227	CH_3 Vibration
1371		1180	Asymmetric C-O-C Stretching
1279		1100	Symmetric stretching of C-O bond
1223	C-C Stretch	1056	C-O Stretching, CH_2 rocking
1192	CH_2 Wagging	1044	C-O Stretching and C-H bending
1160	CH_2 Twisting		
1123	C-C Stretch		
936	C=O Stretch		
721 709	CH_2 Rocking (α) CH_2 Rocking (γ)		

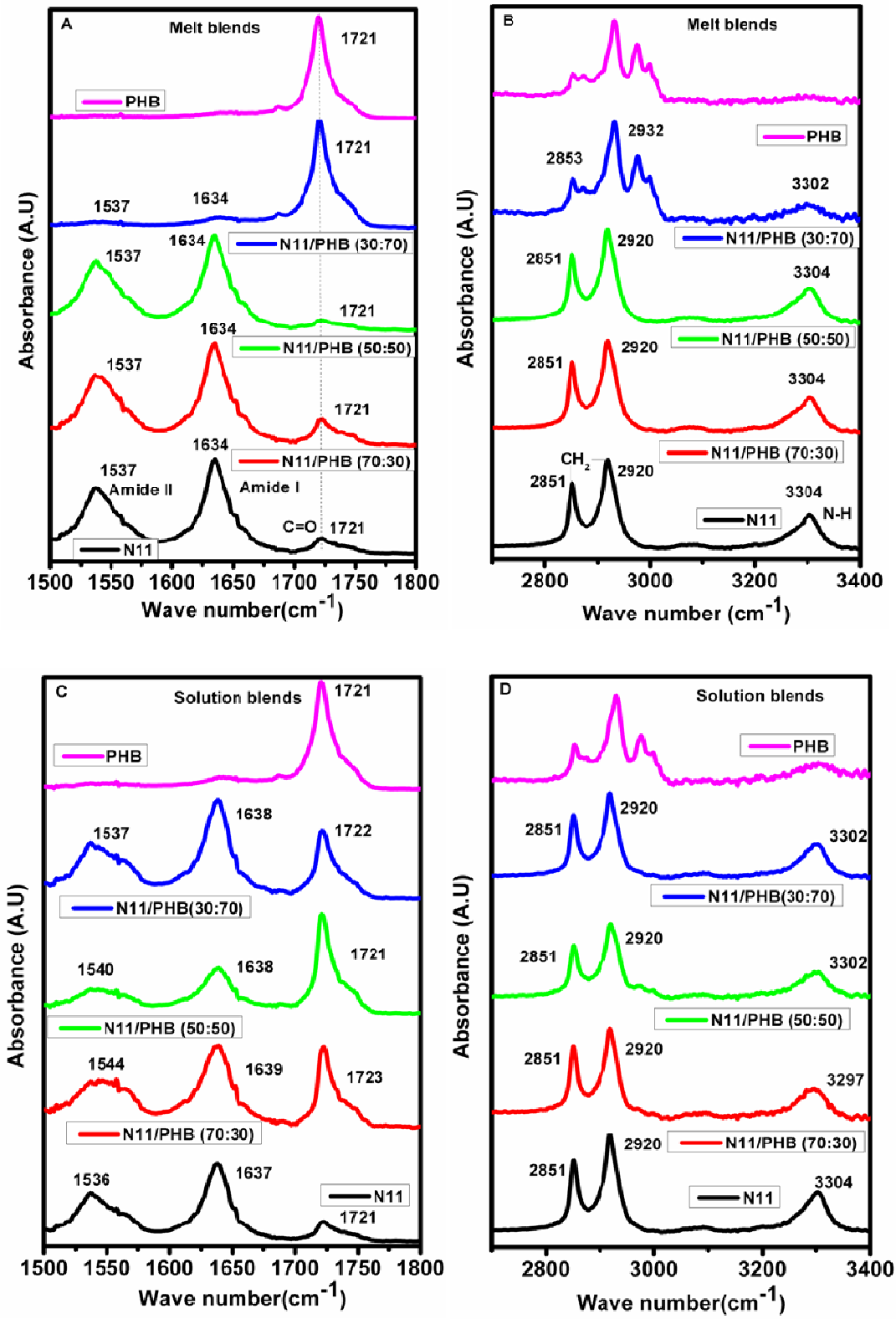
A
Melt blends
PHB
N11/PHB (30:70)
N11/PHB (50:50)
N11/PHB (70:30)
N11
1721
1537
1634
Amide II
Amide I
C=O
Absorbance (A.U)
Wave number(cm-1)
B
Melt blends
PHB
N11/PHB (30:70)
N11/PHB (50:50)
N11/PHB (70:30)
N11
2932
2853
3302
2920
2851
3304
CH2
N-H
Absorbance (A.U)
Wave number (cm-1)
C
Solution blends
PHB
N11/PHB(30:70)
N11/PHB (50:50)
N11/PHB (70:30)
N11
1638
1722
1540
1544
1639
1723
1536
1637
Absorbance (A.U)
Wave number(cm-1)
D
Solution blends
PHB
N11/PHB(30:70)
N11/PHB (50:50)
N11/PHB (70:30)
N11
2920
2851
3302
3297
3304
Absorbance (A.U)
Wave number(cm-1)

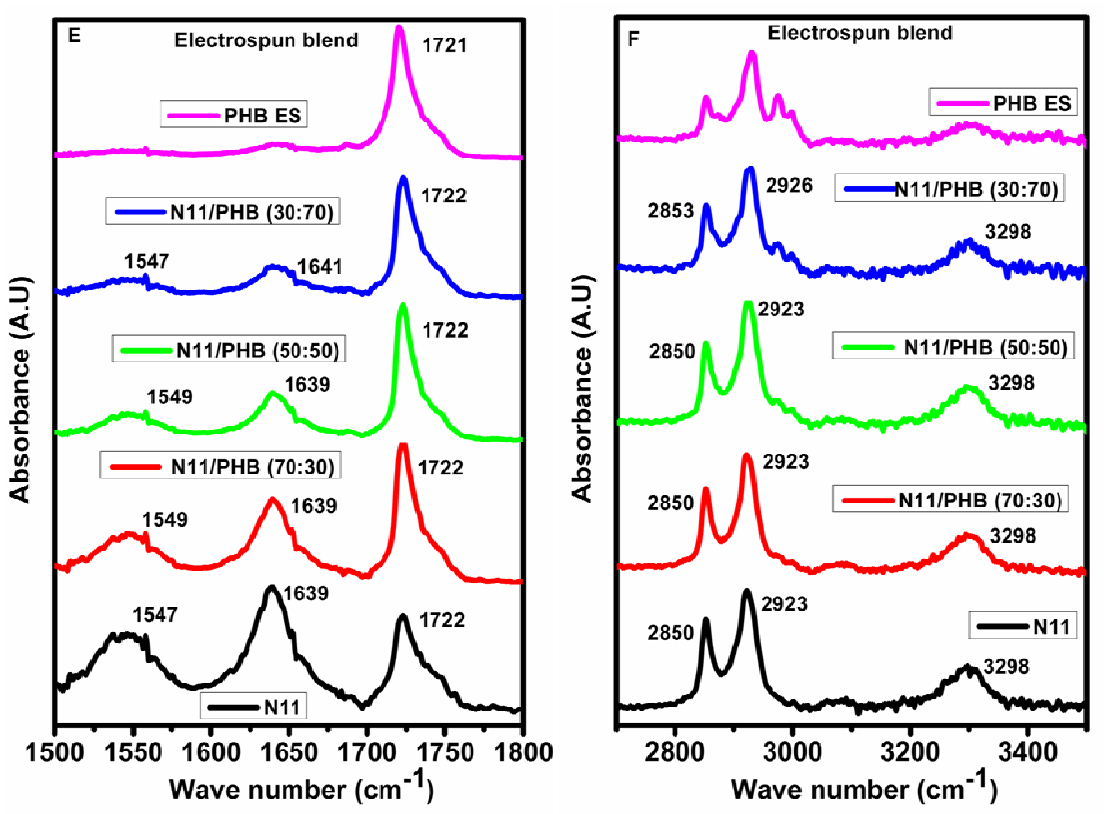

Figure 5.5 ATR spectra of Nylon11, PHB and their melt blends (A and B), solution blends (C and D) and electrospun blends (E and F).

5.1.3.6 Thermo Gravimetric Analysis (TGA)

One of the main drawbacks of the PHB is thermal instability. The decomposition temperature of PHB is closer to its melting temperature and is lower than that of Nylon11. This makes PHB difficult to melt process. Increasing thermal stability of the PHB ultimately improves the processing. The thermal decomposition temperatures of Nylon11/PHB melt, solution and electrospun blends are given in the Table 5.4.

Table 5.4 The thermal decomposition temperature of Nylon11, PHB and their melt, solution and electrospun blends.

Blend compositions	**Melt blends**		**Solution blends**		**Electrospun blends**	
	First derivative peak temperature (°C)		First derivative peak temperature (°C)		First derivative peak temperature (°C)	
	N11	PHB	N11	PHB	N11	PHB
N11	440	-	459	-	475	-
N11/PHB(70:30)	454	300	431	303	479	301
N11/PHB(50:50)	455	304	444	306	485	326
N11/PHB(30:70)	459	280	461	299	476	324
PHB	-	280	-	289	-	304

Figure 5.6 shows that TGA weight loss curve of PHB, Nylon11 and their melt, solution and electrospun blends. The weight loss of pure PHB and pure Nylon11 occurred in one step. The thermal stability of the Nylon11 was better than that of the pure PHB. The thermal decomposition temperature (first derivative peak temperature) of Nylon11 was approximately 440 °C[28], while that of pure PHB was 280 °C. All blends showed two step degradation, the first step corresponding to PHB and the second to Nylon11. The blending of PHB with the Nylon11 significantly improved the thermal stability of the PHB[29]. The enhanced thermal stability in the blending system improved the processing ability of the PHB. The decomposition temperatures of Nylon11, PHB and their electrospun blends were slightly higher than the corresponding solution blends and melt blends.

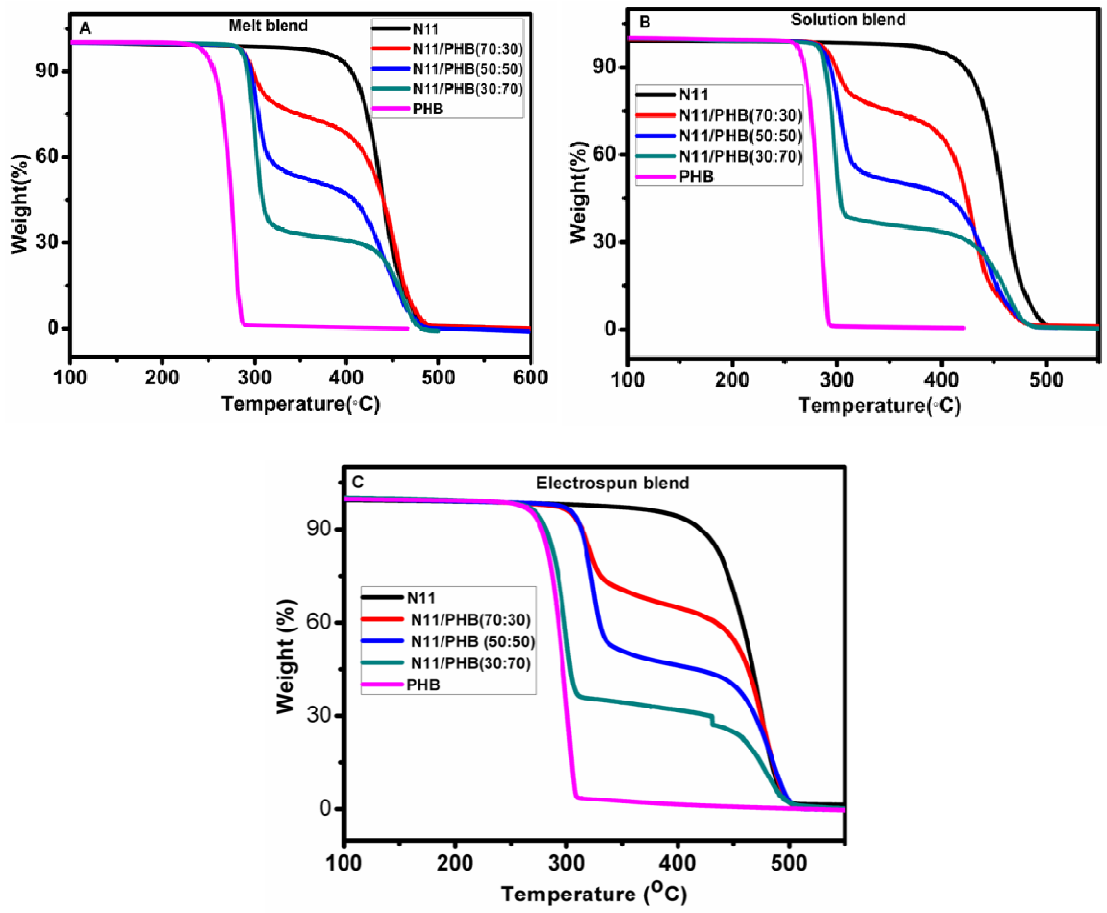

Figure 5.6 TGA curves of Nylon11, PHB and their melt (A), solution (B) and electrospun blends (C).

5.1.3.7 Dynamic Mechanical Thermal Analysis (DMTA)

The α transition (glass transition temperature) of PHB was around -11 °C and for Nylon11 it is 37 °C (shown in Figure 5.7 B). The PHB rich blends Nylon11/PHB (30:70) show the Tg value near to the Tg of PHB. Nylon11 rich blends Nylon11/PHB (70:30) showed value near to the Nylon11. However Nylon11/PHB (50:50) blends showed Tg near that of Nylon11. The single broad relaxation observed in the DMA suggests that the two polymers might be partially miscible in the amorphous phase.

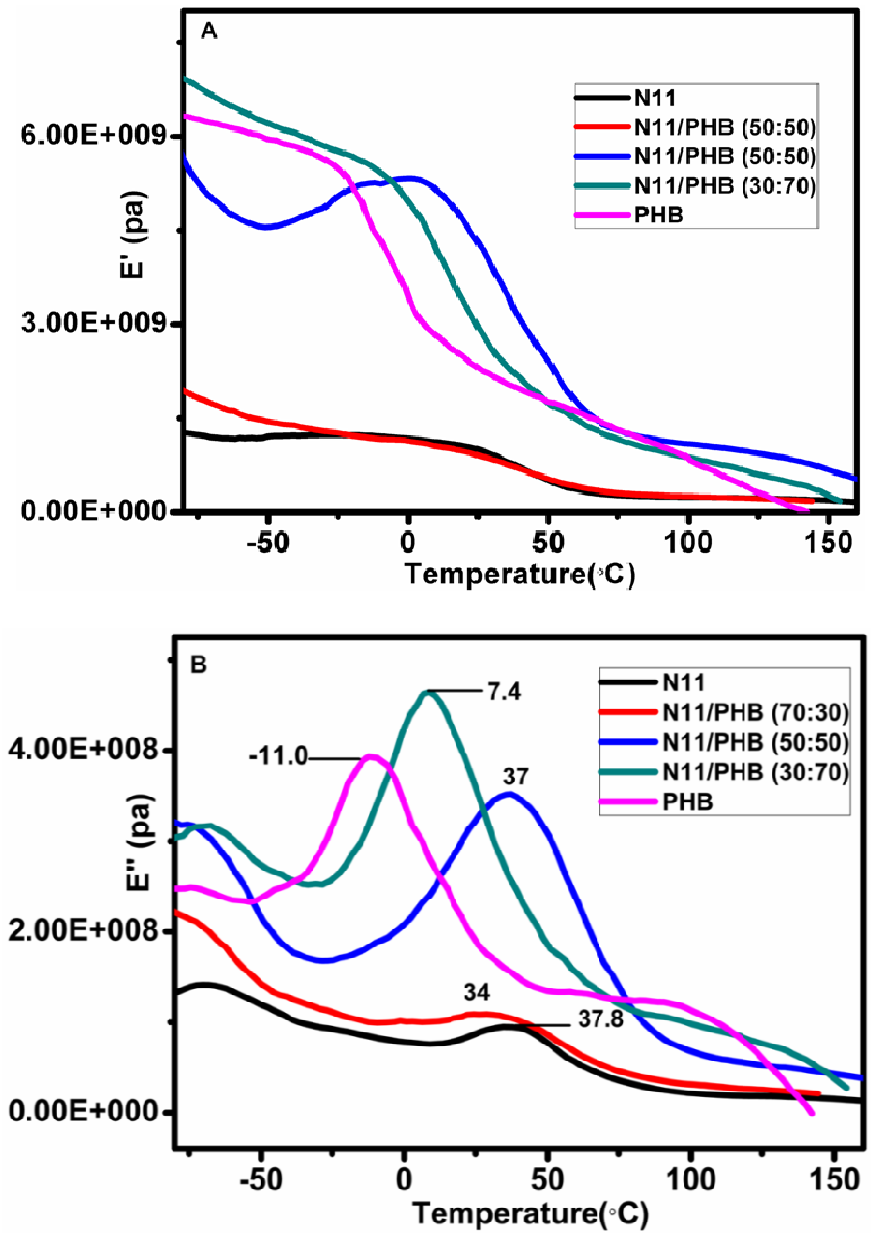

Figure 5.7 Storage modulus (A) and loss modulus (B) of Nylon11, PHB and their melt blends.

5.1.3.8 Water Contact Angle Measurement

The water contact angle of Nylon11, PHB and their blends is listed in the Table 5.5. Nylon11/PHB melt pressed films and solution cast films exhibit contact angle less than 90°[30]. Electrospun mats of Nylon11, PHB and their blends are more hydrophobic in nature[31], showing contact angle greater than 90°. This is because of air pockets and multiple contact points on the electrospun mats.

Table 5.5 Water contact angle measurement of Nylon11, PHB and their blends (standard deviation ± 4 °).

Sample	Water contact angle (°)		
	Electrospun fibers	**Solution films**	**Melt pressed film**
PHB	120	82	66
Nylon11/PHB(30:70)	121	75	73
Nylon11/PHB(50:50)	124	83	72
Nylon11/PHB(70:50)	125	64	70
Nylon11	135	73	73

5.1.3.9 Cell Culture Study

Cell culture procedure was same as described in the chapter 3. Figure 5.8 shows the SEM images of Nylon11, PHB and Nylon11/PHB (50:50) electrospun blends. Cell culture studies on Nylon11 electrospun mat, PHB electrospun mat and Nylon11/PHB (50:50) electrospun mats show that HEK 293 cells adhere and spread on all the electrospun mat surfaces[32].

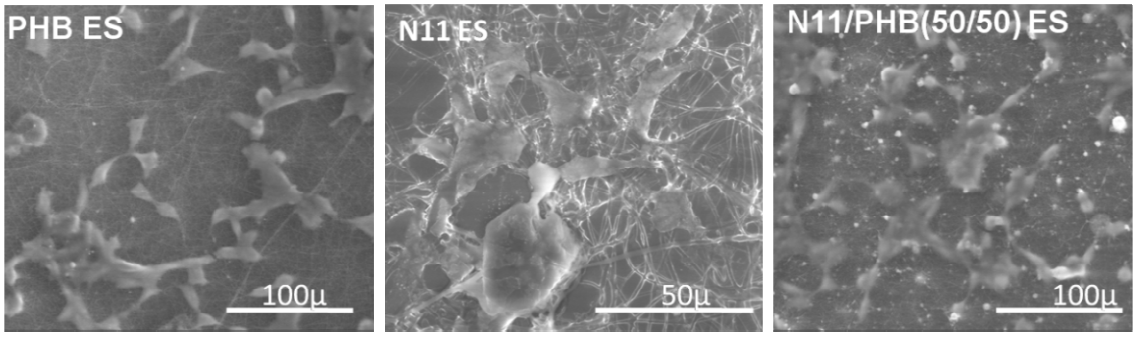

Figure 5.8 Morphological studies of HEK293 cells on Nylon11, PHB and Nylon11/PHB (50:50) electrospun mats.

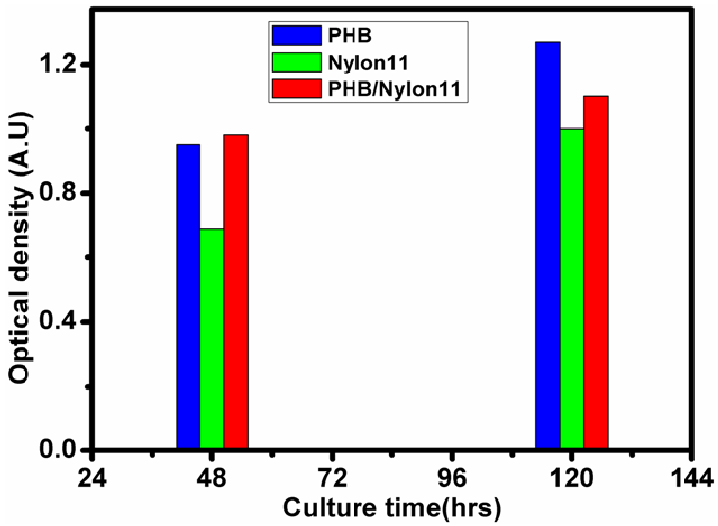

Figure 5.9 MTT assay results of HEK293 cells on Nylon11, PHB and Nylon11/PHB (50:50) electrospun mats.

Figure 5.9 shows MTT assay results of Nylon11, PHB and Nylon11/PHB (50:50) electrospun mats. MTT assay results of 2nd and 5th days show that PHB electrospun mat give better response followed by the blends and Nylon11 electrospun mats.

5.2 Nylon11/ZnO Electrospun Mats

5.2.1 Introduction

Of late there is growing interest in developing flexible biocompatible energy conversion devices that can convert easily available mechanical energy into electrical energy for powering electronic devices. Simultaneously, the combination of nanotechnology and piezoelectricity has resulted in the development of a new class of piezoelectric nano structured materials. Such materials are known to exhibit enhanced piezoelectric effect, which makes them useful for developing a wide range of applications in nano electromechanical systems, nano sensors[33], transducer[34], nano generator, nano resonators, diodes[35] and piezoelectric field effect transistors. Piezoelectric nanostructure can be in the form of nanowires, nano films, nano plates, nano ribbons and nano rings[36]. Nanostructure can be achieved by thin film coating, spin coating, solution cast film and electrospinning process. Recently electrospinning has been widely explored and demonstrated as a suitable method for preparation of nanocomposites[37]. The composite nanofibers have potential applications in filtration, protective clothing, electronics, energy storage devices, sensors and tissue engineering.

Zinc Oxide (ZnO) is a semi-conducting material which exhibits piezoelectric and pyroelecric properties. It has high thermal conductivity, heat capacity and higher melting temperature. Among numerous semiconducting materials, ZnO with a wide band gap of 3.4 eV and high electron mobility, has many promising applications in optoelectronics[38], solar cells[39], chemical sensor[40] and photo detector[41]. Due to its band gap in the UV range, ZnO acts as a good UV blocking agent and also has anti-microbial activity[42]. In cosmetics industry, ZnO nanoparticles are used in sunscreen creams and anti-microbial agents.

We have used Nylon11 electrospun nanofibers embedded with ZnO nanoparticles to create a biocompatible nano-scaled piezoelectric material. The Nylon11/ZnO electrospun mats were prepared by using electrospinning process. These mats were further characterized by using SEM, TEM, XRD, DSC and TGA. The piezo-electric response of Nylon11/ZnO electrospun mats was compared with Nylon11 electrospun mats.

5.2.2 Materials and Methods

5.2.2.1 Materials

Nylon11 pellets and ZnO nanoparticles were purchased from Sigma Aldrich Chemicals. Formic acid was procured from Merck, India.

5.2.2.2 Solution and Nanocomposites Preparation

Nylon11 solutions were prepared at a fixed concentration of 20wt/vol% in formic acid. 5wt% of ZnO was directly added to the solvent along with Nylon11 pellets. Sonication was done for 5 min to disperse ZnO. In the next step, solutions were prepared in a constant temperature bath at 70 °C for 3 hr in formic acid. Electrospinning of Nylon11 and Nylon11/ZnO nanofibers were done at the following conditions:

Solution concentration: 20 wt/vol%

ZnO: 5 wt%

Voltage: 20 kV

Flow rate: 0.2 ml/min

Distance between the electrodes: 10 cm

5.2.2.3 Characterization

The morphologies of Nylon11 and Nylon11/ZnO electrospun mats were studied by using Leica-440 Scanning Electron Microscope (SEM) operated at 20 kV. Electrospun mats were directly mounted on the SEM sample holder and the micrographs of representative areas were recorded at different magnifications. The sample surfaces were coated with gold to avoid specimen charging. Particle size of ZnO was characterized using Transmission Electron Microscopy (JEOL–JEM-2010 UHR) at accelerating voltage of 200 kV and 80 kV. Crystalline structures of the samples were characterized using a Rigaku Model Dmax 2500 X-ray diffractometer with Cu/K_α radiation, operating at 40 kV and 100 mA. The samples were scanned over the 2 θ range of 10 to 80 °. DSC studies of Nylon11 and Nylon11/ZnO electrospun mats were performed using Differential Scanning Calorimeter (DSC-Q100, TA Instrument) over a temperature range of 0-220 °C and at heating and cooling rates of 10 °C/min. The tests were carried out in Nitrogen atmosphere. The melting point (T_m), crystallization temperature (T_c) and % crystallinity were

determined from the first heating and cooling respectively. The viscoelastic properties of Nylon11 and Nylon11/ZnO electrospun mats were measured using Dynamic Mechanical Thermal Analyzer (Rheometric Scientific Inc. model IIIE). A rectangular tension-compression geometry was used. The test was carried out in linear viscoelastic region over the temperature range of -20 °C to 150 °C at a constant frequency of 10 rad/s with 0.02% strain. Thermal stability of Nylon11 and Nylon11/ZnO electrospun mats was studied using Perkin Elmer Simultaneous Thermal Analyzer 6000 (STA6000) over the temperature range of 30 to 550 °C at a heating rate of 20 °C/min. The tests were carried out in a Nitrogen atmosphere. The percent weight loss of sample was measured as a function of temperature. A DMA coupled with an oscilloscope was used to measure the piezoelectric response of the materials. Electrospun samples were placed in between the copper electrodes. The thicknesses of the Nylon11/ZnO electrospun mats were 0.1 mm. Strain was applied to the electrospun mats placed between the Cu electrodes, while the response was measured using an oscilloscope.

5.2.3 Results and Discussion

5.2.3.1 Morphological Studies of Nylon11 and Nylon11/ZnO Electrospun Mats

Figure 5.10 show SEM micrographs of Nylon11/ZnO electrospun mats (Figure 5.10 A) and EDAX analysis of the mats (Figure 5.10 B). The electrospun nanofibers in both mats exhibited ribbon shape or flat fibers having an average width of 700-800 nm. From the EDAX (Elemental analysis) mapping shown in Figure 5.10 B, it is clear that ZnO was present all over the Nylon11 electrospun mat surfaces.

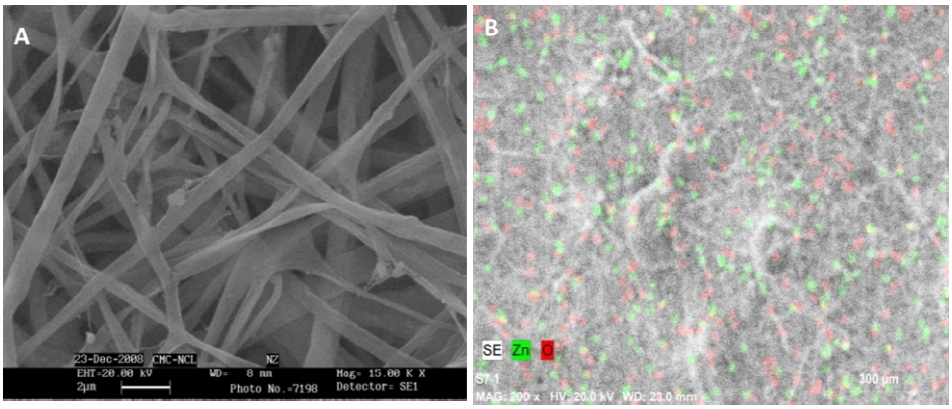

Figure 5.10 SEM micrograph of Nylon11/ZnO electrospun mats (A) (scale bar = 2µm), EDAX mapping of Nylon11/ZnO electrospun mat (B) (scale bar = 300 µm).

5.2.3.2. Transmission Electron Microscopy (TEM)

Figure 5.11 show TEM images of ZnO nanoparticles and Nylon11/ZnO nanocomposites. The size of ZnO nanoparticles was approximately 50 to 70 nm. TEM images of the Nylon11/ZnO composites fibers show nanoparticles are uniformly dispersed in the Nylon11 mat.

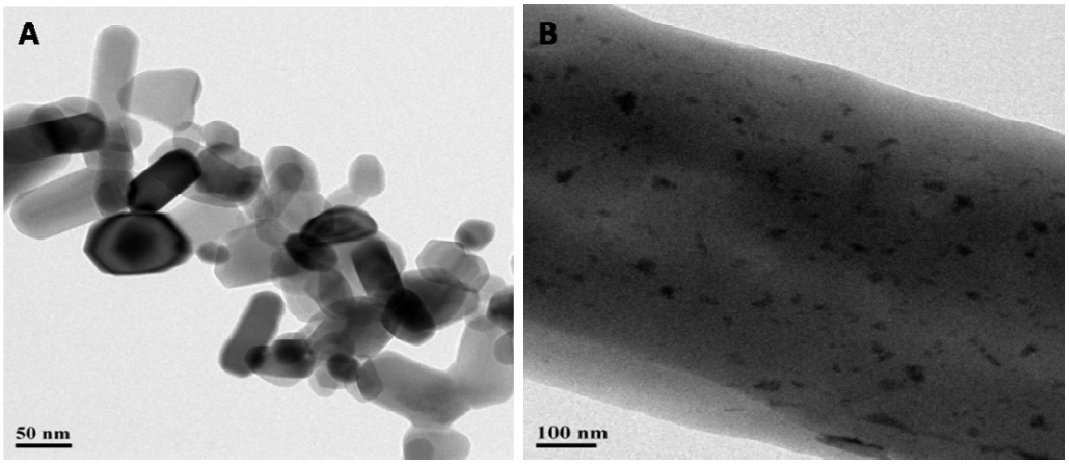

Figure 5.11 TEM images of ZnO (A) Nylon11/ZnO electrospun mat (B).

5.2.3.3 X-Ray Diffraction (XRD)

The data presented in Figure 5.12 are X-ray powder diffraction of ZnO and Nylon11/ZnO nanofibers. The peak at 21.6 ° corresponds to the gamma crystalline structure of Nylon11 electrospun mats. The XRD pattern of hexagonal ZnO shows three prominent peaks at 2θ values of 31.4 °, 34.4 ° and 36.3 °, which are the reflection from the crystallographic (100), (002) and (101) planes respectively[43].

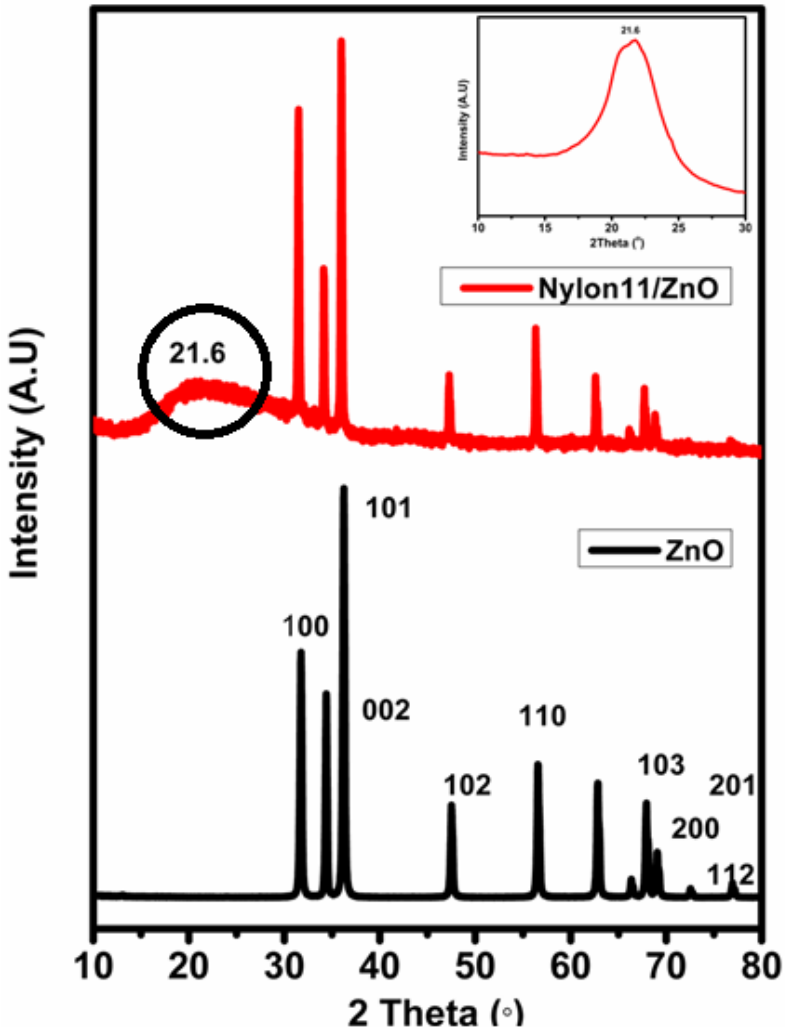

Figure 5.12 X-ray powder diffraction patterns of ZnO and Nylon11/ZnO nanofibers. Inset shows magnified XRD peak for Nylon11 corresponding to the γ crystalline structure.

5.2.3.4. Differential Scanning Calorimetry (DSC)

The melting point of Nylon11 electrospun fibers was 186.7 °C. The melting point of Nylon11/ZnO nanofibers were 187.4 °C. Table 5.6 shows melting temperature, crystallization temperature and % crystallinity of Nylon11 and Nylon11/ZnO electrospun mat. DSC results revealed that melting temperature and crystalline temperature of Nylon11 did not change with incorporation of ZnO nanoparticles.

Table 5.6 Melting temperature and % crystallinity of Nylon11 and Nylon11/ZnO electrospun mats.

Sample	First heating			% Crystallinity
	Melting temperature (T_m°C)	Tc (°C)	Heat of fusion (ΔH_f)J/g	
Nylon11 electrospun mat	186.7	165.5	61.2	29.7
Nylon11/ZnO electrospun mats	187.4	166.2	57.7	29.4

5.2.2.5 Dynamic Mechanical Thermal Analysis (DMTA)

Figure 5.13 show loss modulus of Nylon11 and Nylon11/ZnO electrospun mats. The α transition (Tg) of Nylon11 electrospun mat was 53.2 °C and for Nylon11/ZnO electrospun mats 69.7 °C. A 17 °C shift in the Tg could be attributed to the strong interfacial interaction between the polymer and filler.

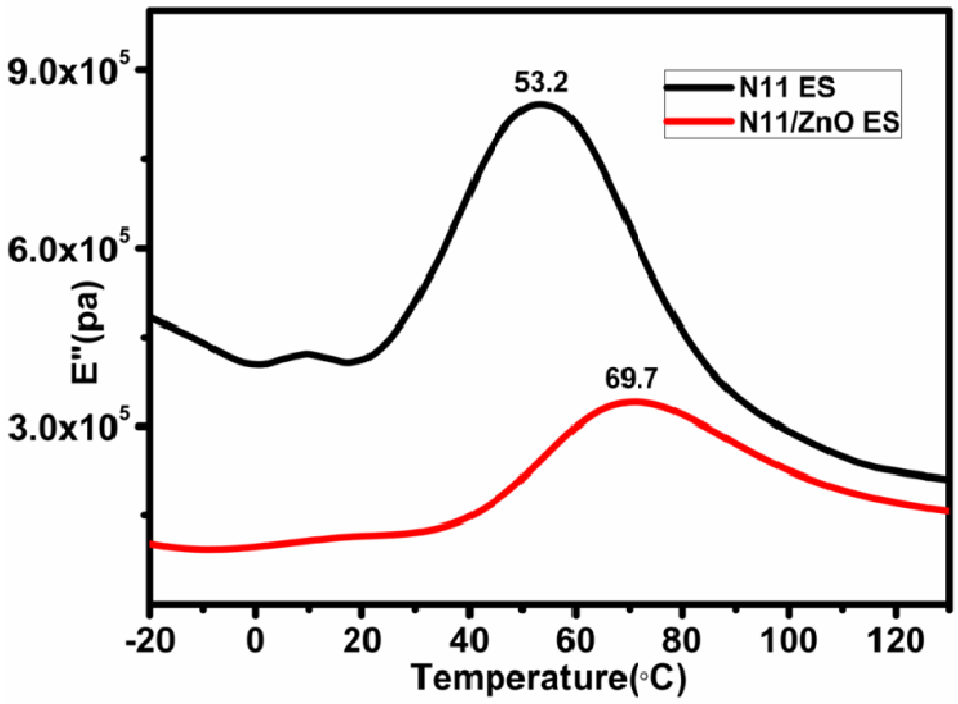

Figure 5.13 Storage modulus (E') and Loss modulus (E") of Nylon11 and Nylon11/ZnO electrospun mats.

5.2.3.6 Thermo Gravimetric Analysis (TGA)

Figure 5.14 shows the weight loss % and degradation temperature (first derivation peak temperature) of Nylon11 and Nylon11/ZnO electrospun mats. The degradation of Nylon11 starts at 425 °C, whereas the onset degradation temperature of Nylon11/ZnO electrospun mats was 416 °C. This is around 10 °C lower than the base polymer. The decomposition temperature (first derivative peak temperature) of Nylon11 was 484 °C. The decomposition temperature of Nylon11/ZnO electrospun mats was 476 °C. Incorporation of ZnO reduced the decomposition temperature of Nylon11 electrospun mats. This is possibly due to the catalytic activity of ZnO resulting in oxidation and earlier decomposition of Nylon11. Similar result was reported where the thermal degradation temperature of polymer was decreased with the presence of ZnO[44].

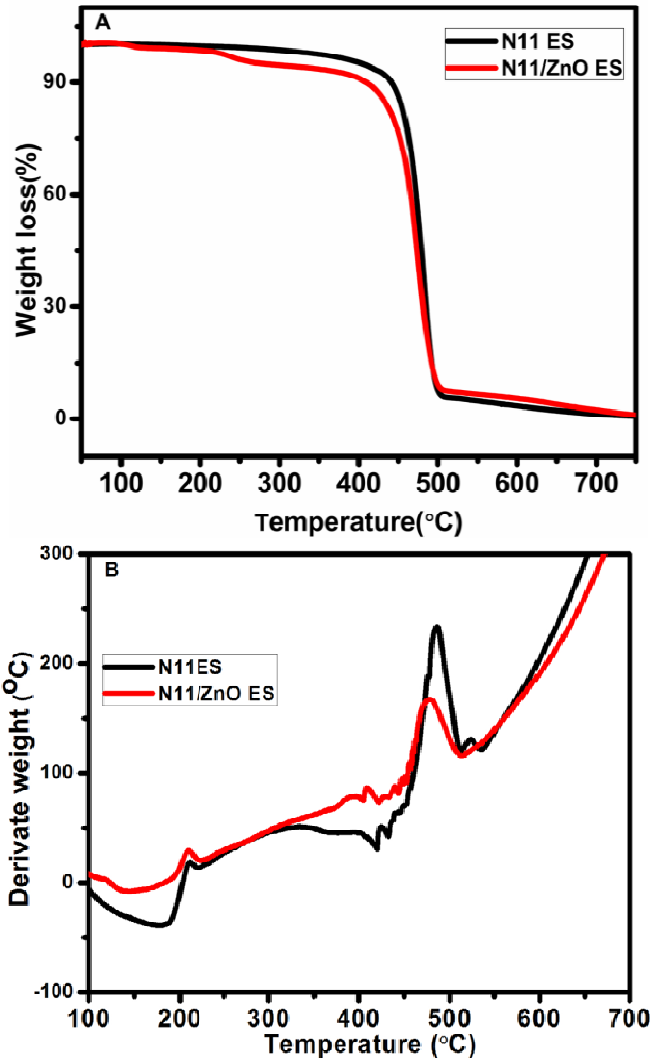

Figure 5.14 Weight loss (A) and first derivative peak temperature (B) of Nylon11 and Nylon11/ZnO electrospun mats.

The residue was calculated at 700 °C for Nylon11 electrospun mats and Nylon11/ZnO electrospun mats. Nylon11 electrospun mats exhibits 1.27 % and Nylon11/ZnO electrospun mats results 2.3 %. This suggests that small piece of the Nylon11/ZnO mats tested by TGA had about 1 % by weight of ZnO on their surfaces. The overall ZnO weight percent was about 5 %. Thus the ZnO was possibly non uniformily dispersed in the nanofibers.

5.2.3.7 Piezoelectric Response of Nylon11 Electrospun Mats

Figure 5.15 shows the piezoelectric response of Nylon11 and Nylon11/ZnO electrospun mats. When the strain is applied to the fibrous mats, piezoelectric charges are generated which build up the potential difference.

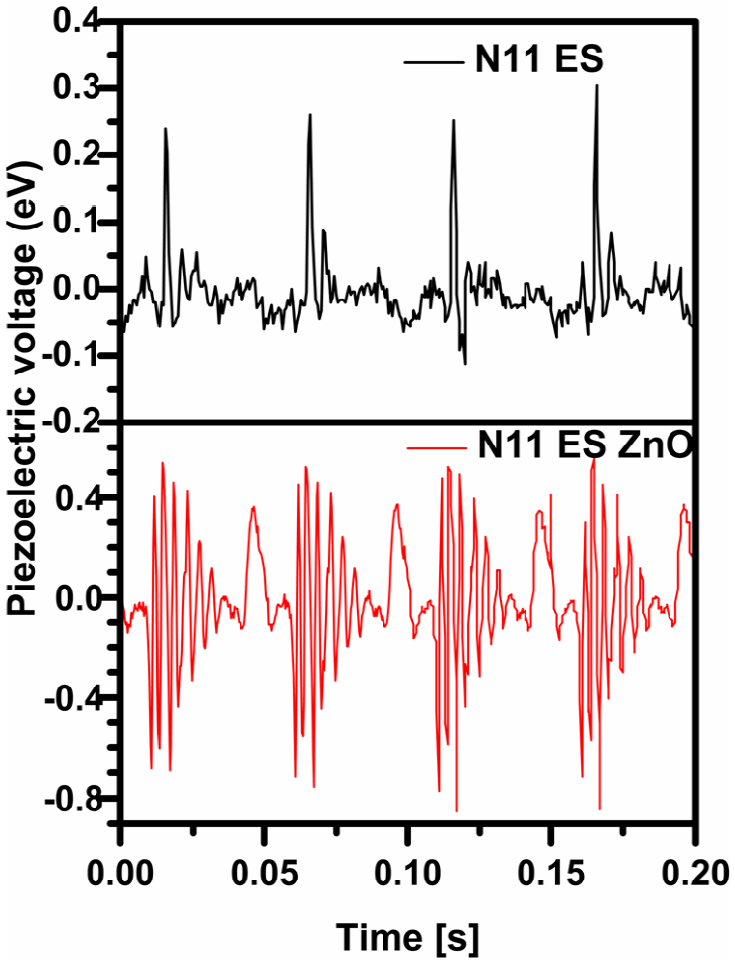

Figure 5.15 Piezoelectric responses of Nylon11 and Nylon11/ZnO nanocomposites.

It can be seen that piezoelectric response of Nylon11 electrospun mat peak to peak voltage was 0.3 V. Piezoelectric response of Nylon11/ZnO electrospun mats peak to

peak voltage was 1.2 V. Nylon11/ZnO nanocomposites showed better piezoelectric response compared to Nylon11 electrospun mat[45].

5.4. Conclusions

Nylon11/PHB blends were successfully prepared by melt, solution and electrospinning process. Solution viscosity of blends was lower than the base polymer. Conductivity of the blend solutions increased with increasing concentration of the Nylon11. Melt viscosity of Nylon11 film exhibited higher values compared to PHB melt. However, in blends viscosity values increased with increasing the concentration of the Nylon11. SEM images revealed that PHB exhibited branched and beaded fiber morphology, whereas Nylon11 electrospun mats show ribbon like fibers. However Nylon11/PHB (50:50) blends show uniform circular fiber.

Wide angle X-ray diffraction results show that PHB crystallized in alpha and beta form that coexisted in all the three blends. Nylon11 crystallized in α form in melt blends, while coexistence of α and γ form was seen in solution blends. The electrospun mats showed predominantly γ form. In DSC, Nylon11 and PHB exhibited separate melting and crystallization temperatures. From the DSC results it was confirmed that Nylon/PHB blends are immiscible. Solution blends exhibited higher crystallinity when compared to the melt blend and electrospun mats. DMA study shows that Tg of Nylon11/PHB melt blends were intermediate between the Tg of Nylon11 and PHB. TGA studies showed that thermal stability of PHB was increased in blends. Hydrophilicity measurement shows that Nylon11/PHB melt and solution blends were relatively more hydrophilic in nature than PHB, Nylon11 and Nylon11/PHB electrospun mats. SEM images show that cells are able to adhere and spread over on all the three mat surfaces. MTT assay revealed that PHB electrospun mat show improved proliferation rate followed by Nylon11/PHB (50:50) blends and Nylon11.

EDAX and TEM images show that ZnO nanoparticles were uniformly dispersed on the Nylon11 electrospun mat. ZnO nanoparticles did not induce any changes in the thermal properties of Nylon11. DMA study showed that Nylon11/ZnO electrospun mat exhibited higher Tg than Nylon11. The decomposition temperature of Nylon11/ZnO electrospun mats was decreased when compared to Nylon11 electrospun mats. The Nylon11/ZnO electrospun mats show better piezoelectric response compared to the Nylon11 electrospun mat.

5.5 References

1. Chem, J. M., Jo, S. B., Lee, H. and Cho, K. Polymer blends with semiconducting nanowires for organic electronics. Journal of Materials Chemistry 22, 4244–4260 (2012).
2. Belorgey, G. and Purdhomme, R.E. Miscibility of polycaprolactone / chlorinated polyethylene blends. Journal of Polymer Science:Polymer Physics Edition, 20, 191–203 (1982).
3. Sakurai, K., Maegawa, T. and Takahashi, T. Glass transition temperature of chitosan and miscibility of chitosan/poly(N -vinyl pyrrolidone) blends. Polymer 41, 7051–7056 (2000).
4. Yang, J., Feng, C., Dai, J., Zhang, N. and Huang, T. Compatibilization of immiscible nylon6/poly (vinylidene fluoride) blends using graphene oxides. Polymer International 62, 1085–1093 (2013).
5. Komalan, C., George, K. E., Kumar, P. A. S., Varughese, K. T. and Thomas, S. Dynamic mechanical analysis of binary and ternary polymer blends based on nylon copolymer/EPDM rubber and EPM grafted maleic anhydride compatibilizer. eXPRESS Polymer Letters 10, 641–653 (2007).
6. Xu, S., Luo, R., Wu, L., Xu, K. and Chen, G. Blending and characterizations of microbial poly (3-hydroxybutyrate) with dendrimers. Journal of Applied Polymer Science 102, 3782–3790 (2006).
7. Koning, C., Duin, M. Van, Pagnoulle, C. and Jerome, R. Strategies for compatibilization of polymer blends. Progress in Polymer Science 23, 707–757 (1998).
8. Shalumon, K. T., Anulekha, K. H., Girish, C. M., Prasanth, R. and Jayakumar, R. Single step electrospinning of chitosan/poly (caprolactone) nanofibers using formic acid / acetone solvent mixture. Carbohydrate Polymers 80, 413–419 (2010).
9. Zhou, Y., Yang, D., Chen, X., Xu, Q. and Lu, F. Electrospun water-soluble carboxyethyl chitosan/Poly (vinyl alcohol) nanofibrous membrane as potential wound dressing for skin regeneration. Biomacromolecules 9, 349–354 (2008).
10. Chen, F., Li, X., Mo, X. and He, C. Electrospun chitosan-P(LLA- CL) nanofibers for biomimetic extracellular matrix. Journal of Biomaterials Science Polymer Edition 19, 677–691 (2008).

11. Hu, G., Wang, B. and Zhou, X. Effect of EPDM-MAH compatibilizer on the mechanical properties and morphology of nylon 11/PE blends. Materials Letters 58, 3457–3460 (2004).
12. Paolo, F., Mantia, L. A. and Valenza, A. Mechanical properties-structure relationships for immiscible blends of low density polyethylene with Nylon-6. European Polymer Journal 25, 553–556 (1989).
13. Kulkarni, S. O., Kanekar, P. P., Jog, J. P., Patil, P. A., Nilegaonkar, S. S. Sarnaik, S. S. and Kshirsagar, P. R. Characterisation of copolymer, poly (hydroxybutyrate-co-hydroxyvalerate) (PHB-co-PHV) produced by Halomonas campisalis (MCM B-1027), its biodegradability and potential application. Bioresource Technology 102, 6625–6628 (2011).
14. Mahishi, L. H., Tripathi, G. and Rawal, S. K. Poly (3-hydroxybutyrate) (PHB) synthesis by recombinant Escherichia coli harbouring Streptomyces aureofaciens PHB biosynthesis genes□: Effect of various carbon and nitrogen sources. Microbiological Research 158, 19–27 (2003).
15. Li, X., Zhang, Y. and Chen, G. Biomaterials nanofibrous polyhydroxyalkanoate matrices as cell growth supporting materials. Biomaterials 29, 3720–3728 (2008).
16. Unger, M., Sato, H., Ozaki, Y. and Siesler, H. W. Crystallization behavior of poly (3-hydroxybutyrate) (PHB), Poly (e -caprolactone) (PCL) and their blend (50□: 50 wt .%) studied by 2D FT-IR correlation spectroscopy. Macromolecular Symposia 305, 90–100 (2011).
17. Godbole, S., Gote, S., Latkar, M. and Chakrabarti, T. Preparation and characterization of biodegradable poly-3-hydroxybutyrate – starch blend films. Bioresource Technology 86, 33–37 (2003).
18. Sombatmankhong, K., Suwantong, O., Waleetorncheepsawat, S. and Supaphol, P. Electrospun fiber mats of poly (3-Hydroxybutyrate), Poly (3Hydroxybutyrate- co -3-Hydroxyvalerate), and their blends. Journal of Polymer Science: Part B: Polymer Physics 44, 2923–2933 (2006).
19. Uyar, T. and Besenbacher, F. Electrospinning of uniform polystyrene fibers□: The effect of solvent conductivity. Polymer 49, 5336–5343 (2008).
20. Wang, C., Hsu, C. and Hwang, I. Scaling laws and internal structure for characterizing electrospun poly [(R) -3-hydroxybutyrate] fibers. Polymer 49, 4188–4195 (2008).

21. Gogolewski, S. and Pennings, A. J. Crystallization of polyamides under elevated pressure□: 5 . Pressure-induced crystallization from the melt and annealing of folded-chain crystals of nylon-11, poly (aminoundecaneamide) under pressure. Polymer 18, 660–666 (1977).
22. T. Sasaki. Notes on the polymorphism in Nylon11. Polymer Letters 3, 557–560 (1965).
23. Al-Rawajfeh, A. E., Al-Salah, H. A. and Al-Rhael, I. Miscibility, crystallinity and morphology of polymer blends of polyamide-6/ Poly (β -hydroxybutyrate). Jordan Journal of Chemistry 1, 155–170 (2006).
24. Qiu, Z., Ikehara, T. and Nishi, T. Poly (hydroxybutyrate)/poly (butylene succinate) blends□: miscibility and nonisothermal crystallization. Polymer 44, 2503–2508 (2003).
25. Nair, S. S., Ramesh, C. and Tashiro, K. Polymorphism in Nylon-11□: Characterization using HTWAXS and HTFTIR. Macromolecular Symposia 242, 216–226 (2006).
26. Catiker, E. and Sancaktar, E. Blends of Poly (3-hydroxybutyrate) with Poly (b -alanine) and Its Derivatives. Applied Polymer Science 40484, 1–8 (2014).
27. Furukawa, T., Sato, H., Murakami, R., Zhang, J., Duan, Y. X., Noda, I., Ochiai, S. and Ozaki, Y. Structure, dispersibility, and crystallinity of Poly(hydroxybutyrate)/Poly(L-lactic acid) blends studied by FT-IR microspectroscopy and differential scanning calorimetry. Macromolecules 38, 6445–6454 (2005).
28. Liu, T., Lim, K. P., Tjiu, W. C., Pramoda, K. P. and Chen, Z. Preparation and characterization of nylon11 / organoclay nanocomposites. Polymer 44, 3529–3535 (2003).
29. Mano, J. F., Koniarova, D., Reis, R. L., Azure, C. De and Gualtar, C. De. Thermal properties of thermoplastic starch/synthetic polymer blends with potential biomedical applicability. Journal of Materials Science: Materials in Medicine 4, 127–135 (2003).
30. Thomas, S. P., Thomas, S., Abraham, R. and Bandyopadhyay, S. Polystyrene /calcium phosphate nanocomposites□: Contact angle studies based on water and methylene iodide. eXPRESS Polymer Letters 2, 528–538 (2008).
31. Jeon, H. and Kim, G. Preparation and characterization of an electrospun polycaprolactone (PCL) fibrous mat and multi-layered PCL scaffolds having a

nanosized pattern-surface for tissue regeneration. Journal of Materials Chemistry B 2, 171–180 (2014).

32. Sombatmankhong, K., Sanchavanakit, N., Pavasant, P. and Supaphol, P. Bone scaffolds from electrospun fiber mats of poly (3-hydroxybutyrate), poly (3-hydroxybutyrate- co -3-hydroxyvalerate) and their blend. Polymer 48, 1419–1427 (2007).
33. Ding, B., Wang, M., Yu, J. and Sun, G. Gas sensors based on electrospun nanofibers. Sensors 9, 1609–1624 (2009).
34. Gun, J., Rizkov, D., Lev, O. and Schoning, M. J. Oxygen plasma-treated gold nanoparticle-based field-effect devices as transducer structures for bio-chemical sensing. Microchim Acta 164, 395–404 (2009).
35. Hussain, A. M. Neppolian, B., Kim, S. H., Kim, J. Y., Choi, H. C., Lee, K., Park, S. J. and Heeger, A.J. Improved performance of polymer light-emitting diodes with nanocomposites. Applied Physics Letters 94, 7–9 (2009).
36. Fang, X.Q., Liu, J.X. and Gupta, V. Fundamental formulations and recent achievements in piezoelectric nano-structures: A review. Nanoscale 5, 1716–26 (2013).
37. Wu, H. and Pan, W. Preparation of Zinc Oxide nanofibers by electrospinning. Journal of the American Chemical Society 701, 699–701 (2006).
38. Chem, J. M., Park, J. S., Lee, J. M., Hwang, S. K., Lee, H. J., Lee, B. R., Park, H., Kim, J. S., Yoo, S., Song, M. H. and Kim, S.O. A ZnO/N-doped carbon nanotube nanocomposite charge transport layer for high performance optoelectronics. Journal of Materials Chemistry 22, 12695–12700 (2012).
39. Son, D., Im, J., Kim, H. and Park, N. 11% efficient perovskite solar cell based on ZnO nanorods: An effective charge collection system. The Journal of Physical Chemistry 118, 16567–16573 (2014).
40. Choi, S., Ankonina, G., Youn, D., Oh, S. and Hong, J. Hollow ZnO nanofibers fabricated using electrospun polymer templates. ACS Nano 3, 2623–2631 (2009).
41. Soci, C., Zhang, A., Xiang, B., Dayeh, S. A., Aplin, D. P. R., Park, J., Bao, X. Y., Lo, Y. H. and Wang, D. ZnO Nanowire UV Photodetectors with high internal gain. Nano Letters 7, 1003–1009 (2007).

42. Ghule, K., Ghule, A. V., Chen, B. and Ling, Y. Preparation and characterization of ZnO nanoparticles coated paper and its antibacterial activity study. Green Chemistry 8, 1034–1041 (2006).
43. Baek, J., Park, J, Kang, J., Kim, D., Koh, S. and Kang, Y. Fabrication and thermal oxidation of ZnO nanofibers prepared via electrospinning technique. Bulletin of the Korean Chemical Society 33, 2694–2698 (2012).
44. Kayaci, F., Ozgit-akgun, C., Donmez, I., Biyikli, N. and Uyar, T. Polymer − inorganic core−shell nano fibers by electrospinning and atomic layer deposition: Flexible Nylon−ZnO core−shell nano fiber mats and their photocatalytic activity. Applied Materials and Interfaces 4, 6185–6194 (2012).
45. Li, Z., Zhang, X. and Li, G. In situ ZnO nanowire growth to promote the PVDF piezo phase and the ZnO – PVDF hybrid self-rectified nanogenerator as a touch sensor. Physical Chemistry Chemical Physics 16, 5475–5479 (2014).

Chapter 6

Recommendations for further work

Based on the results presented in the previous three chapters and the inferences drawn therefrom, three specific recommendations are proposed to take the work forward. These are presented in this chapter.

In chapter 3 the main results of electrospinning of Nylon11 were presented. Specially, the effects of electrospinning process parameters on the morphology of the mats and the size of the nanofibers were discussed. In chapter 4, surface modification of Nylon11 electrospun mats was described. Two surface modification techniques namely, plasma treatment and attachment of gold nanoparticles were demonstrated. Based on the work presented in chapter 3 and 4 the following recommendations for future work are suggested.

It would be useful to design multi-layered scaffold in which the base layer could be a high strength, macroporous Nylon11 substrate such as a woven fabric on which layers of electrospun Nylon11 non-woven fabric of varying fiber porosity can be deposited using the knowledge of the effect of electrospinning process variables on mat morphology and fiber size obtained from the present work. Such multi-layered structures will be able to provide optimal combination of strength, porosity and 3D structure that is favorable for cell culture or other biomedical applications such as wound dressing. Further, these multi-layered mats can be surface treated using the techniques presented in this work. Specifically, the gold nanoparticles can be used as a substrate to attach various functional groups such as growth factors and cleavable drugs so as to make cell culture scaffolds or dressing pads. These ideas can be taken up as future work.

The second recommendation for future work originates in the interesting observation described in chapter 4 namely, the longevity of hydrophilicity of surface modified mats. It was shown in chapter 4 that a water droplet spreads gradually with increasing time on plasma treated mats. This is an unusual observation because it suggests that in the presence of a water drop, the polar functional groups created by plasma treatment such which get buried in the surface layer with aging, are reoriented back to the surface. Such reorientation driven possibly by the presence of a water droplet has never been observed before, and therefore should be investigated in detail.

The third recommendation is based on the work presented in chapter 5 on Nylon11/PHB blends and Nylon11/ZnO nanocomposites. While Nylon11 takes a long time for biodegradation, PHB degrades more rapidly. Thus electrospun blends of Nylon11 and PHB might show good control on the time required for biodegradation. Also, etching/biodegradation of PHB could result in porous nanofibers. Thus the degradation studies of Nylon11/PHB blends are recommended. Also, the ability of Nylon11 to incorporate fillers during electrospinning was demonstrated on

Nylon1/ZnO composites. Another nanofiller of interest could be hydroxyapatite (HAP). Nylon11/HAP nanocomposites could find applications in bone tissue engineering. Preliminary work on Nylon11/HAP electrospun nanocomposites was done as a part of this work. Figure 6.1 shows the morphology of HAP nanoparticles and Nylon11/HAP electrospun fibers. It is clearly seen that the HAP nano-needles were uniformly dispersed in the electrospun fibers. Interestingly a large number of HAP nano-needles were found to be oriented along the fiber direction. Thus, our third recommendation is to study the biodegradability of Nylon11/PHB and Nylon11/HAP electrospun blends and composites, and evaluate them particularly for bone cell culture application.

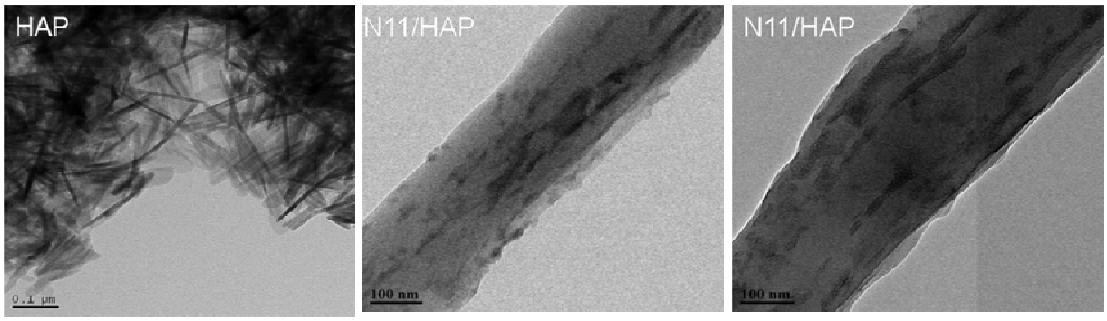

Figure 6.1 TEM images of HAP and Nylon11/HAP electrospun mat.

List of Publications

1. M. Dhanalakshmi, Ashish K. Lele and Jyoti P. Jog. Electrospinning of Nylon11: Effect of processing parameters on morphology and microstructure. Accepted in Materials Today Communications, (2015). DOI: 10.1016/j.mtcomm.2015.01.002.

2. M. Dhanalakshmi and J. P. Jog. Preparation and characterization of electrospun fibers of Nylon11. eXPRESS Polymer Letter 2, 540–545 (2008).

3. M. Dhanalakshmi, Ashish K. Lele and Jyoti P. Jog. Surface modification of Nylon11 electrospun mats (manuscript under preparation).